



**HYDROTALCITE-LIKE COMPOUNDS FOR THE VALORISATION OF RENEWABLE
FEEDSTOCKS**
Mayra García Álvarez

Dipòsit Legal: T. 724-2012

ADVERTIMENT. L'accés als continguts d'aquesta tesi doctoral i la seva utilització ha de respectar els drets de la persona autora. Pot ser utilitzada per a consulta o estudi personal, així com en activitats o materials d'investigació i docència en els termes establerts a l'art. 32 del Text Refós de la Llei de Propietat Intel·lectual (RDL 1/1996). Per altres utilitzacions es requereix l'autorització prèvia i expressa de la persona autora. En qualsevol cas, en la utilització dels seus continguts caldrà indicar de forma clara el nom i cognoms de la persona autora i el títol de la tesi doctoral. No s'autoritza la seva reproducció o altres formes d'explotació efectuades amb finalitats de lucre ni la seva comunicació pública des d'un lloc aliè al servei TDX. Tampoc s'autoritza la presentació del seu contingut en una finestra o marc aliè a TDX (framing). Aquesta reserva de drets afecta tant als continguts de la tesi com als seus resums i índexs.

ADVERTENCIA. El acceso a los contenidos de esta tesis doctoral y su utilización debe respetar los derechos de la persona autora. Puede ser utilizada para consulta o estudio personal, así como en actividades o materiales de investigación y docencia en los términos establecidos en el art. 32 del Texto Refundido de la Ley de Propiedad Intelectual (RDL 1/1996). Para otros usos se requiere la autorización previa y expresa de la persona autora. En cualquier caso, en la utilización de sus contenidos se deberá indicar de forma clara el nombre y apellidos de la persona autora y el título de la tesis doctoral. No se autoriza su reproducción u otras formas de explotación efectuadas con fines lucrativos ni su comunicación pública desde un sitio ajeno al servicio TDR. Tampoco se autoriza la presentación de su contenido en una ventana o marco ajeno a TDR (framing). Esta reserva de derechos afecta tanto al contenido de la tesis como a sus resúmenes e índices.

WARNING. Access to the contents of this doctoral thesis and its use must respect the rights of the author. It can be used for reference or private study, as well as research and learning activities or materials in the terms established by the 32nd article of the Spanish Consolidated Copyright Act (RDL 1/1996). Express and previous authorization of the author is required for any other uses. In any case, when using its content, full name of the author and title of the thesis must be clearly indicated. Reproduction or other forms of for profit use or public communication from outside TDX service is not allowed. Presentation of its content in a window or frame external to TDX (framing) is not authorized either. These rights affect both the content of the thesis and its abstracts and indexes.

Mayra García Álvarez

Hydrotalcite-like compounds for the valorisation of renewable feedstocks

PhD THESIS

Supervised by Prof. Dr. Francesc Medina Cabello

Departament d'Enginyeria Química



UNIVERSITAT ROVIRA I VIRGILI

Tarragona 2012

UNIVERSITAT ROVIRA I VIRGILI

HYDROTALCITE-LIKE COMPOUNDS FOR THE VALORISATION OF RENEWABLE FEEDSTOCKS

Mayra García Álvarez

Dipòsit Legal: T. 724-2012



Departament d'Ingenyeria Química
Av. Països Catalans, 26
Campus Sescelades
43007, Tarragona
Telf. 977 55 8675
Fax. 977 55 9621

Francesc Medina Cabello, Catedrático de la Universidad Rovira i Virgili
(Escuela Técnica Superior de Ingeniería Química, Departamento de Ingeniería
Química),

CERTIFICA:

Que el presente trabajo, titulado “Hydrotalcite-like compounds for the valorisation of renewable feedstocks”, que presenta Mayra García Álvarez para la obtención del título de Doctor, ha sido realizado bajo mi dirección en el Departamento de Ingeniería Química de esta Universidad y que cumple los requisitos para poder optar a la Mención Europea.

Tarragona, 15 de marzo de 2012

Francesc Medina Cabello

UNIVERSITAT ROVIRA I VIRGILI

HYDROTALCITE-LIKE COMPOUNDS FOR THE VALORISATION OF RENEWABLE FEEDSTOCKS

Mayra García Álvarez

Dipòsit Legal: T. 724-2012

En primer lugar, quiero expresar mi agradecimiento a mi supervisor Dr. Francesc Medina por acogerme en su grupo y darme la oportunidad de realizar la tesis, además de por el tiempo invertido durante el desarrollo de la misma. Espero que el resultado final de este trabajo esté a la altura de los conocimientos y apoyos brindados.

Quiero agradecer al Ministerio de Ciencia e Innovación por los 4 años de beca de doctorado y por el apoyo económico recibido durante mis dos estancias en Francia.

Je voudrais exprimer mes sincères remerciements au Prof. Figueras pour tout son support et son aide pendant, et même après, mon séjour à Lyon. J'aimerais également remercier le Dr. Didier Tichit pour m'avoir accepté dans son groupe à Montpellier et pour toutes les connaissances que j'ai acquises sous sa tutelle pendant mon séjour.

También quiero agradecer la ayuda y colaboración de los técnicos del Servei de Recursos y a todo el personal del departamento de Ingeniería Química.

A todos los miembros del grupo de Catálisis Heterogénea (CatHeter).

Los buenos momentos que he pasado en Tarragona durante la tesis se los tengo que agradecer a mis compañeros de laboratorio y, en especial a personas como Noe, Vero, Sandra, Susana, Oscar, Abelín y Luis con los que he compartido cafés, cenas, playas, paellas y eventos varios... y lo que nos queda. Gracias muy especialmente a Antón y Alvarito con los que aprendí muy *bones practiques* y un *altre manera de fer Europa* y que, además me han ayudado en cuestiones científico-técnicas. No me quiero olvidar de los compañeros que ya han encontrado otros caminos y con quienes he pasado muy buenos momentos: Beteley, Kaveh... y Foix (o como a él le gusta que lo llamen: Sr. Grasso...) con el que tanto me he reído en estos 4 años y lo que es mejor, ¡que me ha cuidado los gatos en vacaciones! A Foix, Vero y Susana les debo la tranquilidad de irme de vacaciones sabiendo que los gatines están en buenas manos.

A mi familia, que se lo debo todo y todo se merecen.

Y a Enrique, mi compañero de viaje.

UNIVERSITAT ROVIRA I VIRGILI

HYDROTALCITE-LIKE COMPOUNDS FOR THE VALORISATION OF RENEWABLE FEEDSTOCKS

Mayra García Álvarez

Dipòsit Legal: T. 724-2012

UNIVERSITAT ROVIRA I VIRGILI

HYDROTALCITE-LIKE COMPOUNDS FOR THE VALORISATION OF RENEWABLE FEEDSTOCKS

Mayra García Álvarez

Dipòsit Legal: T. 724-2012

UNIVERSITAT ROVIRA I VIRGILI

HYDROTALCITE-LIKE COMPOUNDS FOR THE VALORISATION OF RENEWABLE FEEDSTOCKS

Mayra García Álvarez

Dipòsit Legal: T. 724-2012

Table of contents

CHAPTER 1. GENERAL INTRODUCTION AND SCOPE	1
<hr/>	
1.1. Heterogeneous basic catalysis	3
1.2. Layered double hydroxides	7
1.2.1. Structure	7
1.2.2. Interlayer	11
1.2.3. Preparation methods	11
1.2.4. Applications	15
1.3. Biodiesel production and glycerol market	17
1.3.1. Uses of glycerol	17
1.3.2. Glycerol carbonate	19
1.4. General context	21
1.5. Objectives	22
1.6. Reference	23
CHAPTER 2. HYDROTALCITE-LIKE COMPOUNDS FOR VALORISATION OF GLYCEROL	27
<hr/>	
2.1. Introduction	29
2.2. Enhanced use of renewable resources: Transesterification of glycerol by hydrotalcite-like compounds	35
2.2.1. Introduction	35
2.2.2. Experimental	37
2.2.3. Results and discussion	38
2.2.4. Conclusions	45
2.3. Tunable basic and textural properties of HT derived materials for transesterification of glycerol	49
2.3.1. Introduction	49
2.3.2. Experimental	51
2.3.3. Results and discussion	53
2.3.4. Conclusions	71

CHAPTER 3. SUPPORTED HT-LIKE MATERIALS FOR TRANSESTERIFICATION OF GLYCEROL 77

3.1. Introduction	79
3.2. From glycerol to glycerol carbonate: Transesterification over hydrotalcites supported on carbon nanofibers as highly active catalysts	81
3.2.1. Introduction	81
3.2.2. Experimental	83
3.2.3. Results and discussion	85
3.2.4. Conclusions	94
3.3. Synthesis of glycerol carbonates by transesterification of glycerol in a continuous system using supported hydrotalcites as catalysts	99
3.3.1. Introduction	99
3.3.2. Experimental	101
3.3.3. Results and discussion	103
3.3.4. Conclusions	119

CHAPTER 4. STUDY OF THE ULTRASOUND TREATMENT EFFECT ON LDH 123

4.1. Introduction	125
4.2. Structure evolution of layered double hydroxides activated by induced reconstruction	129
4.2.1. Introduction	129
4.2.2. Experimental	130
4.2.3. Results and discussion	133
4.2.4. Conclusions	152

CHAPTER 5. GENERAL CONCLUSIONS 155

Appendix 0. Determination of products	159
Appendix I. List of abbreviations	163
Appendix II. Index of tables	167
Appendix III. Index of figures	171
Appendix IV. Index of schemes	177
Appendix V. Contributions to conferences	181
Appendix VI. List of publications	185

UNIVERSITAT ROVIRA I VIRGILI

HYDROTALCITE-LIKE COMPOUNDS FOR THE VALORISATION OF RENEWABLE FEEDSTOCKS

Mayra García Álvarez

Dipòsit Legal: T. 724-2012

CHAPTER 1

GENERAL INTRODUCTION AND SCOPE

UNIVERSITAT ROVIRA I VIRGILI

HYDROTALCITE-LIKE COMPOUNDS FOR THE VALORISATION OF RENEWABLE FEEDSTOCKS

Mayra García Álvarez

Dipòsit Legal: T. 724-2012

CHAPTER 1

GENERAL INTRODUCTION AND SCOPE

1.1. HETEROGENEOUS BASIC CATALYSIS

More than 90% of the chemical manufacturing processes in the use of throughout the world utilise catalysts in one form or another: much of the food we eat and the medicines we take, the cosmetics, many of the building materials, and almost all the transport fuels are produced by catalysed reactions. Among chemical reactions which are promoted by catalysts are the acid-catalysed and base-catalysed reactions which are initiated by acid-base interaction between reactants and catalysts. In homogeneous catalysis, a huge number of acid-catalysed and base-catalysed reactions are known; however, in heterogeneous systems, acid-catalysed reactions have been attracted more attention, with more than 100 industrial processes operating in the world,¹ with respect to base-catalysed reactions which have been studied in lesser extent. The cracking and several refining processes are the largest processes in chemical industries and involve acid catalysed reactions. The first studies about heterogeneous acid catalysis in petroleum refinery come from 1950s and from that moment, the generation of acidic sites on the solids was deeply investigated.

In contrast to this extensive knowledge about heterogeneous acidic catalysts, much less studies have been done in the field of heterogeneous basic catalysis with only a few industrial processes. Nevertheless, most of the reactions of great interest for the chemical and pharmaceutical industry are carried out in basic medium. Until recently, most of these reactions have been catalysed by traditional homogeneous catalysts such as sodium, potassium hydroxide or carbonate.^{2,3,4} This kind of catalysts involves several disadvantages like loss of catalyst due to the separation difficulties at the end of the reaction, corrosion problems in the equipment used, as well as generation of residual effluents which must be subsequently treated to minimise the environmental impact. Replacement of homogeneous basic catalysts by solid base catalysts in chemical processes is one of the aims for the chemical technology of the future in order to simplify the industrial processes and avoid the generation of unacceptable wastes. Since the 1970s a number of reactions have been catalysed

1.1. HETEROGENEOUS BASIC CATALYSIS

by using different materials considered as solid base catalysts when pretreated at high temperature. This sort of basic materials is listed in Table 1.1.1.^{5,6,7} The basic sites are constituted, in most of the cases, by coordinatively unsaturated oxide anions.⁸ In this case, the solid acts as a Lewis base by donation of an electron pair to form anionic intermediates that undergoes catalytic cycles. If the solid acts as a base by abstracting of a proton of the reactant may be called Brønsted base.

Hattori^{5,9} proposed four parameters to recognise a solid base catalyst:

- 1) Characterisation of the surface by various methods such as acid-base indicators (i.e. Hammett indicators), adsorption of acidic molecules (CO₂, nitromethane, CH₃CN...) and several spectroscopic methods (UV, IR, NMR...) indicate that basic sites exist on the surface.
- 2) Catalytic activities can be correlated with the amount and/or strength of basic sites. The active sites are susceptible of poisoning by acidic molecules such as HCl, CO₂ and H₂O.
- 3) Reactions proceeding over the basic materials are similar to the homogeneous base-catalysed reactions (i.e. similar activity and products obtained).
- 4) Mechanistic studies of the reactions and spectroscopic observations of the surface species indicate that anionic species are involved in the reactions.

The highest drawback that presents the catalysis with solid bases is the rapid deactivation due to the adsorption of poisoning agents such as CO₂ or H₂O. Generation of surface basic sites requires high-temperature pretreatments to remove the adsorbed molecules. The nature of the basic sites generated depends on the pretreatment, since the molecules adsorbed on the surface are successively desorbed according to the strength of interaction with the active sites. The finding that proper pretreatment leads to active and efficient solids acting as base catalysts has allowed the progress of heterogeneous basic catalysis in industrial and environmental processes. Thus, during the past decade, catalysis on solid bases has become a rather popular field of research and the number of reaction types screened has expanded considerably (from petroleum industry until the manufacture of molecules in fine chemistry).

Reactions summarised below demonstrate the importance of basic solids as heterogeneous catalysts in industrial and chemical processes:

1) C-C bond formation (condensation reactions, alkylations...)

As an example is the Degussa process for the production of acrolein through the condensation of acetaldehyde and formaldehyde over Na silicate/silica catalysts.¹⁰ Several solid catalytic materials have been developed to achieve the aldol self-condensation of acetone and butanal in the synthesis of the industrially important compounds MIBK and 2-ethylhexanol.^{5,6} These materials consist on supported alkali and/or alkaline-earth oxides. Alkali-

exchanged zeolites¹¹ and anionic exchanged resins¹² also exhibit interesting catalytic behaviour as aldol condensation catalysts.

2) Olefin double-bond isomerisation

Isomerisation of safrole to isosafrole or 1,2-propadiene to propyne are some examples of double bond isomerisation. These reactions require of strong bases (such as Na/NaOH/Al₂O₃) to produce the abstraction of an allylic proton and forming the *cis* and *trans* forms of the allyl anion.

3) Dehydration

Basic catalysts are active for a number of dehydration reactions. Among the more important is the gas-phase process for the synthesis of 2,6-xyleneol in presence of MgO.

4) Polyalkoxylation

Basic solids are applied industrially for polyalkoxylation reactions to produce non-ionic surfactants. Calcined Mg-Al and Ni-Al hydrotalcites have been patented as catalysts for this kind of reactions.¹³

5) Esterification and transesterification reactions

One of the industrial processes using solid base catalysts is the esterification of ethylene oxide with alcohol in the presence of hydrotalcites.¹ IFP¹⁴ developed a continuous fixed-bed process for the transesterification of triglycerides using zinc aluminates as catalysts in order to obtain biodiesel. Several other solids, such as sodated alumina,¹⁵ and alkali earth oxides and hydroxides^{16,17} have been found to be active for the biodiesel production.

The interest in the development of new processes based on heterogeneous bases is growing in order to develop more sustainable processes in the industrial chemistry, but this is still at an early stage.

Despite to the number of processes described above, the characterisation and evaluation of the basicity of solid surfaces is not an easy matter, but numerous efforts are being done nowadays in order to better understand their surface chemistry as a step for the development of new and modified basic materials which act as heterogeneous catalysts and the industrial processes based on them.

1.1. HETEROGENEOUS BASIC CATALYSIS

Table 1.1.1. *Types of heterogeneous basic catalysts*

a) <u>Metal oxides</u>
Alkaline earth oxides
Alkali metal oxides
Rare earth oxides
ThO ₂ , ZrO ₂ , ZnO, TiO ₂
b) <u>Zeolites</u>
Alkali ion-exchanged zeolites
Alkali ion-added zeolites
c) <u>Supported alkali metal ions</u>
Alkali metal ions on alumina
Alkali metal ions on silica
Alkali metal ions on activated carbon
Alkali metal on alkaline earth oxides
Alkali metals and alkaline metal hydroxides on alumina
d) <u>Clay minerals</u>
Hydrotalcites
Chrysolite
Sepiolite
e) <u>Non-oxides</u>
KF supported on alumina
Lanthanide imide and nitride on zeolites
Metal nitrides, sulphides, carbides, phosphides
Activated carbons
Anionic exchange resins
Organic bases grafted on microporous or mesoporous materials

Table adapted from reference 5.

1.2. LAYERED DOUBLE HYDROXIDES

Layered materials (anionic and cationic clays, layered perovskite, pillared clays...) possess a structure consisting of stacked sheets. A large spectrum of structural, textural and compositional modifications is possible for layered materials allowing a wide tuning and control of the catalytic activity¹⁸ (refs. therein). Therefore, this family of materials represent an interesting opportunity in heterogeneous catalysis.

Layered structures can be classified as follows:

- 1) Layered structures having a neutral layer, e.g. brucite ($\text{Mg}(\text{OH})_2$) and other hydroxides, phosphates and chalcogenides.
- 2) Layered structures having negatively charged layers with compensating cations in the interlayer space, e.g. cationic clays such as montmorillonite, hectorite, etc.
- 3) Layered materials having positively charged layers with compensating anions in the interlayer space. The most common of which are the layered double hydroxides (LDH).

The second class is commonly found in nature while LDH, also called hydrotalcites (HT) or anionic clays, are typically synthesised.

1.2.1. Structure

Layered double hydroxides^{19,20,21,22} are a well-know class of layered materials with large use in catalysis^{19,23,24,25,26,27} although often they are used as precursor of catalysts more than as a layered material itself.

Layered double hydroxides have been known for over 150 years since the discovery of the mineral hydrotalcite. Although the stoichiometry of hydrotalcite, $[\text{Mg}_6\text{Al}_2(\text{OH})_{16}]\text{CO}_3 \cdot 4\text{H}_2\text{O}$, was first correctly determined by Manasse in 1915, it was not until pioneering single crystal X-ray diffraction studies on mineral samples that the main structural features of LDHs were understood.

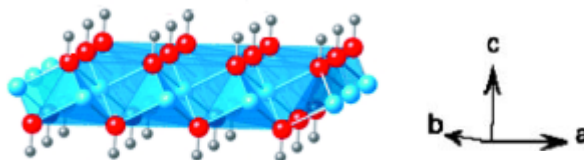


Figure 1.2.1. Projection of a brucite-like layer.

The basic layer structure of LDHs is based on that of brucite, $\text{Mg}(\text{OH})_2$ with edge-sharing hydroxyl octahedra occupied by Mg^{II} cations. These edge-sharing octahedral

1.2. LAYERED DOUBLE HYDROXIDES

units form infinite layers with the OH ions sitting perpendicular to the plane of the layers as shown in Figure 1.2.1.²² In LDHs, a fraction of the divalent cations in the brucite lattice is isomorphically substituted by trivalent cations such that the layers acquire a positive charge, which is balanced by intercalation of anions between the layers. Crystallisation water molecules are also found in the interlayer space. An example of this structure can be seen in Figure 1.2.2.

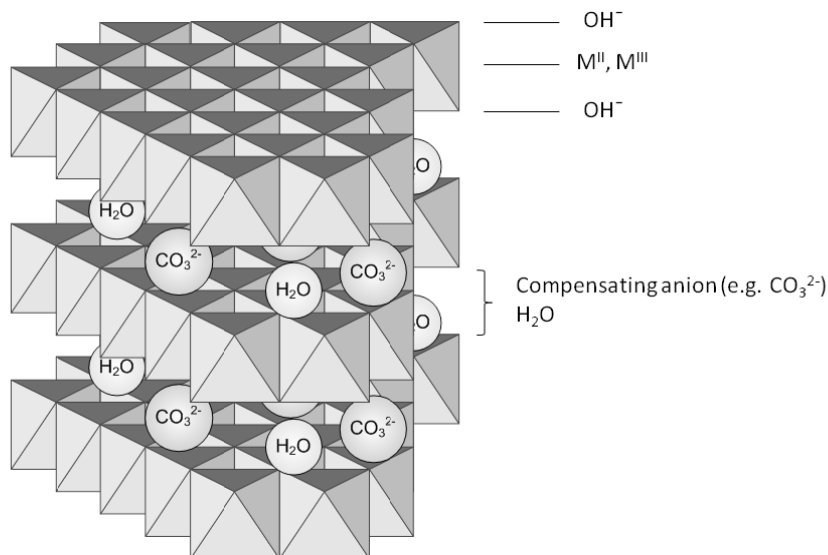


Figure 1.2.2. Idealised structure of a layered double hydroxide (LDH).

The brucite-like sheets of LDHs can stack one on the other with two different symmetries, hexagonal and rhombohedral. At the most basic level, these symmetries could be classified in terms of the number of sheets stacked along the *c* axis of the unit cell. Thus, the hexagonal polytypes have two layers in the unit cell while rhombohedral symmetry presents polytypes having three sheets for unit cell.^{20,28} The identity of the polytype present in a LDH sample may be determined by powder X-ray diffraction. For the sake of simplicity, the indexing of powder patterns for rhombohedral polytypes is based on a triple hexagonal unit cell as show Figure 1.2.3. Despite this cell is not primitive, it is used to better visualise and allow the comparison with hexagonal structures. From the reflections displayed in the PXRD pattern the cell parameters *a* and *c* can be obtained.

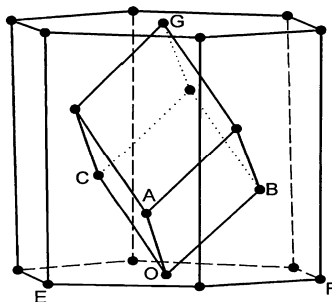


Figure 1.2.3. Relationship between the triple hexagonal cell with axes OE, OF, OG to the primitive rhombohedral cell with axes OA, OB, OC . Taken from reference 22.

A series of strong basal ($00l$) reflections at low angles allow the direct determination of the basal spacing normal to the ($00l$) plane (c_0) which corresponds to the thickness of one brucite-like layer plus the interlayer. For a rhombohedral polytype (3R), the unit cell parameter $c = 3c_0$. Higher order ($00l$) planes generally have spacings corresponding to $c = c_0/2; c_0/3...$ if there is not high degree of disorder in the interlayer.

The position of the (110) reflection at high angles (close to $2\theta = 60^\circ$, for Cu K_α radiation) allows to calculate the value of the lattice parameter $a_0 = 2d_{(110)}$. This value corresponds to the distance between two metal cations and maybe related with the cationic composition in the layer by means of the Vegard's law.

Finally, the positions of the ($01l$) and/or ($10l$) reflections (found at intermediate angles) can be used to determine the stacking pattern of the layers.

Large variety of hydrotalcite-like compounds, having the general formula $[M^{II}_{1-x}M^{III}_x(OH)_2]^{x+}[A^{n-}]_{x/n} \cdot yH_2O$, can be obtained by varying the identity and relative proportions of divalent and trivalent cations (having an ionic radius not so different to that of Mg^{2+}) in the layer as well as the nature of the interlayer anion. Moreover, many ternary LDHs involving mixtures of different M^{II} and/or M^{III} cations can also be prepared and even quaternary LDHs have been reported^{22,29}. The divalent and trivalent cations found in LDHs belong mainly to the third and fourth period of the periodic classification of the elements:

Divalent cations: Mg, Mn, Fe, Co, Ni, Cu, Zn

Trivalent cations: Al, Mn, Fe, Co, Ni, Cr, Ga

1.2. LAYERED DOUBLE HYDROXIDES

		DIVALENT CATIONS							
		Mg	Fe	Co	Ni	Cu	Zn	Ca	Li
TRIVALENT CATIONS	Al								
	Cr								
	Fe								
	Co								
	Ni								
	Ga								
	In								
	V								
	Ti								

Figure 1.2.4. Association of divalent and trivalent cations in LDHs. Adapted from reference 19.

In fact, the range of materials that can be obtained is even larger. Monovalent cation Li^+ is also able to form LDH structures and, recently, the formation of LDHs by incorporation of tetravalent cations has been discussed²². Some of the associations of divalent and trivalent cations in LDHs that have been found in literature are displayed in Figure 1.2.4.

It is claimed^{19,20,22,30} that pure hydrotalcite-like phases can only be formed for stoichiometries in the range $0.2 < x < 0.33$. Higher values of $x = 0.33$ may lead to the formation of $\text{Al}(\text{OH})_3$ (usually not detected by PXRD) due to the increment of neighbouring Al^{3+} octahedra. Similarly, lower values of $x = 0.2$ may lead to a high density of Mg^{2+} octahedra and $\text{Mg}(\text{OH})_2$ is formed. However, there are several publications claiming that LDHs can be formed with x values outside to this range ($0.2 < x < 0.33$). For example, pure lamellar phases are reported for values of $x = 0.15 - 0.34$ in MgAl-LDHs ^{28,31} and even LDHs have been obtained with reported values of x to as low as 0.07 (Mg/Ga-CO_3)³² or as high as 0.5 for $\text{Fe}^{\text{II}}/\text{Fe}^{\text{III}}$ LDHs.³³

There are many difficulties in determining the exact value of x in hydrotalcite-like compounds (i.e. the exact metallic composition forming the brucite-like layers). Chemical analysis gives information about the metal content of all the solid phase. Thus, this could lead to erroneous values of x if the LHD phase is mixed with metal oxides and/or hydroxides, especially when the synthesis mixture contains either very high or very low $\text{M}^{\text{II}}/\text{M}^{\text{III}}$ molar ratios. On occasions, these impurities can be identified by X-ray diffraction, but usually they are amorphous, thus difficulting their detection. In this case, spectroscopic techniques, such as FTIR,³⁴ can be useful to identified small amounts of impurities.

Structural parameters can be an useful tool to locate impurities in the LDH composition. As noted before, the value of the unit cell parameter a is equivalent to the mean distance between adjacent cation centers in the brucite-like layer

assuming an ideal octahedron: $a = \sqrt[2]{2d(M-O)}$. The metal-oxygen bond length $d(M-O)$ is related to the ionic radius by the equation: $d(M-O) = (1-x)r(M^{II}) + xr(M^{III})$, hence $a = \sqrt[2]{2z}$, which gives the direct relationship between the a parameter and the x value. In LDHs, the parameter a decreases with increasing Al^{3+} content (i.e. increasing x value), thus obeying the Vegard's law. When there is no correlation between a and x , this may indicate that other non-LDH phases are also present.³⁵

1.2.2. Interlayer

The interlayer galleries of LDHs contain both anions and water molecules usually randomly distributed. They are forming a network of hydrogen bonds between layer hydroxyl groups, anions and water molecules. Practically, there is not limitation to the nature of anions compensating the positive charge of the layers. Thus, we can prepare LHDs with:

- 1) Inorganic anions
 - a) Halides: F^- , Cl^- , Br^- , I^-
 - b) Oxo-anions: OH^- , NO_3^- , CO_3^{2-} , SO_4^{2-} ...
 - c) Oxo and polyoxometalates: $[CrO_4]^{2-}$, $[V_{10}O_{28}]^{6-}$, $[Mo_7O_{24}]^{6-}$...
 - d) Anionic complexes: $[Fe(CN)_6]^{3-}$, $[PdCl_4]^{2-}$...
- 2) Organic anions: adipic, oxalic, malonic...

The number of anions, size, orientation and strength of the bonds between them and the layer hydroxyl groups determine the thickness of the interlayer. Then, the c_0 parameter, being equivalent to the interlayer thickness plus the thickness of one brucite-like layer²⁰ (4.8 \AA)³⁶ is affected by the nature of the interlayer anion. However, the thickness of the interlayer region is not always proportional to the size of the host anion. That is due to the bonding between the OH^- groups belonging to the layers (which are strongly polarised) and the interlayer molecules, which involves electrostatic effects and hydrogen bonding. Regarding to the water molecules, they may occupy the space between the anions and the layers.

1.2.3. Preparation methods

A number of synthetic techniques have been successfully employed in the preparation of LDHs. Most of the synthetic hydrotalcite-like compounds are prepared by precipitation of the chosen M(II) and M(III) metal salts by means of an alkaline solution. Other methods are based on the anion exchange capacities of LDHs or in the reconstruction of the calcined structure due to the so-called "memory effect". These are the most common techniques of preparation and modification of LDHs reported during last decade, however several other methods has also been reported (sol-gel method, hydrolysis of urea...).

1.2. LAYERED DOUBLE HYDROXIDES

Coprecipitation

The coprecipitation method is the most commonly used to synthesise LDHs. It consists in the simultaneous precipitation of aqueous solutions of soluble metal salts containing the anion that will be incorporated into the structure. The anion can proceed from the metallic salt or from the basic solution used to produce the precipitation of the metals. This method allows the direct preparation of LDHs with a wide variety of interlamellar anions. Therefore is the method usually chosen for the preparation of organic-anion-containing LDHs. Coprecipitation can be carried out at:

1) Low supersaturation

It is performed by slow addition of mixed solutions of divalent and trivalent metal salts in the chosen ratio into a reactor containing an aqueous solution of the desired anion. A second alkaline solution is added into the reactor simultaneously, keeping the pH constant at the selected value. The rate of addition has to be controlled in order to obtain a more homogeneous phase. These conditions usually lead to the formation of precipitates with higher crystallinity since the rate of crystal growth is higher than the rate of nucleation.²²

Many kinds of anion-intercalated LDHs can be prepared³⁷ by using this method if the adequate conditions are given (e.g. avoiding the contamination due to the CO₂), such as CO₃²⁻, halides, and organic compounds including biomolecules or pharmaceutical agents.

2) High supersaturation

This method involves the addition of a solution containing a mixture of the corresponding metallic salts to an alkaline solution containing the desired anion. Generally, LDHs obtained at these conditions present poor crystallinity, due to the high number of nuclei formation.

Urea hydrolysis method

Urea is a weak Brønsted base highly soluble in water which has been used for the precipitation of metal ions as hydroxides. The hydrolysis of urea gives a pH of about 9 depending on the temperature of the mixture which allows its use as precipitant agent in the synthesis of LDHs. The crystallinity degree of LDHs has been observed to depend of the temperature of synthesis and the aging time.³⁸ Larger particles are formed at lower temperatures^{38,39} due to the lower nucleation rate which depends on the decomposition rate of the urea. However, this method is not indicated for the preparation of LDHs with low charge density, but allows the preparation of compounds with high charge density which are difficult to obtain with other procedures.³⁸

Sol-gel method

Some reports^{40,41,42,43} have demonstrated that LDHs can also be obtained by the sol-gel method. The solids obtained by this method often exhibit specific surface areas larger than those obtained by coprecipitation methods,⁴¹⁻⁴³ but with controversial results regarding the basicity and the M^{II}/M^{III} molar ratios.⁴⁰⁻⁴²

The sol-gel method involves the formation of a sol by hydrolysis and partial condensation of a metallic precursor and followed by the gel formation. Metallic alkoxides, acetates or acetylacetonates, as well as many inorganic salts can be used as metallic precursors. The properties of the obtained solid depend on the hydrolysis and condensation rates of the metallic precursor,⁴⁴ which can be modified by controlling different parameters of the reaction such as pH, nature and concentration of the metallic precursor, solvent and temperature of synthesis.

Ion-exchange Method

The host anions in LDHs are able to diffuse through the interlayer space. Consequently, LDHs are one of the main anion exchangers used. This feature has been frequently used to prepare new LDH compounds by means of adding different metals as complex in anionic form. In thermodynamic terms, ion exchange in LDHs depends mainly on the electrostatic interactions between the positively-charged sheets and the interlamellar anions and, to a lesser extent, on the free energy involved in the changes of hydration.⁴⁵ Moreover, the equilibrium constants in the anionic-exchange process depend on the size of the anion. Hence, the anionic exchange is favoured for anions with high charge density (i.e. high charge and small ionic radius).¹⁹ The ionic exchange for simple inorganic anions decreases in the order $\text{CO}_3^{2-} > \text{HPO}_4^{2-} > \text{SO}_4^{2-}$ for divalent anions and $\text{OH}^- > \text{F}^- > \text{Cl}^- > \text{Br}^- > \text{NO}_3^- > \text{I}^-$ for monovalent anions. Experimentally, the ion-exchange method consists on the addition of an excess of the desired anion into a suspension of the LDH and keeping in continuous stirring. Different conditions can affect to the ionic exchange. Among others, the most important parameter to control is the pH, which must be compatible with the exchangeable anion and the LDH.

Rehydration using the structural "memory effect"

Calcination of the LDHs at temperatures from 573 to 1073 K leads to a well dispersed metallic mixed oxide, which cannot be achieved by mechanical means. One of the interesting features of calcined LDHs is the ability to regenerate the layered structure when it is exposed to water and anions. An inert atmosphere is required during the reconstruction process to avoid the contamination of CO_3^{2-} formed from the atmospheric CO_2 . This method is usually employed when large anions intercalated are wanted or in the case of intercalation of anions selectively unfavorable to intercalation by ion-exchange methods (e.g. intercalation of OH^-).

1.2. LAYERED DOUBLE HYDROXIDES

The calcination temperature and composition of the LDH sheets have significant influence on the reconstruction process. The reconstruction is reduced on increasing the temperature of calcination, until no reconstruction is observed when the more stable phase spinel is formed. The temperature at which the spinel phases are obtained strongly depends on the nature of the metals forming the brucite-like layers. After calcination of a Zn/Co/Cu/Al LDH at 850 K, for instance, the “memory effect” is lost;⁴⁶ however, Mg/Al LDHs⁴⁷ can be restored after rehydration of the corresponding mixed oxides obtained up to 1023 K.

The reconstruction method is often used to prepare meixnerite-like compounds, i.e. LDHs containing hydroxyl compensating anions. These kinds of compounds are widely used as catalysts in basic reactions because of its Brønsted basicity.

Miscellaneous methods

In addition to the methods described above, several other methods have been applied in the preparation of LDHs. Among others:

i. Salt-oxide method

It is a simple solid-liquid reaction. Experimentally, it consists in the slow addition of a trivalent metal solution into a suspension of the divalent metal oxide or hydroxide. The mixture is kept during a few days at room temperature in order to favour the reaction between the precursors.

This method was used to prepare LDHs with different combinations of divalent and trivalent cations and anions; in particular [ZnCr-Cl], [ZnCr-NO₃], [ZnAl-Cl] and [ZnAl-NO₃] systems.

ii. Surface synthesis

When a material is supported on the surface of a support, the resulting hybrid or composite material is expected that presents improved properties such as mechanical performance, thermal stability and a high degree of dispersion. The synthesis of LDH on the surface of Al₂O₃ has been reported^{48,49,50} by using aqueous ammonia and urea as precipitant agents or by impregnation of metallic salts following of calcination and hydrothermal treatment.⁵¹ In the same line, de Jong *et al.*^{52,53} have synthesised LDHs supported over carbon nanofibers by subsequent incipient wetness impregnation of the metallic salts and adjusting the pH with a NaOH and Na₂CO₃ solution.

iii. Templated synthesis

Templated-direct synthesis has been attracted attention in the field of material science during the last years. Using self-assembled aggregates as a template, inorganic materials can be directed to an ordered structure with specific morphology

and size. There have been only a few reports of the synthesis of LDHs using this method.²²

A wide number of methods for the synthesis of LDHs can be used. The choice of the method will depend on the application of the final material and the characteristics we want to obtain.

1.2.4. Applications

LDHs present many interesting properties when they are either in calcined form or as the LDH itself. Many applications have been found for hydrotalcites, mainly after calcination. The controlled thermal decomposition of LDH compounds leads to a well disperse mixture of oxides which have high specific surface area compared to those observed in the parent material. The mixed oxides obtained can be used as catalysts or catalytic supports in a great variety of reactions.^{19,20,22} This mixture of oxides presents acid-base properties which can be modulated by changing the calcination temperature, the nature and amount of structural cations and also of the anions which are compensating the positive charge, as well as the preparative method. Generally the approach applied for activation of LDHs involves a thermal treatment, but in some cases the next step of activation consists on the reconstruction of the layered structure by rehydration of the mixed oxides in an appropriate medium. If the medium is decarbonated water, hydroxyl ions from water can enter into the interlayer of the reformed LDH resulting in the generation of Brønsted basic sites.⁵⁴

LDHs represent one of the most technologically promising materials as a consequence of their low cost, easy preparation and the large number of composition variables that can be used. At present, even though a great deal of applications of LDHs in the field of heterogeneous catalysis, covering a wide range of areas, have made substantial progress, especially in the past decade. Due to the properties abovementioned, there are many possible applications of LDHs, not only as catalysts but as well as scavengers of ions in water purification or as component in medicals. Different possible applications of LDHs are schematised in Figure 1.2.5.

1.2. LAYERED DOUBLE HYDROXIDES

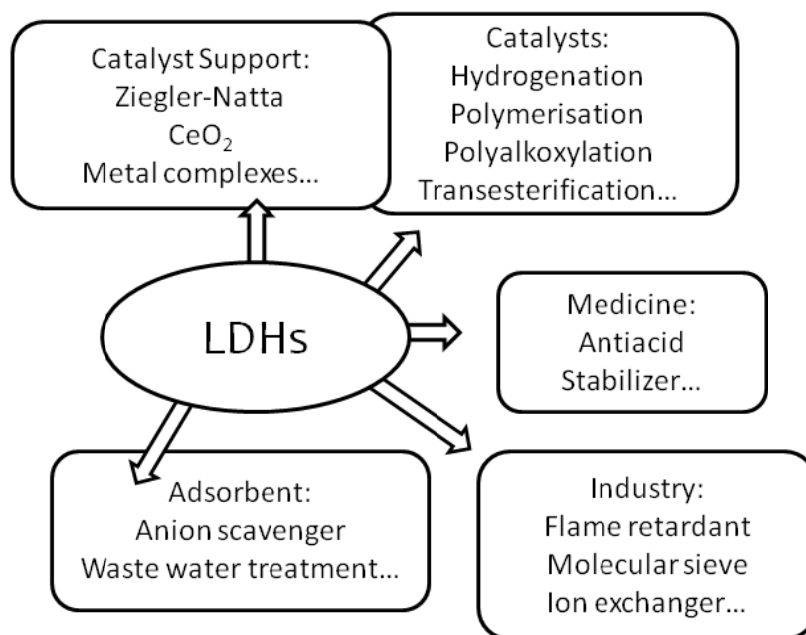


Figure 1.2.5. Possible applications of LDH compounds. Adapted from reference 20.

As basic catalyst, activated LDHs are of current interest in several organic reactions. Many workers have reported the use of rehydrated LDHs in a large number of reactions such as Knoevenagel condensations,⁵⁵ Michael additions,⁵⁶ Claisen-Smith condensations⁵⁷ and epoxidation reactions.⁵⁸ Further, calcined LDHs (with acid and basic sites) are found to be very active and selective in a wide variety of base-catalysed reactions. For example, reactions of condensation of alcohols,⁵⁹ Merwein-Ponndorf-Verley (MPV) reduction,^{60,61} condensations,^{62,63,64} esterification and transesterification reactions, hydrogenation,⁶⁵ oxidative dehydrogenation^{66,67} of propane and n-butane, isomerisations⁶⁸ and polymerisation⁶⁹ have been reported. The nature, strength and relative amount of these sites mainly depend on the nature and molar ratio of the brucite-like layer cations as well as the calcination temperature.

In the last decade, an increasing interest have been growth in using LDH and derived LDH materials for biodiesel production by transesterification of fatty acids with an alcohol.

1.3. BIODIESEL PRODUCTION AND GLYCEROL MARKET

Petroleum is an important feedstock of our society because of the requirements of power, clothing, agriculture and a multitude of synthetic materials and chemicals. Unfortunately, petroleum is a non-renewable resource and due to its rapid depleting, there is an urgent necessity of developing new alternative fuels. Because its primary feedstock are vegetable or animal fats, biodiesel is considered and as a renewable and governments are providing incentives that encourage the rapid growth of biodiesel industry.

With a production growth of 17% in 2009 with respect to 2008, the European Union remains the major producer of biodiesel in the world. In 2009, biodiesel production in the EU reached $10.2 \cdot 10^3$ million of litres (i.e. 55-60% of the world production) and overall, the production of biodiesel worldwide in 2009 was about $18 \cdot 10^3$ million of litres (i.e., +11% with respect to 2008).⁷⁰ It is expected that the production of biodiesel grow up to a 17% in the next years (2012). The production of biodiesel utilises surplus vegetable oils, fats and waste restaurant greases. For every 10 kilograms of biodiesel produced, about 1 kg of a crude glycerol by-product is obtained.⁷¹ This crude glycerol can be purified by several steps such as vacuum distillation or ion exchange refining, but these techniques are not practical for small biodiesel plants. The increased trend of biodiesel production has a considerable influence on the glycerol market and, of course, in its price. While the glycerol price was around 1200 €/ton between 2000 and 2003, from 2004 to 2006 it decreased to 500-700 €/ton⁷² and its price is pushing down as the biodiesel market increases.

1.3.1. Uses of glycerol

Glycerol is a colorless, odourless, viscous, non toxic and hygroscopic liquid with sweet taste. Pure glycerol is a trihydric alcohol soluble in water and alcohols in almost all proportions. Compared with the hydrocarbon feedstocks currently used in classic petrochemistry, is already a highly functionalised molecule.

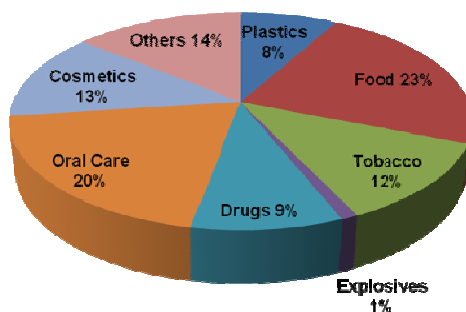
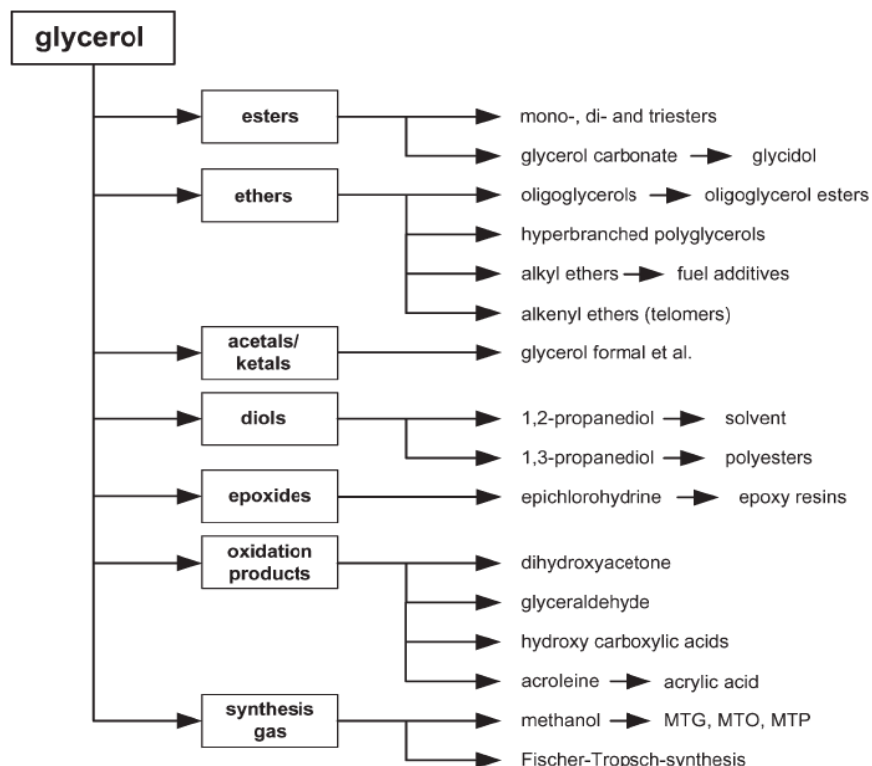


Figure 1.3.1. Distribution of various uses of glycerol.

1.3. BIODIESEL PRODUCTION AND GLYCEROL MARKET

Of course, glycerol is a commodity chemical with multitude of uses. For instance, glycerol is traditionally used in pharmaceuticals, cosmetics (hair and skin care), soaps and teeth pastes because of its properties as humectant, lubricant and solvent. It has similar role as a food additive and it helps to food preservation. It is also directly used as sweetener in candies and cakes and its use as wetting agent on tobacco is widespread.⁷³ A distribution of glycerol uses is showed in Figure 1.3.1.

Glycerol is also used as a raw material for polyols synthesis. These are required for the manufacture of polyeter polyols for flexible foams and as plasticiser in alkyd resins and cellophane. It is needless to emphasise its long standing use as basic chemical for nitroglycerine production.



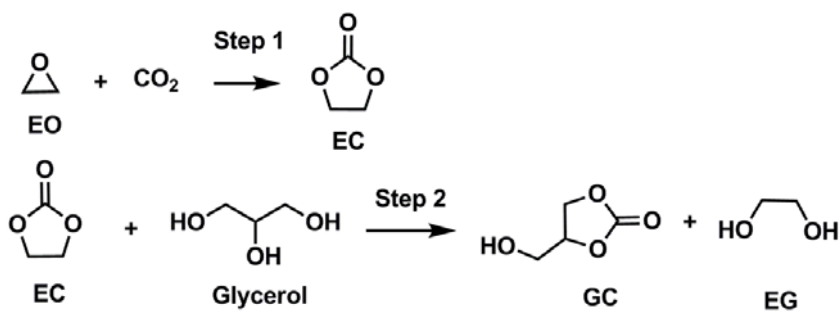
Scheme 1.3.1. *Compilation of the main glycerol modifications. Taken from reference 72.*

Despite the mentioned uses of glycerol, the high surplus of glycerol raises the question of how this additional glycerol can be used widely. Some simple chemical modifications of glycerol are carried out in industry through catalysis, especially in the synthesis of some esters and polyethers. From a technical point of view, the structure of glycerol (with three available hydroxyl groups) allows its chemical modification in several different forms. And due to the similar structure to sugars, conversion to glucose, xylose, etc would increase the profitability of glycerol. Of course, new catalytic conversions require a controlled defunctionalisation. There is an immense activity in the valorisation of glycerol, since a great number of patents and publications have been found in the near last years. More specifically, glycerol oxidation, dehydration, hydrogenolysis, oligomerisation/polymerisation, polyol formation and synthesis of several miscellaneous products can be dealt with. An overview of the main transformations is compiled in Scheme 1.3.1.

1.3.2. Glycerol carbonate

Among the most interesting derivatives of glycerol are the glycerol carbonate (4-hydroxymethyl-1,3-dioxolan-2-one, CAS #931-40-8) and its esters. They are relatively new materials in the chemical industry and, due to their properties (low toxicity, low flammability and low vapour pressure), have great potential as new component in gas-separation membranes, non-volatile solvents for dyes, lacquers, pharmaceuticals,⁷⁴ detergents, adhesives, cosmetics, and biolubricants,⁷⁵ and for the synthesis of new functionalised polymers such as polyglycerol.⁷⁶ Likewise, glycerol carbonate can be used as a substitute for important petro-derived compounds such as ethylene carbonate or propylene carbonate,⁷⁷ used in the synthesis of polymers such as polyesters, polyurethanes, polycarbonates and polyamides, surfactants, lubricating oils⁷² and very valuable intermediates as glycidol.⁷⁸

The present industrial synthesis of glycerol carbonate involves two steps⁷², as illustrated in Scheme 1.3.2.: first ethylene oxide reacts with carbon dioxide to yield the cyclic ethylene carbonate which then reacts further with glycerol to yield glycerol carbonate and ethylene glycol.

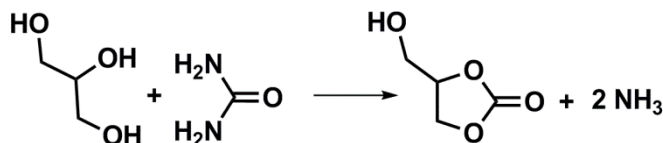


Scheme 1.3.2. Synthesis of glycerol carbonate.

1.3. BIODIESEL PRODUCTION AND GLYCEROL MARKET

Glycerol carbonate can also be synthesised by the catalytic transesterification of glycerol and dimethyl carbonate using either lipase⁷⁹ or homogeneous basic catalysts.^{75,80} Another method involves the use of CO or phosgene in the presence of metallic catalysts.⁸¹ In this case, the reactants are non-desirable due to the high toxicity that present and even the flammability presented by CO.

Glycerol and carbon dioxide are considered two of the main candidates to be used as building blocks for chemical synthesis, because both are widely available at low prices due to their excess production. Obviously, it would be more economic to convert glycerol into glycerol carbonate directly by carboxylation with CO₂. This synthesis is, nowadays, an interesting target of scientific groups. For example, Aresta *et al.*⁸² have investigated the conversion of glycerol by direct carboxylation with CO₂ at 50 bars of pressure and 180 °C and using several metal complexes of tin as catalysts (such as di(*n*-butyl)tin oxide, tin dimethoxide and di(*n*-butyl)tin dimethoxide). Low conversions to glycerol carbonate were achieved, being the best conversion around a 7% due to the lower reactivity of CO₂. Similar tin catalysts were investigated by Ballivet–Tkatchenko⁸³ in the direct synthesis of dimethyl carbonate working in supercritical carbon dioxide. More promising yields have been recently reported by George *et al.* (up to 35%).⁸⁴



Scheme 1.3.3. Synthesis of glycerol carbonate from glycerol and urea.

Catalysts based on zinc, Zn(CH₃C₆H₄-SO₃)₂, were used by Yoo *et al.*⁸⁵ to synthesise glycerol carbonate from glycerol and urea as shown in Scheme 1.3.3. Low pressure, 140 °C and equimolar amounts of glycerol and urea were the reaction conditions to obtain glycerol carbonate. In this case, the conversion achieved was 85% after 1 hour of reaction. In the same line of research, Climent *et al.*⁸⁶ also recently reported that solids with well balanced acid-base pairs such as Zn/Al mixed oxides from hydrotalcite-like compounds are efficient catalysts for the transesterification of glycerol with ethylene carbonate or carbonylation of glycerol with urea to obtain glycerol carbonate. In this case, the formation of GC proceeds in two consecutive steps: first glycerol reacts with urea to form glycerol carbamate and a molecule of NH₃. Then, the oxygen of the secondary hydroxyl group reacts with the carbonylic carbon atom again in an intramolecular reaction to yield the glycerol carbonate and a second molecule of NH₃ is generated. The second step involves the reaction of the free hydroxyl group of the GC, which can react with urea to give the carbamate of glycerol carbonate. So, the reaction conditions may be carefully chosen to avoid a

decrease in selectivity of GC. As shown by Cavino-Casilda *et al.*,⁸⁷ the first step occurs faster than the second step, which is relatively slow.

Other reactions involving homogeneous catalysis have also been described in literature. For example, the reaction among glycerol halo-derivatives with alkaline hydrogen carbonates (KHCO_3 , NaHCO_3 ...).⁸⁸

One of the most interests of GC lies in its use as intermediate in chemical synthesis, as above mentioned. Unlike other cyclic carbonates, the GC presents high reactivity due to its hydroxyl free group and the ring carbon atoms. Therefore, GC can act both as a nucleophile and as an electrophile. For example, Moulongui and Pellet⁸⁹ have reported the synthesis of glycerol carbonate esters by acylation of GC with aliphatic acyl chlorides in the presence of triethyl amine (TEA) as HCl scavenger and dimethyl formamide (DMF) as solvent. The obtained esters have good thermal and oxidation stability and surfactant properties.

A very interesting chemical obtained from GC is the glycidol, which is use as a raw material for obtaining polyglycerols esters, glycidyl esters, pharmaceuticals, cosmetics, detergents and so on. Currently, it is a high value chemical and consequently, more economic routes for its synthesis are being developed. Such a route could be the decarboxylation of GC which is usually carried out by continuously distilling glycidol under low vacuum in presence of catalysts as zeolites.⁷⁸

The importance of glycerol carbonate for industry is demonstrated and the interest for developing different synthetic procedures for GC manufacturing is growing in parallel with its applications.

1.4. GENERAL CONTEXT

The high co-production of glycerol, linked to the biodiesel production (over 100 g/kg of biodiesel) represents a considerable technical and economic burden. On the one hand, glycerol is not fully exploited on the market, which is even more so with the increase in the production and use of bio-diesel; on the other hand, the presence of residual glycerol, as such and as mono-, di- and triglycerides, in bio-diesel is not tolerated, due to problems of de-mixing and fouling. Narrow specification ranges have been then established fixing the free glycerol content in bio-diesel lower than 0.02% by weight, and the total glycerol, i.e. both in free form and partially or totally esterified, lower than 0.25% by weight. Complex separation and purification operations are therefore required to meet these specifications. After refining, it can reach high-purity grade for pharmaceutical and industrial uses. However, the price of glycerol is being pushed down as supplies increase as a result of increased biodiesel production.

The state of the art reveals that the valorisation of glycerol is nowadays an important target of scientific groups. Catalytic processing of glycerol to more valuable chemicals

1.5. OBJECTIVES

is demonstrated by the large number of patents and articles reported until now, as explained along this introduction.

Glycerol carbonate is one of the most interesting chemicals obtained from glycerol. Before the development of this work, there were only few references in the literature concerning the production of glycerol carbonate and even less involving the use of basic solid catalysts. To the best of our knowledge, only one patent⁹⁰ was published regarding the use of basic solids (commercial Mg/Al-hydrotalcite Macrosorb CT 100) as heterogeneous catalysts for the conversion of glycerol. This produced a mixture of oligomers containing only 23% glycerol carbonate.

1.5. OBJECTIVES

Because of the abovementioned literature background, the main objective of this dissertation was the study of the valorisation of glycerol to glycerol carbonate using basic solid catalysts. The transesterification of glycerol towards glycerol carbonate by transesterification with an organic carbonate such as diethyl carbonate and a solid base had not been studied until these days. The basic materials used as catalysts in this work were based mainly in layered double hydroxides since they have revealed to be very active basic catalysts in several reactions.

Therefore, one more specific objective of this thesis is the comparison of the properties among the materials obtained by following different protocols of preparation and activation. These methods involve the preparation of LDHs by conventional methods such as co-precipitation or the preparation of supported materials by surface synthesis. The activation of the catalysts was done by calcination, rehydration in gas-phase, rehydration in liquid phase and applying ultrasonication and anion exchange.

The influence of these parameters on the structural, textural and basic properties has been studied by applying several physico-chemical techniques and the catalytic properties have been studied in the reaction of transesterification of glycerol with diethyl carbonate.

1.6. REFERENCE

1. K. Tanabe, W.F. Holderich, *Appl. Catal. A*, **181** (1999) 399.
2. H. Hattori, *Appl. Catal. A*, **222** (2001) 247–259.
3. W. F. Hölderich, *Catal. Today*, **62** (2000) 115–130.
4. H. Pines, J. A. Veseley, V. N. Ipatieff, *J. Am. Chem. Soc.*, **77** (1955) 6314–6321.
5. H. Hattori, *J. Japan Petroleum Inst.*, **47** (2) (2004) 67-81.
6. G. Busca, *Ind. Eng. Chem. Res.*, **48** (2009) 6486-6511.
7. J. Weitkamp, M. Hunger, U. Ryma, *Micropor. Mesopor. Mater.*, **48** (2001) 255-270.
8. C. Chizalet, G. Costentin, M. Che, F. Delbecq, P. Sautet, *J. Phys. Chem. B*, **110** (2006) 15878-15886.
9. H. Hattori, *Chem. Rev.*, **95** (1995) 537-558.
10. W. Weissermel, H.J. Arpe, *Industrial Organic Chemistry*, 3rd ed., VCH: Berlin, 1997 (and references therein)
11. J. Li, J. Thai, R.J. Davis, *Catal. Today*, **116** (2006) 226-233.
12. G. Gelbard, *Ind. Eng. Chem. Res.*, **44** (2005) 8468-8498.
13. E. Bialowas, J. Szymanowski, *Ind. Eng. Chem. Res.*, **43** (2004) 6267-6280.
14. L. Bournay, D. Casanave, B. Delfort, G. Hillion, J.A. Chodorge, *Catal. Today*, **106** (2005) 190-192.
15. M. Di Serio, M. Cozzolino, M. Giordano, R. Tesser, P. Patrono, E. Santacesarea, *Ind. Eng. Chem. Res.*, **46** (2007) 6379-6384.
16. G. Arzamendi, I. Campo, E. Arguinarena, M. Sanchez, M. Montes, L.M. Gadia, *Chem. Eng. J.*, **134** (2007) 123-130.
17. M. Kouzo, T. Kasuno, M. Tajika, Y. Sugimoto, S. Yamanaka, J. Hidaka, *Fuel*, **87** (2008) 2796-2806.
18. G. Centi, S. Perathoner, *Micropor. Mesopor. Mater.*, **107** (2008) 3-15.
19. V. Rives, Ed., *Layered Double Hydroxides: Present and Future*, Nova Sci. Pub., Inc., New York (2001), and references therein.
20. F. Cavani, F. Trifirò, A. Vaccari, *Catal. Today*, **11** (1991) 173.
21. A.I. Khare, D. O'Hare, *J. Mater. Chem.*, **12** (2002) 3191.
22. D.G. Evans, X. Duan, Ed., *Layered Double Hydroxides*, Springer-Verlag, Berlin (2006).

1.6. REFERENCE

-
23. B.F. Sels, D.E. De Vos, P.A. Jacobs, *Catal. Rev.-Sci. Eng.*, **43** (2001) 443.
 24. A. Albertazzi, F.D. Basile, A. Vaccari, *Int. Sci. Technol.*, **1** (2004) 496.
 25. D. Tichit, B. Coq, *Cattech*, **7** (2003) 206.
 26. F. Figueras, M.L. Kantam, B.M. Choudary, *Curr. Org. Chem.*, **10** (2006) 1627.
 27. K. Kaneda, K. Mori, T. Mizugaki, K. Ebitani, *Curr. Org. Chem*, **10** (2006) 241.
 28. A.S. Booking, V.A. Drits, *Clays Clay Miner.*, **41** (1993) 551.
 29. R.K. Allada, A. Navrotsky, H.T. Berbeco, W.H. Casey, *Science*, **296** (2002) 721.
 30. T. Sate, H. Fujita, T. Endo and M. Shimada, *React. Solids*, **5** (1988) 219.
 31. D.G. Cantrell, L.G. Gillie, A.F. Lee and K. Wilson, *Appl. Catal. A: Gen.*, **287** (2005) 183.
 32. E. López-Salinas, M. García-Sánchez, J.A. Montoya, D.R. Acosta, J.A. Abasolo, I. Schifter, *Langmuir*, **13** (1997) 4748.
 33. L. Legrand, M. Abdelmoula, A. Géhin, A. Chaussé, J.M.R. Génin, *Electrochim. Acta*, **46** (2001) 1815.
 34. H.C. Zeng, Z.P. Xu, M. Qian, *Chem. Mater.*, **9** (1998) 2277.
 35. M. Kaneyosi, W. Jones, *J. Mater. Chem.*, **9** (1999) 905.
 36. S. Carlino, M.J. Hudson, *J. Mater. Chem.*, **5** (1995) 1433.
 37. S. Miyata, *Clays Clay Minerals*, **23** (1975) 369.
 38. U. Constantino, F. Marmottini, M. Nocchetti, R. Vivani, *Eur. J. Inorg. Chem.* (1998) 1439.
 39. M. Ogawa, H. Kaiho, *Langmuir*, **18** (2002) 4240.
 40. T. López, P. Bosch, E. Ramos, R. Gómez, O. Navarro, D. Acosta, F. Figueras, *Langmuir*, **12** (1996) 189.
 41. F. Prinetto, G. Ghiotti, P. Graffin, D. Tichit, *Micropor. Mesopor. Mater.*, **39** (2000) 229.
 42. M.A. Aramendia, V. Borau, C. Jiménez, J.M. Marinas, J.R. Ruíz, F.J. Urbano, *J. Solid State Chem.*, **168** (2002) 156.
 43. M. Jitianu, M. Baloiu, M. Zaharescu, A. Jitianu, A. Ivanov, *J. Sol-Gel Sci. Technol.*, **19** (2000) 453.
 44. J. Livage, M. Henry, C. Sánchez, *Prog. Solid State Chem.*, **18** (1988) 259.
 45. N. Morel-Desrosiers, J. Pisson, Y. Israëlì, C. Taviot-Ghèho, J.P. Besse, J.P. Morel, *J. Mater. Chem.*, **13** (2003) 2582.

-
46. A.J. Marchi, C.R. Apesteguía, *Appl. Clay Sci.*, **13** (1998) 35.
 47. J. Rocha, M. del Arco, V. Rives, M.A. Ulibarri, *J. Mater. Chem.*, **9** (1999) 2499.
 48. E. Merlen, P. Gueroult, J.B. d'Espinose de la Caillerie, B. Rebours, C. Bobin, O. Clause, *Appl. Clay Sci.*, **10** (1995) 45.
 49. J.B. d'Espinose de la Caillerie, M. Kermarec, O. Clause, *J. Am. Chem. Soc.*, **117** (1995) 11471.
 50. F. Zhang, J. Chen, P. Chen, Z. Sun, S. Xu, *AIChE Journal*, **0** (2011) 1.
 51. M.G. Álvarez, M. Pliskova, A.M. Segarra, F. Figueras, F. Medina, *Appl. Catal. B*,
 52. F. Winter, A.J. van Dillen, K.P. de Jong, *Chem. Commun.*, (2005) 3977.
 53. F. Winter, V. Koot, A.J. van Dillen, J.W. Geus, K.P. de Jong, **236** (2005) 91.
 54. V.R.L. Constantino, T.J. Pinnavaia, *Inorg. Chem.*, **34** (1995) 883.
 55. U. Constantino, M. Curini, F. Montanari, M. Nocchetti, O. Rosati, *J. Mol. Catal. A: Chem.*, **195** (2003) 245.
 56. B.M. Choudary, M.L. Khantam, C.R.V. Reddy, K.K. Rao, F. Figueras, *J. Mol. Catal. A: Chem.*, **146** (1999) 279.
 57. M.J. Climent, A. Corma, S. Iborra, A. Vely, *J. Catal.*, **221** (2004) 474.
 58. I. Khirm, F. Medina, X. Rodríguez, Y. Cesteros, P. Salagre, J. Sueiras, *Appl. Catal. A: Gen.*, **272** (2004) 175.
 59. J.L. Di Cosimo, C.R. Apesteguía, M.J.L. Ginés, E. Iglesia, *J. Catal.*, **190** (2000) 261.
 60. P.S. Khumbar, J. Sánchez-Valente, J. López, F. Figueras, *Chem. Comm* (1998) 535.
 61. M.A. Aramendía, V. Borau, C. Jiménez, J.M. Marinas, J.R. Ruíz, F.J. Urbano, *Appl. Catal. A: Gen.*, **249** (2003) 1.
 62. M.J. Climent, A. Corma, R. Guil-López, S. Iborra, J. Primo, *Catal. Lett.*, **59** (1999) 33.
 63. J.L. Di Cosimo, V. K. Díez, C.R. Apesteguía, *Appl. Clay Sci.*, **13** (1998) 433.
 64. C.N. Pérez, C. A. Pérez, C. A. Henriques, J.L.F. Monteiro, *Appl. Catal. A: Gen.*, **272** (2004) 229.
 65. F.M. Cabello, D. Tichit, B. Coq, A. Vaccari, N.T. Dung, *J. Catal.*, **167** (1997) 142.
 66. M.J. Holgado, V. Rives, M.S. San Román, *Appl. Catal. A: Gen.*, **214** (2001) 219.
 67. M.J. Holgado, F.M. Labajos, M.M.J. Sontero, V. Rives, *Mater. Res. Bull.*, **38** (2003) 1879.
 68. C.T. Fishel, R.J. Davis, *Langmuir*, **10** (1994) 159.

1.6. REFERENCE

-
69. D.E. Laycock, R.J. Collacott, D.A. Skelton, M.F. Tchir, *J. Catal.*, **130** (1991) 354.
 70. <http://www.biofuels-platform.ch>
 71. D. Fabbri, V. Benovi, M. Notari and F. Rivetti, *Fuel*, **86** (2007) 690.
 72. A. Behr, J. Eilting, K. Irawadi, J. Leschinski, F. Lindner, *Green Chem.*, **10** (2008) 13.
 73. <http://www.1911encyclopedia.org/Glycerin>
 74. Ger. Pat. 10 110 855 A1 (2001).
 75. D. Herault, A. Eggers, A. Strube and J. Reinhard, DE 101108855A1 (2002).
 76. G. Rokicki, P. Rakoczy, P. Parzuchowski and M. Sobiecki, *Green Chem.*, **7** (2005) 529.
 77. W.C. Shieh, S. Dell, O. Repič, *J. Org. Chem.*, **67** (2002) 2188.
 78. J.W. Yoo, Z. Mouloungui, A. Gaset, WO 9840371 (1998).
 79. S.C. Kim, Y.H. Kim, H. Lee, D.Y. Yoon, B.K. Song, *J. Mol. Catal. B: Enzim.*, **49** (2007) 75.
 80. P.U. Naik, L. Peritjean, K. Refes, L. Picquet Mand Plasseraud, *Adv. Synth. Catal.* **351** (2009) 1753.
 81. J.H. Teles, N. Rieber, W. Harder, US Patent 5359094 (1994).
 82. M. Aresta, A. Dibenedetto, F. Nocito and C. Pastore, *J. Mol Catal. A: Chem.*, **257** (2006) 149.
 83. D. Ballivet-Tkatchenko, S. Chambrey, R. Keiski, R. Ligabue, L. Plasseraud, P. Richard, H. Turunen, *Catal. Today*, **115** (2006) 80.
 84. J. George, Y. Patel, S. Muthukumar, P. Munshi, *J. Mol. Catal. A*, **304** (2009) 1.
 85. J.W. Yoo and Z. Mouloungui, *Stud. Surf. Sci. Catal.*, **146** (2003) 757.
 86. M.J. Climent, A. Corma, P. De Frutos, S. Iborra, M. Noy, A. Velty, P. Concepción, *J. Catal.*, **269** (2010) 140.
 87. V. Cavino-Casilda, G. Mul, J.F. Fernández, F. Rubio-Marcos, M.A. Bañares, *Appl. Catal. A*, **409-410** (2011) 106.
 88. O. Gómez-Jiménez-Aberasturi, J.R. Ochoa-Gómez, A. Pesquera-Rodríguez, C. Ramírez-López, A. Alonso-Vicario, J. Torrecilla-Soria, *J. Chem. Technol. Biotechnol.* **85** (2010) 1663.
 89. Z. Mouloungui, S. Pelet, *Eur. J. Lipid Sci. Technol.*, **103** (2001) 216.
 90. J.J.W. Eshuis, J.A.M. Laan and G. Roberts, WO 9516723 (1995).

CHAPTER 2

HYDROTALCITE-LIKE COMPOUNDS FOR VALORISATION OF GLYCEROL

Article:

Enhanced use of renewable resources: Transesterification of glycerol catalysed by hydrotalcite-like compounds.

Mayra G. Álvarez, Anna M. Segarra, Sandra Contreras, Jesús E. Sueiras, Francisco Medina and François Figueras
(*Published in Chemical Engineering Journal*, 161 (2010) 340-345)

Article:

Tunable basic and textural properties of hydrotalcite derived materials for transesterification of glycerol.

Mayra G. Álvarez, Ricardo J. Chimentao, Francesc Medina and François Figueras
(*Published in Applied Clay Science*, 58 (2012) 16-24)

UNIVERSITAT ROVIRA I VIRGILI

HYDROTALCITE-LIKE COMPOUNDS FOR THE VALORISATION OF RENEWABLE FEEDSTOCKS

Mayra García Álvarez

Dipòsit Legal: T. 724-2012

CHAPTER 2

HYDROTALCITE-LIKE COMPOUNDS FOR VALORISATION OF GLYCEROL

2.1. INTRODUCTION

Hydrotalcite-like compounds or layered double hydroxides constitute a class of materials with a wide range of applications in the field of catalysis. They have been the subject of several reviews, books and research articles.

Among others, two important characteristics of hydrotalcites should be remembered briefly. First, HTs have a considerable anion-exchange capacity which is especially interesting when immobilizing homogeneous catalysts or when large anions want to be intercalated into the structure. The second characteristic is that hydrotalcites behave as a solid base. The basic character of hydrotalcites is dependent. Whereas the basicity of a hydrated hydrotalcite comes mainly of structural and interlamellar hydroxyls, strong Lewis metal-oxygen coordinated basic pairs ($M-O^{2-}$) are mainly present in the calcined ones. The base-tuning capability of these materials makes them as excellent catalysts in a broad spectrum of reactions. In fact, this tuning capability allows preparing specific catalysts for each reaction.

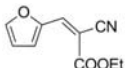
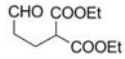
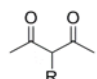
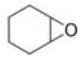
HTs can be used in the as-synthesised form or after different pretreatments. The HTs as such in a solid base or, depending on the elemental composition, may have redox properties. Despite the multiple applications of hydrotalcite-like compounds in the field of catalysis (oxidation, reduction dehydrogenation reactions, halide substitution reactions, polymerisation, acid-catalysed reactions and so on) we have focused this work in the application of HTs as acid-base catalysts.

A multitude of base-catalysed reactions have been studied involving hydrotalcite-like compounds. For example, aldol condensation of aldehydes and ketones has been extensively described over the years. Likewise, Knoevenagel reactions, Michael

2.1. INTRODUCTION

additions, epoxidations, alkylations, acylations, polymerisations, decarboxylations and esterification and transesterification reactions have been widely reported. Table 2.1.1 illustrates some of these reactions.

Table 2.1.1. Base-catalysed reactions involving hydrotalcite-like compounds

Entry	Reagents	Catalyst	Product	Yield (%)	Ref.
<i>Condensation and Claisen-Schmidt</i>					
1	Acetone	MgAl-HT (c)	Diacetone alcohol	23	1
2	n-butylaldehyde	MgAl-HT (c)	2-ethyl-2-hexenal	75	1
3	Benzaldehyde + acetophenone	MgAl-OH (r)	Chalcone	87	3
<i>Knoevenagel reaction</i>					
4	Malononitrile + 2-furfural	MgAl-HT (c) or MgAl-OH (r)		100	4
5	Acrolein + diethyl malonate	MgAl-HT (c)		92	5
<i>Alkylation</i>					
6	2,4-pentanedione + ethyl iodide	MgAl-HT (c)		87	6
<i>Epoxidation</i>					
7	Ciclohexene + H ₂ O ₂ + alkylcyanide	MgAl-HT(c) or MgAl-CO ₃ ²⁻		98	7
8	Limonene	MgAl-HT(c) or MgGa-HT(c)	Limonene oxide	99	8
<i>Transesterification</i>					
9	Ethyl carbonate + Methanol	MgAl-CO ₃ ²⁻	Dimethyl carbonate Ethylene glycol	50	9
10	Triglycerides + glycerol	MgAl-HT (c) or LiAl-HT (c) MgAl-OH (r)	Mono and diglycerides	64 69 80	10

(c) Calcined hydrotalcite

(r) Rehydrated hydrotalcite

Particularly, the transesterification reactions have extensively studied with HTs and offer a convenient route for the preparation of esters. An example is the synthesis of dimethyl carbonate from ethylene carbonate and methanol with MgAl-HTs.⁹

Another example of industrial interest deals with the production of esters of oils and fats. Mono- and di-glycerides are compounds used as emulsifiers in food, pharmaceutical and cosmetic industries. Monoglycerides can be obtained either via direct esterification of glycerol with fatty acids or via transesterification of glycerol with triglycerides or fatty acids. As an example, Mg/Al hydrotalcites activated by calcination and subsequent rehydration have shown to exhibit higher catalytic activity than the decomposed ones for the transesterification of oleic acid methyl ester with glycerol¹⁰ indicating that the kind of basicity (Brønsted or Lewis) is an important factor governing the reaction.

But is the production of biodiesel in where this reaction has attracted more attraction during the past years and several examples of transesterification of vegetal oils with an alcohol can be found in literature. (Table 2.1.2)

As examples, calcined Li/Al, Mg/Al and Mg/Fe layered double hydroxides were found being active in transesterification of glyceryl tributyrates with methanol and in the transesterification reaction of soybean oil with methanol.¹¹ Maximum activity was observed for the Li/Al catalysts when a calcination temperature of 450–500 °C was applied, corresponding to decomposition of the layered double hydroxide to the mixed oxide without formation of crystalline lithium aluminate phases. The Mg/Fe and Mg/Al catalysts exhibited much lower methyl ester yields. Calcined iron or gallium doped Mg/Al-HTs were tested in the transesterification of soybean oil with MeOH¹² showing being effective catalysts. In another work,¹³ transesterification of rapeseed oil with methanol using Mg/Al hydrotalcites with a molar ratio of 3 and calcined at 500 °C converted the methanol ester to about 90% yield. These are only few examples of biodiesel synthesis manifesting a great deal of interest in the field of biocombustibles.¹⁴

The growing production of biodiesel has generated an economic impact due to the excess of glycerol produced. Nowadays, new applications for glycerol are being found including the energy and petrochemical fields. In fact, industry has started to research to find new applications of glycerol as a low cost feedstock for precursor of value-added chemicals. The main transformations of glycerol into more valuable products were already described in Chapter 1.

As a few examples are the oxidation of the secondary hydroxyl group to form 1,3-dihydroxyacetone (ingredient in cosmetics), the etherification of glycerol to form fuel additives, hydrogenolysis to obtain propylene glycol, dehydration for the formation of acrolein (intermediate in the synthesis of polymers) and so on.

With a focus in the valorisation of glycerol, in this chapter is described the conversion of glycerol into glycerol carbonate as more valuable product by means of

2.1. INTRODUCTION

transesterification with diethyl carbonate and using hydrotalcite-like compounds as catalysts.

Table 2.1.2. *Transesterification reactions (biodiesel production) involving hydrotalcite-like compounds*

Triglyceride	Catalyst	Ratio MeOH/oil	Reaction time (h)	Temperature (°C)	Conversion (%)	Ref.
Glyceryl tributyrate	MgAl-HT (c)	3	3	60	75	15
Rapeseed oil	MgAl-HT (c)	6	4	65	90	13
Palm oil	MgAl-HT (c)	30	6	100	87	16
Soybean oil	LiAl-HT (c)	15	2	65	83	11
Cottonseed oil	MgAl-HT (c)	6	12	180-210	87	17
Rice oil	MgAlLa-HT (r)	30	9	100	78	18
Soybean oil	MgAlFe-HT (c)	6	1	80	38	19
Poultry fats	MgAl-HT	60	6	120	98	20

(c) Calcined hydrotalcite

(r) Rehydrated hydrotalcite

References

1. R. Tessier, D. Tichit, F. Figueras and J. Kervenat, FR2729137, 1995.
2. B.J. Arena, J.S. Holmgren, US Patent, 5,144,089, 1992.
3. M.J. Climent, A. Corma, S. Iborra, A. Velty, *Journal of Catalysis* 221 (2004) 474.
4. M.L. Kantam, B.M. Choudary, C.V. Reddy, K.K. Rao, F. Figueras, *Chem. Commun.* (1998) 1033.
5. Y.V.S. Rao, D.E. De Vos, P.A. Jacobs, *Proc. R. Soc. Chem.* (1997) 110.
6. C. Cativiela, F. Figueras, J.I. García, J.A. Mayoral, M.M. Zurbano, *Synth. Commun.*, 25 (1995) 1745.
7. S. Ueno, K. Yamaguchi, K. Yoshida, K. Ebitani, K.J. Kaneda, *Chem. Soc., Chem. Commun.* (1998) 295.
8. M.A. Aramendia, V. Borau, C. Jiménez, J.M. Luque, J.M. Marinas, F.J. Romero, J.R. Ruiz, F.J. Urbano, *Studies Surface Sci. Catal.*, 130 (2000) 1668.
9. Y. Watanabe, T. Tatsumi, *Micropor. Mesopor. Mater.*, 22 (1998) 399.
10. A. Corma, S. Abd Hamid, S. Iborra, A. Velty, *J. Catal.*, 234 (2005) 340.
11. J.L. Shumaker, C. Crofcheck, S.A. Tackett, E. Santillan-Jimenez, T. Morgan, Y. Ji, M. Crocker, T.J. Toops, *Appl. Catal. B: Environmental*, 82 (2008) 120.
12. G.S. Macala, A.W. Robertson, C.L. Johnson, Z.B. Day, R. S. Lewis, M.G. White, A.V. Iretskii, P.C. Ford, *Catal. Lett.*, 122 (2008) 205.
13. H.Y. Zeng, Z. Feng, X. Deng, Y.Q. Li, *Fuel*, 87 (2008) 3071.
14. M. Pagliaro, R. Ciriminna, H. Kimura, M. Rossi, C. Della Pina, *Angew. Chem. Int. Ed.*, 46, (2007) 4434.
15. D.G. Cantrell, L.G. Gillie, A.F. Lee and K. Wilson, *Appl. Catal. A: Gen.*, **287** (2005) 183.
16. W.L. Xie, H. Peng, L.G. Chen, *J. Mol. Catal. A: Chem.*, 246 (2006) 24.
17. N. Barakos, S. Pasias, N. Papayannakos, *Bioresource Technology*, 99 (2008) 5037.
18. P. Chuayplod, W. Trakarnpruk, *Ind. Eng. Chem. Res.*, 48 (2009) 4177.
19. G.S. Macala, A.W. Robertson, C.L. Johnson, Z.B. Day, R.S. Lewis, M.G. White, A.V. Iretskii, P.C. Ford, *Catal. Lett.*, 122 (2008) 205.
20. Y. Liu, E. Lotero, J.G. Goodwin Jr., X. Mo, *Appl. Catal. A: General*, 331 (2007) 138.

UNIVERSITAT ROVIRA I VIRGILI

HYDROTALCITE-LIKE COMPOUNDS FOR THE VALORISATION OF RENEWABLE FEEDSTOCKS

Mayra García Álvarez

Dipòsit Legal: T. 724-2012

2.2. ENHANCED USE OF RENEWABLE RESOURCES: TRANSESTERIFICATION OF GLYCEROL BY HYDROTALCITE- LIKE COMPOUNDS

2.2.1. Introduction

Environmental and political concerns are generating growing interest in renewable alternative fuels such as bio-diesel produced from vegetable oils by transesterification. The high co-production of glycerol, however, linked to this production (over 100 g/kg of biodiesel) represents a considerable technical and economic burden. On the one hand, glycerol is not fully exploited on the market, which is even more so with the increase in the production and use of bio-diesel; on the other hand, the presence of residual glycerol, as such and as mono-, di- and triglycerides, in bio-diesel is not tolerated, due to problems of de-mixing and fouling. Narrow specification ranges have been then established fixing the free glycerol content in bio-diesel lower than 0.02% by weight, and the total glycerol, i.e. both in free form and partially or totally esterified, lower than 0.25% by weight. Complex separation and purification operations are therefore required to meet these specifications. After refining, it can reach high-purity grade for pharmaceutical and industrial uses. However, the price of glycerol is being pushed down as supplies increase as a result of increased bio-diesel production.¹ Therefore, it is especially important to explore new applications for this product as well as alternative strategies for transforming it into new suitable products. Glycerol carbonate (4-hydroxymethyl-1,3-dioxolan-2-one) and its esters are very interesting derivatives of glycerol. They are relatively new materials in the chemical industry and have great potential as a new component in gas-separation membranes, in non-volatile solvents for dyes, lacquers, pharmaceuticals, detergents, adhesives, cosmetics, and biolubricants,² and for the synthesis of new functionalised polymers such as polyglycerol.³ Fuels represent large scale applications, and Notari and Rivetti *et al.*⁴ recently reported that a mixture containing alkyl esters or fatty acids (bio-diesel) and one or more esters of fatty acids of glycerol carbonate (constituting between 10 and 40 percent of the weight) can be used as fuel.

The present industrial synthesis of glycerol carbonate involves two steps:⁵ first ethylene oxide reacts with carbon dioxide to yield the cyclic ethylene carbonate which then reacts further with glycerol to yield glycerol carbonate and ethylene glycol.

The improvement of the economic and environmental feasibility of the industrial synthesis of glycerol carbonate (i.e. reducing the number of steps and waste) entails the obtaining of an optimised direct method for its production. Few references have been found in the literature concerning the production of glycerol carbonate using simplified methodologies. Vieville *et al.*⁶ obtained glycerol carbonate (up to 32% after 1 hour) by direct carbonation of glycerol in supercritical carbon dioxide in the

2.2. ENHANCED USE OF RENEWABLE RESOURCES

presence of zeolites and ion exchange resins, using ethylene carbonate as co-reactant. Aresta *et al.* have recently reported the direct carboxylation of glycerol with carbon dioxide using tin complexes ($n\text{-Bu}_2\text{Sn}(\text{OCH}_3)_2$, $n\text{-Bu}_2\text{SnO}$ and $\text{Sn}(\text{OMe})_2$) as catalysts.⁷ However, the best glycerol conversion achieved after 15 hours of reaction was below 7%. Catalysts based on zinc, $\text{Zn}(\text{CH}_3\text{C}_6\text{H}_4\text{-SO}_3)_2$, were used by Yoo *et al.*⁸ to synthesise glycerol carbonate from glycerol and urea. In this case, the conversion achieved was 85% after 1 hour of reaction.

The non-toxicity, biodegradability and cleaner production process of alkyl carbonates such as dimethyl or diethyl carbonate (DMC or DEC, respectively) make them green reagents that prevent pollution at the source during synthesis.⁹ Moreover, since DEC includes ethoxy and carbonyl groups, it can be used as an effective carbonylating and ethylating agent as well as a raw material for manufacturing polycarbonates.¹⁰ Glycerol carbonate can be obtained via a transesterification reaction of DMC with glycerol using homogeneous catalysts such as $n\text{-Bu}_2\text{Sn}(\text{OCH}_3)_2$, resulting in a 65% conversion after 15 hours.⁷ The usual synthesis uses large quantities of a Brønsted base as a catalyst, K_2CO_3 ; to produce either glycerol carbonate, glycerol dicarbonate or diglycerol tricarbonate depending on the reaction temperature and/or the amount of DMC added³. Mouloungui *et al.*¹¹ reported the synthesis of glycerol carbonate by reaction of glycerol on a cyclic organic carbonate in the presence of a solid catalyst consisting of an anionic, bi-carbonated or hydroxylated, macroporous resin, or alkaline X- or Y-type zeolite. This reaction produces glycol as by product with a selectivity of about 15-30%. To the best of our knowledge, only one patent has been published regarding the use of basic solids (commercial Mg/Al-hydrotalcite Macrosorb CT 100) as heterogeneous catalysts for the conversion of glycerol. This produced a mixture of oligomers containing only 23% glycerol carbonate.¹²

Hydrotalcite-like compounds have the general formula $[\text{M}^{\text{II}}_{1-x}\text{M}^{\text{III}}_x(\text{OH})_2]^{x+} \text{A}^{n-x/n} \cdot n\text{H}_2\text{O}$, where M^{II} and M^{III} stand for a divalent and a trivalent cation, respectively, and A is a charge-balancing anion. The structure consists of brucite-like layers $[\text{Mg}(\text{OH})_2]$ with edge-sharing hydroxyl octahedra occupied by Mg^{II} cations. In hydrotalcites, some divalent cations are isomorphically substituted by trivalent ones which introduce a positive charge that is balanced by anions located in the interlayer. Additionally, crystallisation water molecules are also found in the interlayer.¹³ They are usually prepared by co-precipitation from metal salts in alkaline media at constant pH followed by a hydrothermal treatment of the precipitate. The usual protocol of activation for these materials is controlled thermal decomposition which leads to the formation of mixed oxides showing a good dispersion of metals, a large specific surface area and Lewis basic properties. The rehydration of calcined hydrotalcites under a CO_2 free atmosphere allows the layered structure to be recovered containing interlayer OH^- anions, which provides significant Brønsted basic properties.¹⁴⁻¹⁵ The basic properties of the solid can be tuned by the procedure of rehydration: Roelofs *et al.*¹⁶ reported a higher activity after hydration, followed by washing with ethanol. The higher activity in base catalysed reactions has been reported when they are activated by thermal decomposition followed by rehydration processes using ultrasound.^{17,18}

Cantrell *et al.* showed that the Brønsted basic sites of rehydrated Mg-Al hydrotalcites are effective catalysts for the transesterification of tributyrin with methanol, with an increase of the rate with the Mg content in the Mg-Al hydrotalcites.¹⁹

We report here the results of an exploratory study focussed on the synthesis of glycerol carbonate by the transesterification reaction of glycerol with DEC. Due to the report of Cantrell,¹⁷ a Mg-Al hydrotalcites with Mg/Al molar ratio of 4 was selected as catalyst, since it is known that phase separation occurs above this ratio.

2.2.2. Experimental

i. Catalyst preparation

Parent Mg/Al hydrotalcite-like precursor with a molar ratio of 4 was obtained according to the standard co-precipitation method as follows. The appropriate amounts of $\text{Mg}(\text{NO}_3)_2 \cdot 6\text{H}_2\text{O}$ and $\text{Al}(\text{NO}_3)_3 \cdot 9\text{H}_2\text{O}$ were dissolved in 150 cm^3 of distilled water and added dropwise into a glass vessel which initially contained 200 cm^3 of deionised water. The pH was controlled by adding a 2M NaOH solution and was kept at 10. Both solutions were mixed under vigorous stirring. The suspension was stirred overnight at room temperature. The precipitated solid was filtered and washed several times with water and dried at $110 \text{ }^\circ\text{C}$ to yield the as-synthesised hydrotalcite (HT-as). The solid was calcined in air by heating at $10 \text{ }^\circ\text{C}/\text{min}$ up to $450 \text{ }^\circ\text{C}$ over 3 hours to obtain the corresponding mixed oxides. This solid was named HT04, where 4 refers to Mg/Al molar ratio). A part of the mixed oxide was reconstructed back in decarbonated water by sonication for one hour under an inert atmosphere to maximise the accessibility of the OH groups.^{17,18} This sample was called HTr4.

ii. Catalysts characterisation

Mg and Al elemental chemical analyses were obtained by atomic absorption spectroscopy (AAS) using a Perkin-Elmer 703 instrument, before the samples were dissolved in HNO_3 . Specific surface areas were determined by nitrogen adsorption at $-196 \text{ }^\circ\text{C}$ using a Micromeritics ASAP 2000 equipment. Samples were previously degassed in situ at $120 \text{ }^\circ\text{C}$ under vacuum. Surface areas were calculated using the Brunauer-Emmet-Teller (BET) methods over a P/P_0 range where a linear relationship was maintained. X-ray diffraction (XRD) powder patterns were collected on a Siemens EM-10110BU diffractometer model D5000 fitted with a $\text{Cu K}\alpha$ (1.541 \AA) radiation source. Data were recorded over a 2θ range of $5\text{-}70^\circ$ with an angular step of 0.05° at 3 s/step which resulted in a scan rate of $1^\circ/\text{min}$. Patterns were identified using files from the Joint Committee on Powder Diffraction Standards (JCPDS).

The basicity measurements were obtained by temperature programmed desorption (TPD) of CO_2 on a Thermo Finnigan TPDRO 1100 equipped with a TCD detector. Typically, ca. 0.150 g of sample were placed in a tubular quartz reactor. The sample was pretreated with Ar at $80 \text{ }^\circ\text{C}$ during 1 h and then cooled to room temperature and treated with a CO_2 flow (3% CO_2 in He). The desorption of CO_2 was measured by

2.2. ENHANCED USE OF RENEWABLE RESOURCES

heating the sample from room temperature to 800 °C at a heating rate of 10°C/min in He flow. Water was trapped on magnesium perchlorate. The number of basic sites was calculated from the CO₂ peaks by deconvolution using the software of the equipment, and a calibration of the instrument using a known amount of CaCO₃.

Thermogravimetric analysis (TGA) curves were recorded in a Labsys/Setaran TG thermo balance apparatus from room temperature to 900 °C, at a heating rate of 10 °C/min.

iii. *Standard batch catalytic transesterification reaction*

Glycerol (99%) and DEC (99.5%, GC grade) were purchased from Aldrich and used without any further purification. Ethanol HPLC grade from Aldrich was used as a solvent to characterise the products obtained. Transesterification reactions were performed in a three-neck round bottomed flask equipped with a condenser. Typically, the flasks were charged with an excess of DEC (38.95 g) and glycerol (1.85 g). Freshly activated catalyst (0.3 g) was added and the experiment started with mechanical stirring under argon at 130 °C. Stirring was continued until the completion of the reaction. Aliquots were periodically withdrawn, filtered and quantified by GC-MS analysis. This was performed on a Shimadzu GC-MS (QP 2010) with a Zebron ZW-WAX capillary column.

iv. *Recycling experiments*

We investigated the reuse of the catalyst HTr4 in the transesterification reaction of glycerol with DEC under the same reaction conditions that were used for the standard transesterification reaction. The reaction mixture was removed with a syringe equipped with a microfilter when the reaction had finished, leaving the catalyst in the smallest possible amount of liquid. The reaction mixture was then washed twice with DEC. After that, a new charge of reactants was added to the used catalyst and the next run was performed.

2.2.3. Results and discussion

i. *Characterisation and basic properties of the solids*

Table 2.2.1 gives the results of the chemical analysis of the metals in the samples. The Mg/Al atomic ratio for the as-synthesised hydrotalcite was slightly higher than the atomic ratio fixed in the solution. Generally, the optimal value of x for a pure LDH phase ranges from 0.2 to 0.33.²⁰ However, pure lamellar phases are reported for values of $x = 0.15 - 0.34$ in MgAl-LDHs.^{19,21} X-ray diffraction patterns (not shown) exhibited single phases consistent with a hydrotalcite structure.

Table 2.2.1. Characterisation of catalysts. Chemical composition, PXRD analysis and BET surface areas

Catalyst	Elemental analysis ^a		PXRD analysis			Surface area ^c (m ² g ⁻¹)
	M(II)/M(III)	x	d ₍₀₀₃₎ (Å)	d ₍₁₁₀₎ (Å)	a (Å)	
HT-as	4.29 (4) ^b	0.19	8.01	1.53	3.07	17
HTO4	4.29	---	---	---	4.19	199
HTr4	4.08	0.19	7.67	1.53	3.06	57

^a Atomic Absorption Spectroscopy

^b nominal value

^c using BET method

The XRD pattern of the HT-as sample exhibited symmetric reflections corresponding to the (003), (006) and (009) planes and recorded at 8.01, 4.03 and 2.63 Å, respectively. The indexing was based on rhombohedral symmetry (polytype 3R).²⁰ The value of the lattice parameter *a*, 3.07 Å, was calculated as twice the spacing of plane (110) whose maximum was recorded close to 2θ = 60° and is characteristic of hydrotalcite-like compounds, (JCPDS 22-700). The value of parameter *a* is in the range of that observed for pure hydrotalcite phases with low Al content.^{18,22} After calcination at 450 °C, the layered structure was destroyed and the calcined sample presented the typical features of Mg(Al)Ox mixed oxide (HTO), whose reflections appeared at 2θ = 43° and 63°, thus corresponding to a periclase-like structure (JCPDS 87-0653). Its structural parameters are lower than those in the pure MgO rock salt-type structure, showing that Al³⁺ cations are inserted into the structure.^{23,24} The original layered structure was recovered from the calcined material after rehydration in the absence of CO₂. The sample presented a meixnerite structure (JCPDS 35-0965) because of the well-known “memory effect”²⁵ where the original nitrate anions have been replaced by Brønsted OH sites. The most striking feature of the rehydrated sample was the increased intensity of the basal peaks in the rehydrated samples compared with the original hydrotalcite. This indicates an increase in crystallinity, despite the ultrasound treatment for rehydration, which agrees with data obtained from N₂ adsorption. Rehydration in water could provoke a dissolution of the smaller particles and increase of the larger ones (Ostwald ripening) which could account for this increase of crystallinity. The BET specific surface area for the as-synthesised hydrotalcite was in accordance with those reported in the literature.¹⁵ It can be noticed that the surface area increased from about 17 m²g⁻¹ for the as-synthesised sample to 200 m²g⁻¹ for the calcined sample, and decreased to 57 m²g⁻¹ after rehydration, in spite of the use of ultrasounds.

2.2. ENHANCED USE OF RENEWABLE RESOURCES

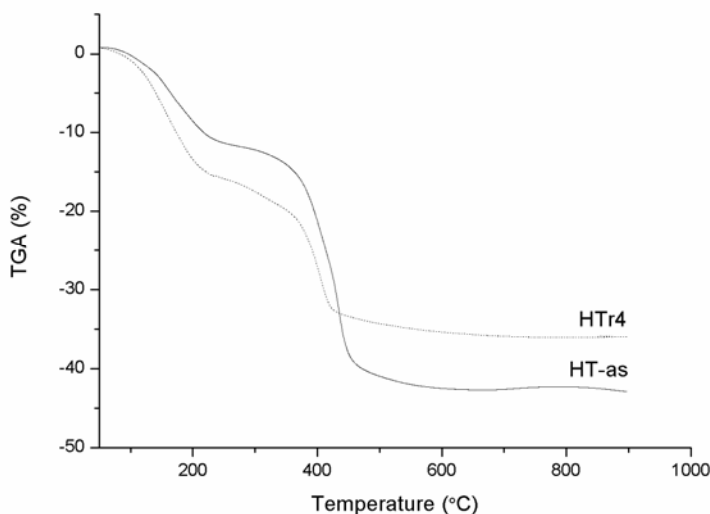


Figure 2.2.1. Thermogravimetric analysis of the hydrotalcite samples.

TGA of as-synthesised and rehydrated samples is displayed in Figure 2.2.1. Both samples exhibited the two characteristic steps of weight loss for hydrotalcite-like compounds.²⁶ A first weight loss of 11.2% in the HT-as sample was observed from about 120 °C to 250 °C and is caused by the elimination of adsorbed and interlayer water. A second weight loss of approximately 25.8% in the temperature range of 380 °C to 700 °C was caused by the loss of hydroxyl groups in the brucite layers and interlayer anions. The first weight loss was greater in the meixnerite-like compound than in the as-synthesised sample, which suggests that the former has more adsorbed water molecules. From the second weight loss, the rehydration degree could be estimated by comparing it with the theoretical weight loss in meixnerite-type materials. The rehydrated sample exhibited a second weight loss of 20.4% (6% lower than the as-synthesised sample), which indicates an incomplete rehydration of the mixed oxide, with a degree of reconstruction of 84.4%.

The basicity of the mixed oxide and rehydrated catalysts was measured by TPD-CO₂ and the basic strength could be assigned according to the temperature at which peaks appeared (Figure 2.2.2). The number of basic sites was estimated by integration of these peaks. A recent calorimetric investigation of CO₂ adsorption, showed a non-uniform surface for the mixed oxide, and very close values for the differential heats of adsorption on MgO and hydrotalcites activated at 400 °C.²⁷

Table 2.2.2. Results of basic properties for the catalysts

Sample	TPD analysis of adsorbed CO ₂			Total evolved CO ₂ (μmol·g ⁻¹)
	Desorption peaks			
	I (150-160 °C)	II (400-500 °C)	III (550-600 °C)	
HTO4 ^a	94	19	61	174
HTr4 ^a	29	64	146	189

^a Fresh catalyst

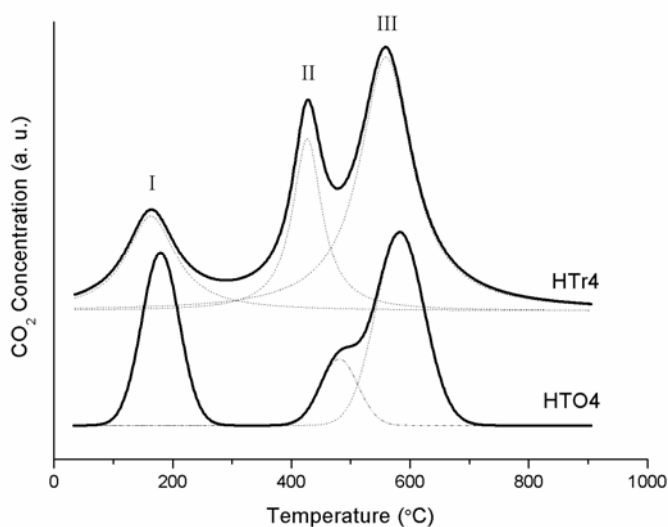


Figure 2.2.2. CO₂ losses during temperature-programmed desorption experiments.

Hydrotalcite loses both water and CO₂ at about 400 °C,²⁴ and since the second peak around 440 °C is more intense on the rehydrated catalyst, it can be assigned to the decomposition of bicarbonate species, formed by adsorption of CO₂ on the Brønsted basic sites. The third broad peak between 480 and 650 °C is observed at the same position on the both calcined and rehydrated samples. This peak could be ascribed to the strong Lewis sites identified to O²⁻ linked to Al or to low coordinatively unsaturated Mg species (corners or edges). The low temperature peak at 150 °C, is more intense on the calcined sample; it can be assigned to an adsorption on Lewis sites identified to oxygens linked to Mg cations localised on basal planes.

Table 2.2.2 shows the similarity in the number of basic sites measured by the adsorption of CO₂ for both HTr4 and HTO4. The main difference is a higher number of Brønsted basic sites on the rehydrated sample HTr4. The investigation of CO₂

2.2. ENHANCED USE OF RENEWABLE RESOURCES

adsorption by calorimetry²⁸ indeed showed that rehydration did not affect the total number of sites, but decreased the strength, which agrees with the present results.

ii. Study of the transesterification reaction of glycerol in batch

The transesterification was performed at 403 K under a small flow of Ar with a molar excess of DEC (17:1) to shift the reaction equilibrium towards the products. The catalytic properties were determined by measuring the glycerol conversion *versus* time (Figure 2.2.3). The rehydrated catalyst HTr4 presented a 99% glycerol conversion after 10 hours of reaction, whereas the mixed oxide catalyst HTO4 achieved only a 76% glycerol conversion after 50 hours of reaction. If we take into account the similar total number of basic sites of these solids and the significantly lower surface area of the rehydrated sample compared to the mixed oxide (57 and 199 m²/g, respectively), HTO4 (with Lewis basic sites) shows definitively poorer catalytic properties than HTr4 (with Brönsted basic sites) (Table 2.2.2). This behaviour suggests that, in terms of activity, the accessibility and the number of base sites is not as important as the type of basicity of the solid, as has been observed in the literature.²⁹ The presence of Brönsted basic sites in the HTr4 catalyst induces a better catalytic activity in the transesterification reaction of glycerol than the HTO4 catalyst, which has a similar quantity of Lewis basic sites. This is probably because the Brönsted basic sites are better at extracting the proton from the alcohol (which presents higher acidity compared with DEC) thus providing the alkoxide anion stabilised at the surface of the solid.

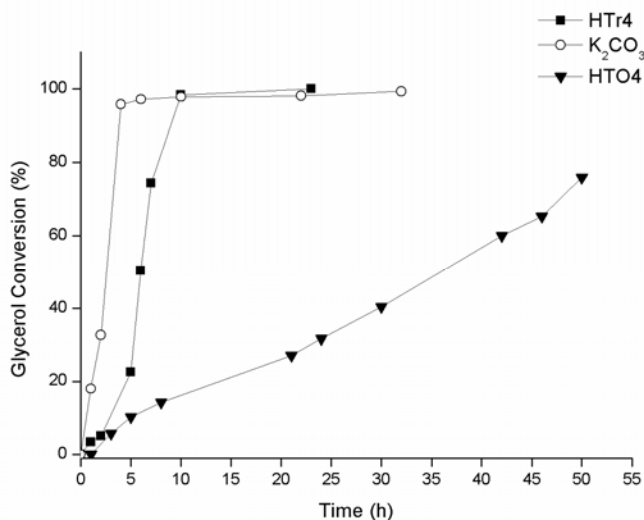
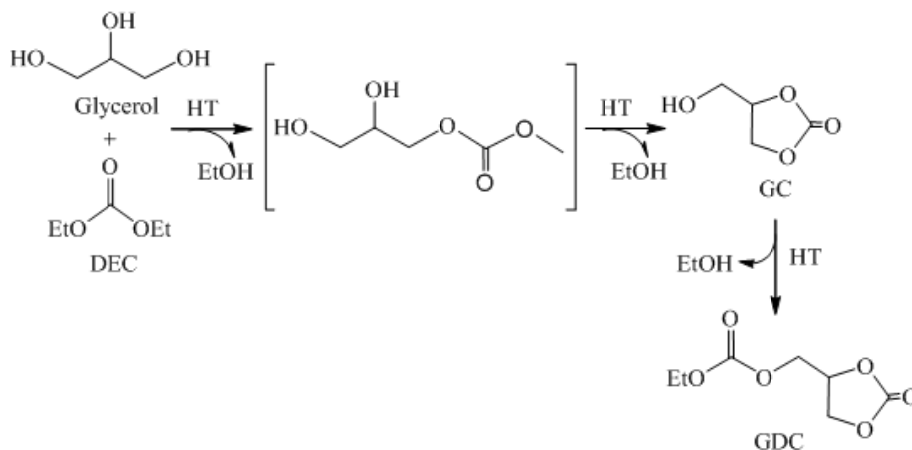


Figure 2.2.3. Conversion of glycerol vs. reaction time.

On the other hand, it should be remembered that the three hydroxyl groups of glycerol can be used for the transesterification reaction. Under the reaction conditions, the primary alcohols are presumably more reactive than the secondary

alcohol. However, once the transesterification of the primary alcohol occurs, the intramolecular reaction between the secondary alcohol and the nearby carbonate group is favoured, thus producing glycerol carbonate. Finally, the transesterification reaction between the glycerol carbonate and the DEC leads to the formation of glycerol dicarbonate, or GDC (Scheme 2.2.1).



Scheme 2.2.1. Consecutive hydrotalcite-catalysed transesterification reaction of glycerol with DEC.

The different catalysts used in the transesterification reaction of glycerol led to different products (see Table 2.2.3). The mixed oxide catalyst HTO4 did not lead to any reaction between the diethyl carbonate with the third OH group of glycerol. The only product obtained was glycerol carbonate after 54 hours of reaction (Entry 1, Table 2.2.3). By contrast, the HTr4 sample catalysed the reaction and, after 10 hours, converted almost all the glycerol to carbonate with a selectivity of 33% to glycerol dicarbonate. After 54 hours of reaction, 83% of the glycerol carbonate was transformed into glycerol dicarbonate (Entry 2, Table 2.2.3).

The homogeneous catalyst K₂CO₃ was also tested under the same reaction conditions when reacting glycerol with DEC. The number of Brönsted basic sites introduced into the homogenous reaction was comparable to the number of Brönsted basic sites found on the HTr4 sample. This catalyst presented a slightly higher activity than the rehydrated catalyst HTr4, giving a conversion of 97% after 6 hours of reaction. However, the maximum GDC achieved was only 53% (Entry 3, Table 2.2.3).

2.2. ENHANCED USE OF RENEWABLE RESOURCES

Table 2.2.3. Synthesis of glycerol carbonate or dicarbonate from glycerol under standard conditions with different catalysts

Entry	Catalyst ^a	Reaction time (h)	Glycerol converted (%) ^b	Yield (%) ^b	
				GC	GDC
1 ^c	HTO4	50	76	76	-
2 ^c	HTr4	10	98	65	33
		29	99	23	76
		54	99	17	82
3	K ₂ CO ₃	10	98	54	44
		32	99	53	46

^a All the reactions were performed under standard conditions. ^b Conversions were determined by GC/MS. ^c 0.3 g of solid catalyst that corresponds to 20 μmol of Brønsted sites.

iii. Recycling experiments

The reuse of the catalyst was investigated in the transesterification reaction of glycerol with DEC with the most active catalyst, HTr4 (Table 2.2.4).

During the experiment, the activity in the consecutive cycles decreased: the time required to reach full conversion 99% of glycerol was 10 hours in the first run, and 24 hours in the second consecutive run. The third consecutive run reached 97% conversion after 60 hours. The same trend was observed for the transesterification of glycerol carbonate with DEC to obtain glycerol dicarbonate. In this case, after 54 hours of reaction, the first run gave an 82% GDC conversion which decreased dramatically in the following runs, yielding only a 4% after 60 hours of reaction in the third consecutive run.

An attempt was done to investigate the structure of the catalyst after reaction, determining the XRD pattern of the catalyst (Figure 2.2.4). The analysis revealed a loss of the crystalline structure of the original meixnerite-like phase after the third cycle. This modification of the solid is reminiscent of that observed upon calcination. Here the solid is not carbonated, but the TGA experiment shows that dehydration starts at about 100 °C. The reaction temperature of 130 °C is then sufficient to provoke a significant dehydration, if we take into account that the reactor is swept by argon, and the reaction time relatively long. It can then be reasonably supposed that the dehydration of the catalyst surface is the cause of the decrease of catalytic activity.

Table 2.2.4. Reutilisation of catalyst HTr4

Run ^a	Reaction time (h)	Glycerol converted (%)	Yield (%) ^b	
			GC	GDC
1	10	98	65	33
	54	99	17	82
2	54	99	34	65
	60	99	31	68
3	60	97	93	4

^aAll the reactions were performed under standard conditions using HTr4 as catalyst.

^b Conversions were determined by GC/MS

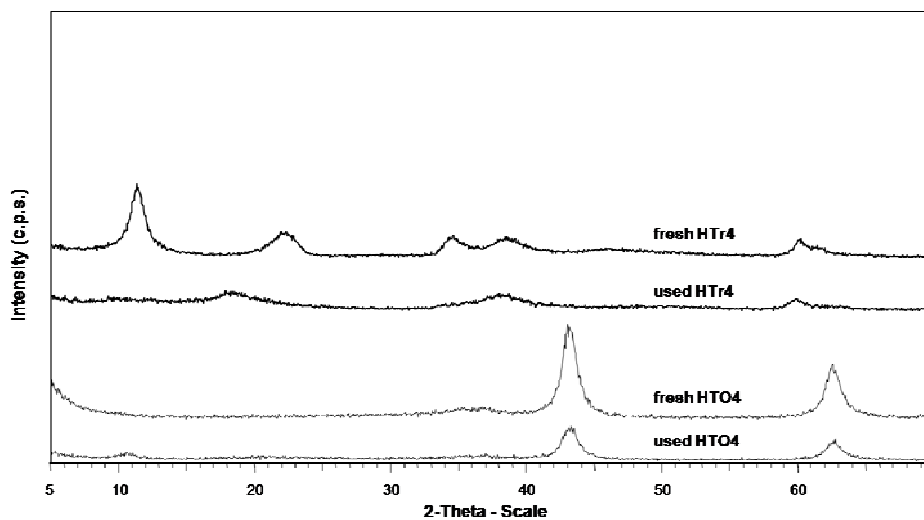


Figure 2.2.4. PXRD patterns for fresh and used catalysts

2.2.4. Conclusions

In conclusion, we have developed an efficient method using heterogeneous catalysts to obtain glycerol carbonate and glycerol dicarbonate from glycerol. The experimental results show that the type of basic centre has a large influence on the activity in the heterogeneous glycolysis reaction. In addition, the absorption capacity of the Brønsted heterogeneous catalyst favours the subsequent transesterification of the glycerol carbonate. HTr4 was the best catalyst and could be recycled a few times.

2.2. ENHANCED USE OF RENEWABLE RESOURCES

Thus it is concluded that Mg/Al mixed oxide catalysts and rehydrated catalysts are promising candidates for the transesterification reaction and would be able to replace homogeneous catalysts that have similar activity. It is however observed that the structure of the meixnerite active phase is lost after reaction, suggesting that the solid is dehydrated in the course of the reaction. This opens a path to a possible stabilisation of catalytic activity.

Reference

1. D. Fabbri, V. Benovi, M. Notari and F. Rivetti, *Fuel*, 86 (2007) 690.
2. D. Herculat, A. Eggers, A. Strube and J. Reinhard, DE101108855A1 (2002).
3. G. Rokicki, P. Rakoczy, P. Parzuchowski and M. Sobiecki, *Green Chem.*, 7 (2005) 529.
4. M. Notari and F. Rivetti, to Polimeri Europa, US20050261144 (2005).
5. A. Behr, J. Eilting, K. Irawadi, J. Leschinski and F. Lindner, *Green Chem.* 10 (2008) 13.
6. C. Vieville, J.W. Yoo, S. Pelet and Z. Mouloungui, *Catal. Lett.*, 56(4) (1999) 245.
7. M. Aresta, A. Dibenedetto, F. Nocito and C. Pastore, *J. Mol. Catal. A: Chem.*, 257 (2006) 149.
8. J.W. Yoo and Z. Mouloungui, *Stud. Surf. Sci. Catal.*, 146 (2003) 757.
9. P. Tundo and M. Selva, *Acc. Chem. Research*, 35(9) (2002) 706.
10. D. Wang, B. Yang, X. Zhai and L. Zhou, *Fuel Process. Technol.* 88 (2007) 807.
11. Z. Mouloungui, J. W. Yoo, C. A. Gachen, A. Gaset and G. Vermeersch, EP0739888.
12. J.J.W. Eshuis, J.A.M. Laan and G. Roberts, WO 9516723 (1995).
13. F. Cavani, F. Trifiró and A. Vaccari, *Catal. Today*, 11 (1991) 173.
14. D.Tichit, M. Naciri Bennani, F. Figueras, R. Tessier and J. Kervennal, *Appl. Clay Sci.* 13 (1998) 401.
15. J. Roelofs, A.J. van Dillen and K.P. de Jong, *Catal. Lett.* 74 (2001) 91.
16. S. Abelló, F. Medina, D. Tichit, J. Pérez-Ramírez, Y. Cesteros, P. Salagre, and J.E. Sueiras, *Chem. Commun.* (2005) 1453.
17. R.J. Chimentão, S. Abelló, F. Medina, J. Llorca, J. E. Sueiras, Y. Cesteros and P. Salagre, *J. Catal.*, 252 (2007) 249.
18. T. Sate, H. Fujita, T. Endo and M. Shimada, *React. Solids*, 5 (1988) 219.
19. A.S. Bookin and V.I. Drits, *Clays Clay Miner.*, 41 (1993) 551.
20. J.I. Di Cosimo, V.K. Diez, M. Xu, E. Iglesia and C.R. Apesteguía, *J. Catal.* 178 (1998) 499.
21. M. Gazzano, W. Kagunya, D. Matteuzzy and A. Vaccari, *J. Phys. Chem. B*, 101 (1997) 4514.
22. D. Tichit, M.N. Bennani, F. Figueras and J.R. Ruiz, *Langmuir*, 14 (1998) 2086.
23. S. Miyata, *Clays & Clay Miner.* 28 (1980) 50-6.

2.2. ENHANCED USE OF RENEWABLE RESOURCES

24. E. Kanezaki, *Inorg. Chem.*, 73 (1998) 2588.
25. H.A. Prescott, Z.J. Li, E. Kemnitz, A. Trunchke, J. Deutsch, H. Lieske and A. Auroux, *J. Catal.*, 234 (2005) 119.
26. J. Sanchez Valente, F. Figueras, M. Gravelle, P. Kumbhar, J. Lopez and J. -P. Besse, *J. Catal.* 189 (2000) 370.
27. A. Corma, S.B.A. Hamid, S. Iborra and A. Velty, *J. Catal.*, 234 (2005) 340.
28. J. Sanchez Valente, F. Figueras, M. Gravelle, P. Kumbhar, J. Lopez and J. -P. Besse, *J. Catal.* 189 (2000) 370.
29. A. Corma, S.B.A. Hamid, S. Iborra and A. Velty, *J. Catal.*, 234 (2005) 340.

2.3. TUNABLE BASIC AND TEXTURAL PROPERTIES OF HYDROTALCITE DERIVED MATERIALS FOR TRANSESTERIFICATION OF GLYCEROL

2.3.1. Introduction

In ages of depleting fossil oil reserves, the utilisation of renewable raw resources to provide new sources of energy and chemical intermediates is one necessary step towards a sustainable development.

The growing production of biodiesel by transesterification of oils with methanol or ethanol is responsible for the surplus production of glycerine. Consequently, the price of glycerine has dropped dramatically and is expected to be lower than that of propylene glycol or sorbitol.¹ Therefore, it is especially important to explore new applications for this product as well as alternative strategies for transforming it into new suitable products. A great number of publications have been reported in this field, highlighting the immense activity in the chemistry of glycerol.² Several important chemicals can be obtained from glycerol via oxidation, esterification, etherification, acetalisation, dehydrogenation, polymerisation and so on. Glycerol carbonate and its esters are most interesting derivatives of glycerol. They are relatively new materials in the chemical industry and, due to their properties (low toxicity, low flammability and low vapour pressure) have great potential as new component in gas-separation membranes, non-volatile solvents for dyes, lacquers, pharmaceuticals, detergents, adhesives, cosmetics, and biolubricants,³ and for the synthesis of new functionalised polymers such as polyglycerol.⁴

Traditionally, the synthesis of glycerol carbonate involves the use of homogeneous bases, such as NaOH or NaHCO₃⁵ introducing several drawbacks such as the corrosion of the reactors, generation of basic aqueous effluents due to the neutralisation of the base as well as the recovery of the product by distillation under reduced pressure.

The improvement of the economic and environmental feasibility of the industrial synthesis of glycerol carbonate (i.e. reducing the number of steps and waste) entails the design of an optimised direct method for its production. Few references have been found in the literature concerning the production of glycerol carbonate using heterogeneous catalysts.⁶⁻⁸

Heterogeneous catalysis has gained importance in the field of basic catalysis and different materials such as oxides, hydroxides and organic modified mesoporous materials have been studied.⁹ For this purpose, layered double hydroxides are probably the most studied materials as basic catalysts in the last few years and there is a vast literature concerning catalysis with this kind of materials.¹⁰⁻¹² For instance, nowadays hydrotalcite-like compounds have gained special relevance in the

2.3. TUNABLE BASIC AND TEXTURAL PROPERTIES OF HT-DERIVED MATERIALS

transesterification of oils for biodiesel synthesis.¹³

We have previously reported the results of an exploratory study focussed on the synthesis of glycerol carbonate by the transesterification of glycerol with diethyl carbonate using heterogeneous catalysts based on Mg/Al hydrotalcite-like compounds with a Mg/Al molar ratio of 4.¹⁴ The results showed that these Mg/Al mixed oxide and its rehydrated form are efficient and reusable catalysts for the transesterification reaction, being able to replace homogeneous catalysts, such as K_2CO_3 , which showed similar activity. Moreover, the non-toxicity, biodegradability and cleaner production process of diethyl carbonate (DEC) make it as a green reagent to be used as carbonylating agent.¹⁵ Along the same research lines,¹⁶ showed that an uncalcined hydrotalcite containing a hydromagnesite phase efficiently catalyses glycerol carbonate synthesis from glycerol and DEC using DMF as solvent. Climent *et al.*,¹ also recently reported that solids with well balanced acid-base pairs such as Zn/Al mixed oxides from hydrotalcite-like compounds are efficient catalysts for the transesterification of glycerol with urea.

Hydrotalcite-like materials also known as LDHs have the general formula $[M^{II}_{1-x}M^{III}_x(OH)_2]^{x+} A^{n-}_{x/n} nH_2O$, where M^{II} and M^{III} stand for a divalent and a trivalent cation octahedrally coordinated with hydroxyl groups sharing edges to form brucite-like layers and A^{n-} is a charge-balancing anion (e.g. CO_3^{2-} , NO_3^- , Cl^- , OH^- or organic anions). The thermal decomposition of hydrotalcites leads to mixed metal oxides, which are characterised by high specific surface areas, homogeneous dispersion of metals and unique acid-base properties, which presumably exposes strong Lewis base sites.¹⁷⁻¹⁹ The basic properties of these sites depend on the Mg-Al ratio in the precursor hydrotalcite.²⁰ These mixed oxides are able to recover the original layered structure by treatment with water. Interestingly, the reconstruction of decomposed Mg-Al hydrotalcite by rehydration at room temperature has been reported to enhance the catalytic activity.²¹ During the rehydration in an inert atmosphere, the brucite-like layers are reformed and the charge-compensating anions are replaced by hydroxyl anions, thus forming Brønsted base sites, however this process results in an important decrease in specific surface area of the material respect to the corresponding mixed oxide.²²

The crystallinity and textural properties of hydrotalcites are essential features for them to be utilised as catalysts^{23,24} and may be affected by various experimental parameters such as pH and temperature of preparation, concentration of used solutions, flow rate during addition of reactants, hydrodynamic conditions in the reactor and/or post synthesis operations (e.g. an ageing of obtained precipitate). The crystal quality of LDHs affects their surface properties and the activity trend.²⁵ Since hydrothermal treatment generally increases crystallinity, the application of ultrasound assisted rehydration on hydrotalcites has been reported as an effective method which permits the synthesis of materials with different surface characteristics leading to important differences in terms of catalytic activity.²⁶ In addition, the change in the nature of the cations in the layers, M^{2+}/M^{3+} molar ratio, nature of the compensating

anions or activation methodology can modify the acid–base properties of these catalysts.^{21,27} Tuning the properties of hydrotalcite by changing the composition of the brucite-like layers or the nature of the interlayer anions offers a wide range of possibilities.

This work presents a study of the role of the Mg/Al molar ratio, of different compensating anions (OH^- , F^- , Cl^- , CO_3^{2-}) and of ultrasound-assisted treatment in the rehydration process on the properties of the layered double hydroxides. To understand their behaviour and how it is possible to modulate and fulfil the specific requirements to improve their properties, the Mg-Al mixed-metal oxides were examined in transesterification of glycerol using diethyl carbonate as co-substrate for the production of glycerol carbonate.

2.3.2. Experimental

i. Catalyst preparation

Parent Mg/Al hydrotalcite-like precursor with a molar ratio of 2, 3 and 4 was obtained according to the standard co-precipitation method as follows. The appropriate amounts of $\text{Mg}(\text{NO}_3)_2 \cdot 6\text{H}_2\text{O}$ (20–40 mmol) and $\text{Al}(\text{NO}_3)_3 \cdot 9\text{H}_2\text{O}$ (10 mmol) were dissolved in 150 cm^3 of distilled water and added dropwise into a glass vessel which initially contained 200 cm^3 of deionised water. The pH was controlled by adding a 2M NaOH solution and was kept at 10. Both solutions were mixed under vigorous stirring. The suspension was stirred overnight at room temperature. The precipitated solid was filtered and washed several times with water ($\approx 3\text{L}$) and dried at 383 K during 24 h to yield the as-synthesised hydrotalcite (HTx-as). The solid was calcined in air by heating at 10 K/min up to 723 K over 3 hours to obtain the corresponding mixed oxides. These solids were named HTOx, where x refers to a nominal Mg/Al molar ratio). A part of the mixed oxides were reconstructed back in decarbonated water by sonication for one hour under an inert atmosphere to maximise the accessibility of the OH^- groups.^{26,28} These samples were called HTx.

Another hydrotalcite containing CO_3^{2-} with an Mg/Al molar ratio of 4 (HT4-CO3) was prepared following the same co-precipitation method and adjusting the pH at 10 with a NaOH/ Na_2CO_3 solution. The different anion-exchanged hydrotalcites were prepared by rehydration in a saturated solution of the desired anion, of the mixed oxide obtained by the calcination of HT4-CO3 as described by Choudary *et al.*²⁹ These samples were called HT4-x, where x represents the corresponding anion.

ii. Catalysts characterisation

Mg and Al elemental chemical analyses were obtained by atomic absorption spectroscopy (AAS) using a Perkin-Elmer 703 instrument, after dissolution of the samples in HNO_3 . Specific surface areas were determined by nitrogen adsorption at 77.2 K using a Micromeritics ASAP 2000 equipment. Samples were previously degassed in situ at 393 K under vacuum. Surface areas were calculated using the

2.3. TUNABLE BASIC AND TEXTURAL PROPERTIES OF HT-DERIVED MATERIALS

Brunauer-Emmet-Teller (BET) methods over a p/p_0 range where a linear relationship was maintained. X-ray diffraction (XRD) powder patterns were collected on a Siemens EM-10110BU diffractometer model D5000 fitted with a Cu K α (1.541 Å) radiation source. Data were recorded over a 2θ range of 5-70° with an angular step of 0.05° at 3 s/ step which resulted in a scan rate of 1°/min. Patterns were identified using files from the Joint Committee on Powder Diffraction Standards (JCPDS).

The basicity measurements were obtained by temperature programmed desorption (TPD) of CO₂ on a Thermo Finnigan TPDRO 1100 equipped with a TCD detector. Typically, ca. 0.150 g of sample were placed in a tubular quartz reactor. The sample was pretreated with Ar at 353 K during 1 h and then cooled to room temperature and treated with a CO₂ flow (3% CO₂ in He). The desorption of CO₂ was measured by heating the sample from room temperature to 1073 K at a heating rate of 10 K/min in He flow. Water was trapped on magnesium perchlorate. The number of basic sites was calculated from the CO₂ peaks by deconvolution using the software of the equipment, and a calibration of the instrument using a known amount of CaCO₃. The Hammett indicator method was used to determine the basicity strength of the anion-exchanged hydrotalcites. Thermogravimetric analysis (TGA) curves were recorded in a Labsys/Setaran TG thermo balance apparatus from room temperature to 1173K, at a heating rate of 10 K/min.

iii. Standard batch catalytic transesterification reaction

Glycerol (99%) and DEC (99.5%, GC grade) were purchased from Aldrich and used without any further purification. Ethanol HPLC grade from Aldrich was used as a solvent to characterise the products obtained. Transesterification reactions were performed in a three-neck round bottomed flask equipped with a condenser. Typically, the flasks were charged with an excess of DEC (38.95 g) and glycerol (1.85 g). Freshly activated catalyst (0.30 g) was added and the experiment started with mechanical stirring under argon at 403 K. Stirring was continued until the completion of the reaction. Aliquots were periodically withdrawn, filtered and quantified by GC analysis equipped with a FID detector. This was performed on a Shimadzu GC (QP 2010) with a Zebron ZW-WAX capillary column.

iv. Recycling experiments

We investigated the reuse of the catalyst HTr3 in the transesterification reaction of glycerol with DEC under the same reaction conditions that were used for the standard transesterification reaction. The reaction mixture was removed with a syringe equipped with a microfilter when the reaction had finished, leaving the catalyst in the smallest possible amount of liquid. The catalyst was then washed twice with DEC at 403 K. After that, a new charge of reactants was added to the used catalyst and the next run was performed.

2.3.3. Results and discussion

i. X-ray diffraction (XRD)

The chemical composition, textural properties and crystalline parameters are shown in Table 2.3.1. X-ray diffraction patterns of the prepared materials with values of $x = \text{Al}/(\text{Mg}+\text{Al})$ between 0.19 and 0.32 exhibited single phases consistent with a hydrotalcite structure. Generally, the optimal value of x for a pure LDH phase ranges from 0.2 to 0.33.³⁰ However, pure lamellar phases are reported for values of $x = 0.15 - 0.34$ in MgAl-LDHs.³¹ The value of the lattice parameter a was calculated as twice the spacing of plane (110) whose maximum was recorded close to $2\theta = 60^\circ$ and is characteristic of hydrotalcite-like compounds, (JCPDS 22-700). The indexing was based on rhombohedral symmetry (polytype 3R).³¹ The a values (Table 2.3.1) are in the range of that observed for pure hydrotalcite phases³² and decreases linearly with increasing Al content, obeying the Vegard's law.

Table 2.3.1. Composition, textural and crystalline properties of the prepared materials

Solid	Molar ratio		x	Lattice parameters (Å)			Surface area (m ² /g)	Pore volume (cm ³ /g)	Pore diameter (Å)
	Solution	Solid ^a		$d_{(006)}$	a	c			
HT2-as	2	2.09	0.32	8.69	3.04	26.07	38	--	--
HT3-as	3	2.85	0.26	8.83	3.06	26.49	20	--	--
HT4-as	4	4.29	0.19	8.89	3.07	26.67	17	--	--
HTO2	--	--	--	--	4.19	--	42	0.18	170
HTO3	--	--	--	--	4.19	--	202	0.33	66
HTO4	--	--	--	--	4.19	--	199	0.48	97
HTr2	2	2.05	0.32	7.58	3.04	22.74	106	0.47	168
HTr3	3	2.91	0.25	7.77	3.06	23.31	56	0.22	172
HTr4	4	4.08	0.19	7.73	3.06	23.19	47	0.14	121
HT4-CO3	4	3.85	0.21	7.99	3.07	23.97	77	0.40	208
HT4-Cl	4	3.85	0.21	8.04	3.07	24.09	45	0.35	223
HT4-F	4	3.76	0.21	7.92	3.07	23.76	40	0.35	237

^aMeasured by Atomic Absorption Spectroscopy

2.3. TUNABLE BASIC AND TEXTURAL PROPERTIES OF HT-DERIVED MATERIALS

The X-ray diffraction patterns of materials HT3-as, HTO3 and HTr3 are reported in Figure 2.3.1. After calcination the layered structure was destroyed and the calcined sample presented the typical features of Mg(Al)Ox mixed oxide (HTO), whose reflections appeared at $2\theta = 43^\circ$ and 63° , thus corresponding to a periclase-like structure (JCPDS 87-0653). Its structural parameters are lower than those in the pure MgO rock salt-type structure, showing that Al^{3+} cations are inserted into the structure.^{33,34} The original layered structure was recovered from the calcined material after rehydration in the absence of CO_2 . The sample presented a meixnerite structure (JCPDS 35-0965) because of the well-known “memory effect”³⁵ where the original nitrate anions have been replaced by Brønsted OH^- sites. The most striking feature of the rehydrated samples was the increased intensity of the basal peaks in the rehydrated samples compared with the original hydrotalcite. This indicates an increase in crystallinity, despite the ultrasound treatment for rehydration. Rehydration in water could provoke dissolution of the smaller particles and increase of the larger ones (Ostwald ripening), which could account for this increase of crystallinity.

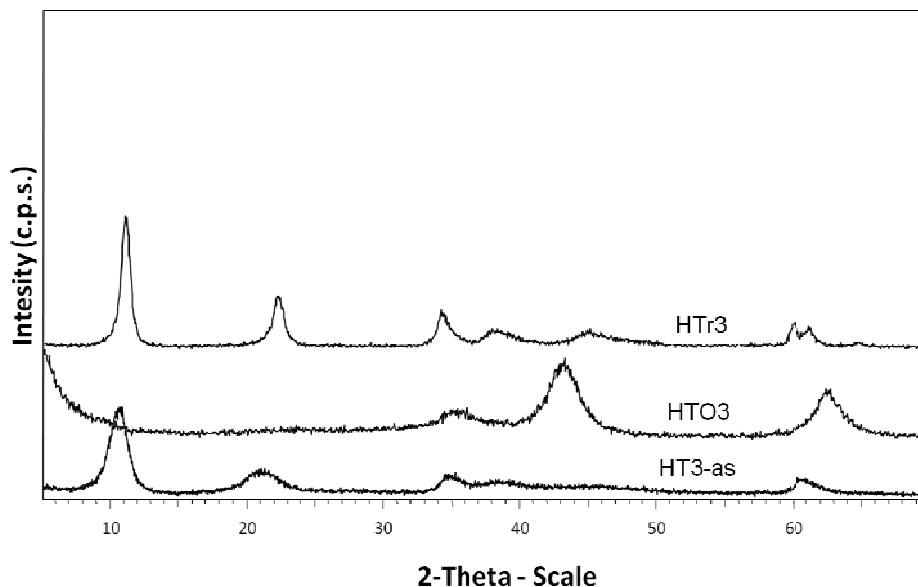


Figure 2.3.1. Powder X-ray diffractograms of as-synthesised, calcined and rehydrated hydrotalcite.

ii. N_2 -physisorption

Measured BET surface areas of the materials are showed in Table 2.3.1. The as-synthesised hydrotalcites were found to span a narrow range from $38 \text{ m}^2/\text{g}$ for HT2-as to $17 \text{ m}^2/\text{g}$ for HT4-as. The adsorption-desorption isotherms of HT2-as HT3-as and

HT4-as at 77.2 K confirm the generation of mesopores during the synthesis and the absence of micropores. (Figure 2.3.2 A)

Upon calcination at 723 K of the as-synthesised hydrotalcites the specific surface areas and the porosities increased significantly. This behaviour is due to the decomposition process of the hydrotalcite (dehydroxylation and loss of the compensating anion) which generates the formation of mesoporous channels through the layers.³⁶ Apparently, there was no correlation between the surface area of the as-synthesised hydrotalcites and the final area of the obtained mixed oxides.

Depending on the treatment condition (calcination or rehydration) the hysteresis loops of the materials were affected in different way. The calcined materials, particularly the HTO3 and HTO4 (Figure 2.3.2 B) presented wider hysteresis loops indicating a progressive generation of interparticle pores during the calcination. On the other hand, the rehydration of mixed oxides led to the recovery of the original structure presenting similar textural properties to those presented by the as-synthesised hydrotalcites and the hysteresis loops turned narrower again (Figure 2.3.3 C).

2.3. TUNABLE BASIC AND TEXTURAL PROPERTIES OF HT-DERIVED MATERIALS

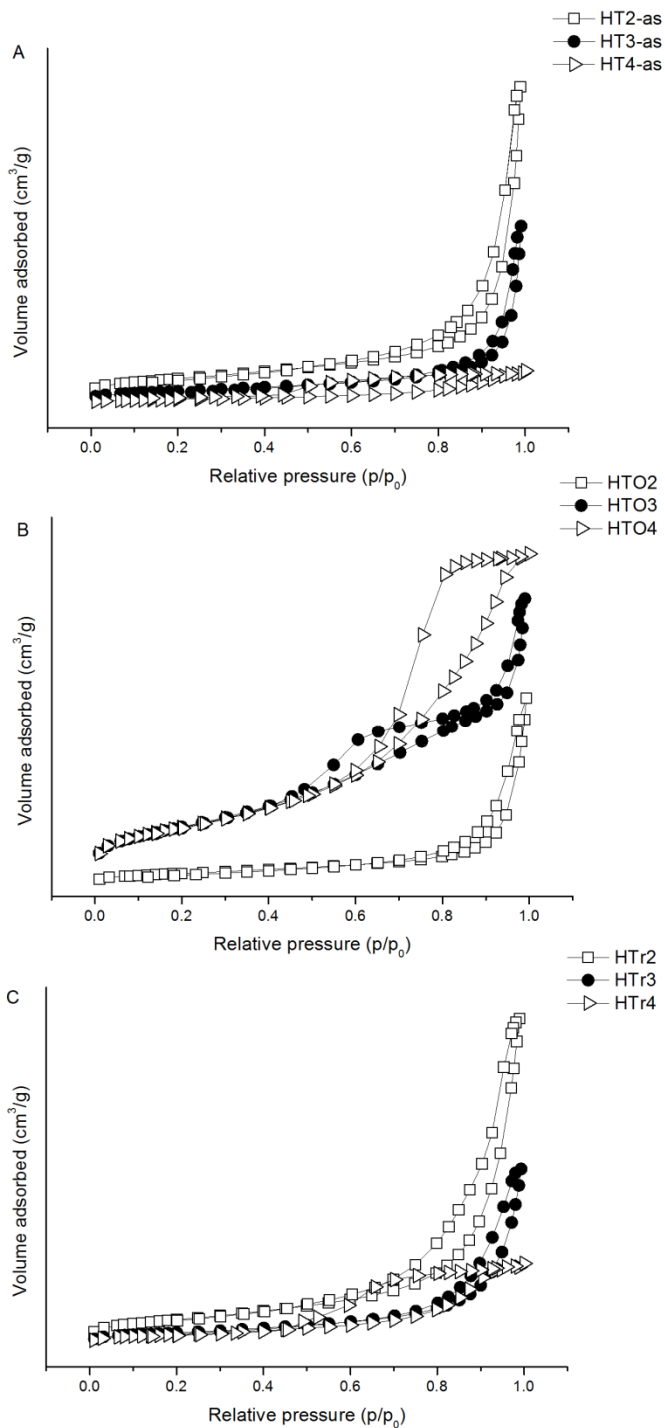


Figure 2.3.2. Nitrogen adsorption isotherms for the prepared materials. A) As-synthesised hydrothermal materials; B) calcined hydrothermal materials and C) rehydrated hydrothermal materials.

The calcined hydrotalcites (HTO3 and HTO4) increased the surface area (202 and 199 m²/g, respectively) with respect to their parent material, however no significant change in BET surface area was observed in the calcined hydrotalcite of Mg/Al molar ratio of 2 compared to that observed for the as-synthesised sample (from 37 m²/g for HT2-as to 42 m²/g for HTO2). After rehydration the specific surface areas and the pore volume of the samples decreased remarkably, however the main pore size increased. These textural changes could be attributed to the formation and growth of the meixnerite particles during the ultrasound-assisted rehydration. In this step, dissolution of the small particles is produced while the bigger particles grow at expenses of small particles until they disappear. This increase in crystallinity is in good agreement with the observed PXRD diffractograms. In addition, the high surface tension of water may lead to form a platelet agglomeration which provokes the closure of small mesopores thereby giving rise to a substantial loss of surface area.³⁷

The hydrotalcite with a Mg/Al molar ratio of 2 (HTr2) exhibited opposite behaviour. When this sample was rehydrated its surface area increased from 38 (HT2-as) to 106 m²/g. It has been found that there is a connection between the crystallinity and the Mg/Al molar ratio of hydrotalcites. Thus, the crystallinity of the Mg/Al hydrotalcites increases with increasing the Mg/Al molar ratio, on contrary to that observed by Sharma and co-workers.³⁸

iii. *Thermogravimetric analysis (TGA)*

The samples exhibited the two mass loss steps typical for hydrotalcite-like compounds during decomposition in air (Figure not shown).³⁹ Thermogravimetric analysis data of rehydrated samples are displayed in Table 2.3.2. A first mass loss of 16, 15 and 17% was observed at temperatures up to 423 K for rehydrated samples HTr2, HTr3 and HTr4, respectively and is caused by the elimination of adsorbed and interlayer water.

A second mass loss (above 550 K) is due to the water removal through condensation of layer and interlayer hydroxyl groups.³² The total mass loss involved was between 35 and 45% in all the rehydrated samples.

The rehydration degree could be estimated by comparing the second mass loss in rehydrated samples with the theoretical mass loss in meixnerite-type materials. Despite the same hydrothermal conditions applied in all the samples, it has been observed a decrease in the rehydration degree with increasing the Mg/Al molar ratio. Thus, except sample HTr2 which was almost totally rehydrated (93%) the rest of the samples showed an incomplete rehydration of the mixed oxide, with a degree of reconstruction of 86% for sample HTr3 and 84% for HTr4.

2.3. TUNABLE BASIC AND TEXTURAL PROPERTIES OF HT-DERIVED MATERIALS

Table 2.3.2. Thermogravimetric analysis of rehydrated and anion-exchanged hydrotalcites

SAMPLE	1 st MASS LOSS (%)	2 nd MASS LOSS (%)	TOTAL MASS LOSS (%)
	(423 K)	(550 K)	(%)
HTr2	16 (0.65) ^a	27 (93%) ^b	43
HTr3	15 (0.60) ^a	20 (86%) ^b	35
HTr4	17 (0.66) ^a	21 (84%) ^b	38
HT4-CO3	12	21	33
HT4-Cl	16	26	42
HT4-F	19	19	38

^aValue corresponding to crystallisation water.

^bValue corresponding to the rehydration degree calculated respect to the theoretical value.

iv. Basicity

The TPD-CO₂ profiles of the mixed oxides and rehydrated materials are presented in Figure 2.3.3. The basic strength could be assigned according to the temperature at which peaks appeared and the number of basic sites was estimated by deconvolution and integration of these peaks.

Calorimetric investigations^{40,41} and FTIR spectroscopic studies of adsorption of CO₂ have shown a non-uniform surface for the mixed oxides.^{20,42,43} The CO₂ desorption of the calcined and rehydrated samples showed three main peaks at about 400 K (weak strength), 700 K (medium strength) and 800 K (high strength). The peak at the highest temperature is predominant in samples with higher Mg/Al molar ratio with a contribution of 45.7% and 48.3% of the total CO₂ evolved for HTO4 and HTr4, respectively. These peaks are attributed to strong Lewis basic sites which can be associated with unsaturated O²⁻ linked to Al or low coordinatively unsaturated Mg species. Moreover, peaks shifted at higher temperatures with increasing Mg/Al molar ratio. For instance, the maxima for the high strength basic sites were observed at 813 K, 836 K and 856 K for HTO2, HTO3 and HTO4, respectively. The same behaviour was observed for rehydrated samples.

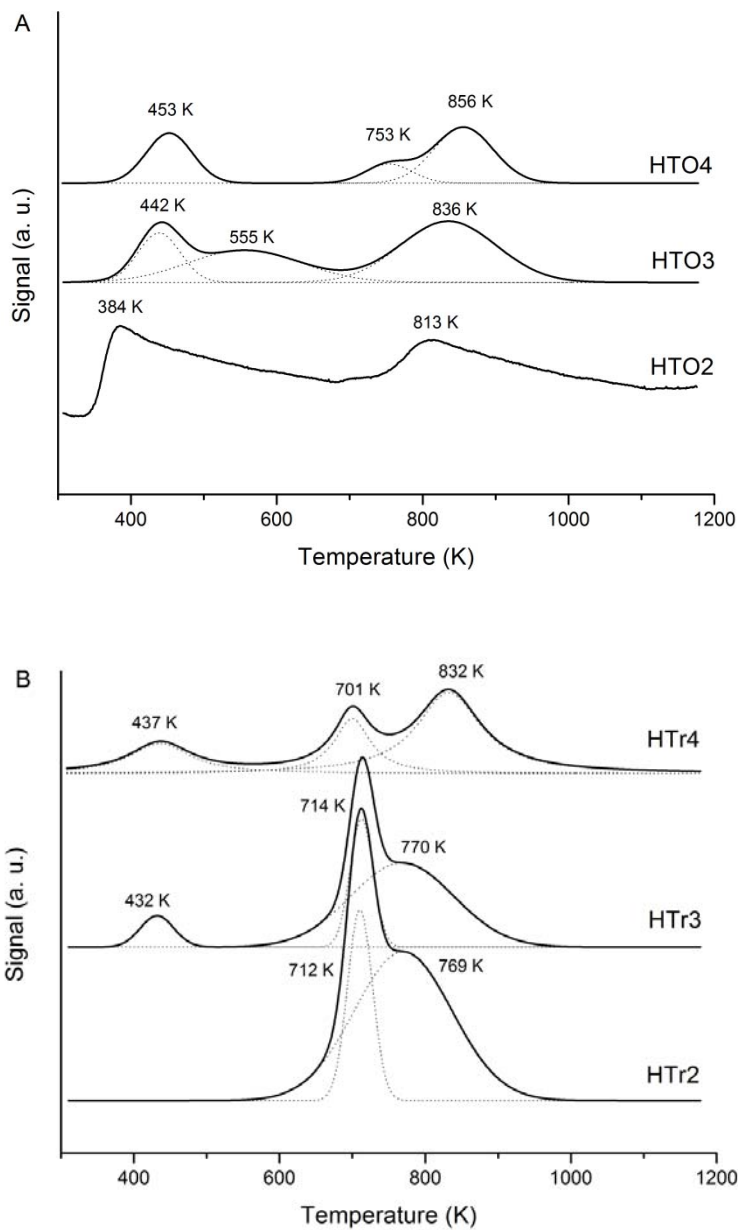


Figure 2.3.3. TPD-CO₂ profiles of: A) calcined hydrotalcites and B) rehydrated hydrotalcites.

2.3. TUNABLE BASIC AND TEXTURAL PROPERTIES OF HT-DERIVED MATERIALS

On the other hand, weak and medium-strength basic sites increased with increasing Al content. The low temperature peak is more intense on calcined samples and can be ascribed to an adsorption at Lewis sites identified to oxygens linked to Mg cations localised on basal planes or CO₂ species adsorbed on weakly basic OH⁻ groups.⁴⁴

As a main difference, the rehydrated samples showed higher peaks at medium temperatures than calcined ones with a contribution of 53.7%, 45.3% and 35.5% of the total CO₂ evolved for HTr2, HTr3 and HTr4 respectively. These peaks can be assigned to the decomposition of bicarbonate species, formed by adsorption of CO₂ on the Brønsted basic sites. A decrease of the number of Brønsted basic sites was noticed when increasing the Mg/Al molar ratio, which can be also due to the partial rehydration of samples HTr3 and HTr4.

The hydrothermal treatment did not lead to an enhancement of the total number of basic sites which are rather similar between the mixed oxide and its corresponding rehydrated form, but a decrease in strength was observed. These results agree with the calorimetric studies for hydrotalcite-type materials reported by Sanchez-Valente and co-workers.⁴¹

Table 2.3.3 reports the distribution of basic sites for calcined and rehydrated materials represented as μmol of desorbed CO₂ normalised per gram of catalyst, as well as the amount of moderate and strong basic sites taking into account the surface area of the samples expressed as μmol of desorbed CO₂ per square meter. From these data the following sequence is established: HTr3 > HTr2 > HTr4 > HT02 > HT03 > HT04.

It is noteworthy the influence of the rehydration in calcined hydrotalcites. Based on data from Table 2.3.3, it seems that when the mixed oxides are submitted to the ultrasound-assisted rehydration the weak basic sites are partially transformed into moderate and strong basic sites. The composition of the parent material also have an influence on the proportion of weak, medium and strong-strength basic sites and the hydrothermal treatment can induce changes in the population of the basic sites, therefore affecting the catalytic behaviour.

Table 2.3.3. Basic properties found for the mixed oxides and rehydrated catalysts

Sample	Desorption peaks			Total evolved CO ₂ (μmol·g ⁻¹)	Evolved CO ₂ (II+III) ^a (μmol·m ⁻²)
	I	II	III		
	(≈ 450 K)	(≈ 700 K)	(≈ 800 K)		
HT02	594 (384)	–	80 (813)	674	1.6
HT03	161 (442, 555)	–	174 (836)	335	0.8
HT04	94 (453)	19 (753)	61 (856)	174	0.4
HTr2	–	275 (712)	237 (769)	512	4.8
HTr3	33 (432)	168 (714)	170 (770)	371	6.0
HTr4	29 (437)	64 (701)	87 (832)	180	3.1

^aEvolved CO₂ of medium (II) and strong-strength (III) basic sites of catalysts. In brackets are given the temperature of maxima (K).

v. Catalytic Activity

The transesterification of glycerol with diethyl carbonate (DEC) was investigated using the mixed oxides and rehydrated samples from the series of Mg/Al hydrotalcite-like materials as catalysts. A representative sample (HT4-as) was employed to exchange different compensating anions (F⁻, Cl⁻, CO₃²⁻) for comparative purposes.

The transesterification was performed at 403 K under a small flow of Ar with a molar excess of DEC (17:1) to shift the reaction equilibrium towards the products and avoid mass transfer problems. The catalytic properties were determined by measuring the glycerol conversion *versus* time.

Figure 2.3.4 displays the reaction profiles for calcined and rehydrated catalysts. Glycerol conversion seems to occur with an induction period and this effect is more pronounced in rehydrated samples, especially on HTr2 catalyst. This behaviour could be due to the great hydrophilic character of the rehydrated hydrotalcite surface. The more pronounced effect showed by the catalyst HTr2 is in agreement with the results found in thermogravimetric analyses since the TGA showed that HTr2 presented the highest hydration degree, as well as the highest amount of adsorbed water molecules. After this period, the glycerol conversion increased greatly to reach a plateau.

2.3. TUNABLE BASIC AND TEXTURAL PROPERTIES OF HT-DERIVED MATERIALS

The rehydrated catalysts presented total glycerol conversion in a shorter period of time. For instance, while the best catalyst found, HTr3, achieved total glycerol conversion in 7 h the corresponding mixed oxide HTO3 achieved only the 13%. If we take into account the similar total number of basic sites of these both solids and the lower surface area of the rehydrated catalyst with respect to the mixed oxide (56 and 202 m²/g, respectively), HTO3 (mainly containing Lewis basic sites) shows definitively poorer catalytic properties than HTr3 (with Brønsted basicity) (Table 2.3.4).

The same behaviour was found for the rest of the catalysts, being more active those that are rehydrated. This fact suggests that the presence of Brønsted basic sites in rehydrated catalysts (HTr2, HTr3 and HTr4) induces a better catalytic activity in the transesterification reaction of glycerol than the calcined catalysts (HTO2, HTO3 and HTO4), which have a similar quantity of Lewis basic sites compared with their respective rehydrated form. This is probably because the Brønsted basic sites are better at extracting the proton from the alcohol (which presents higher acidity compared with DEC) thus providing the alkoxide anion stabilised at the surface of the solid.

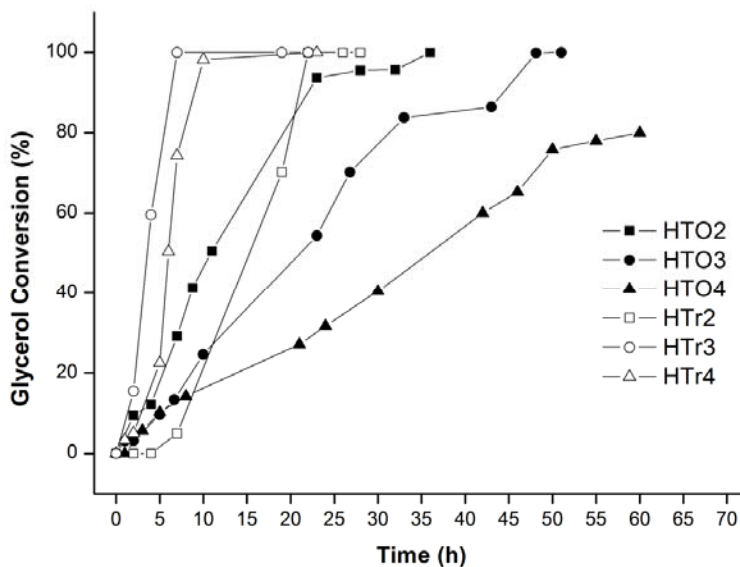


Figure 2.3.4. Catalytic behaviour of calcined and rehydrated catalysts at 403 K and a glycerol : DEC molar ratio 1:17.

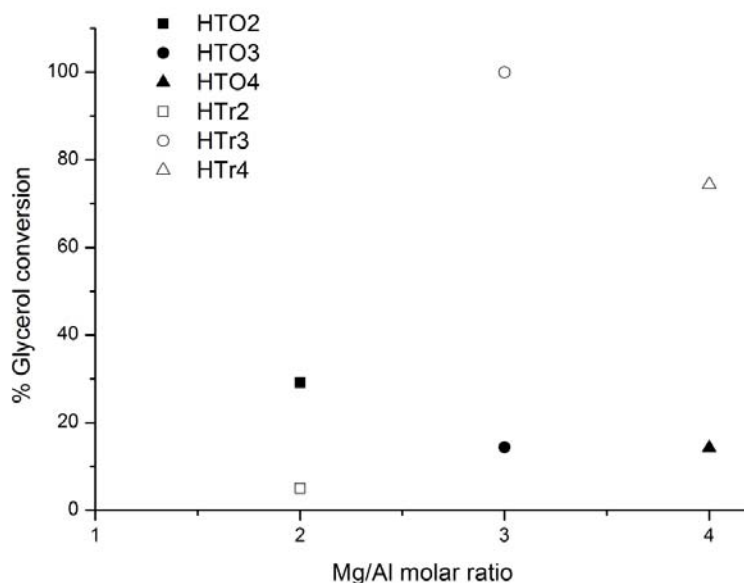


Figure 2.3.5. Influence of the Mg/Al molar ratio in the catalytic activity of calcined and rehydrated catalyst. Conversions after 7 h of reaction at 403 K and standard conditions.

The optimal molar ratio for the transesterification reaction was found for Mg/Al=3 (Figure 2.3.5). This result agrees with those found by many authors in reactions of transesterification of fatty acids for biodiesel synthesis and other reactions in which the Mg/Al molar ratio of 3 was reported as the best in terms of basic activity.⁴⁵⁻⁴⁷

The activity of the catalysts followed the next sequence: HTr3> HTr4> HTr2> HTO2> HTO3> HTO4 apparently manifesting an influence between catalytic performance and the Mg/Al molar ratio of the catalysts. While the rehydrated catalysts showed an increase of the activity with the increasing Mg content, the calcined catalysts showed the opposite behaviour.

As seen previously, the rehydration of mixed oxides did not lead to a significant enhancement of the total number of basic sites, but induces a clear increase of medium basic sites. In this regard, the rehydration of mixed oxides can be seen as a transformation Lewis to Brønsted basicity since medium-strength basic sites (attributed to Brønsted basicity) increase at the expenses of weak-strength basic sites belonging to the corresponding mixed oxide.

Probably, only the medium and strong basic sites take part in the transesterification reaction. Taking this into account, it seems reasonable that rehydrated catalysts present higher catalytic activity. A deeper study of the results obtained by TPD-CO₂ is reported in Table 2.3.4. In terms of basicity (expressed as medium and strong

2.3. TUNABLE BASIC AND TEXTURAL PROPERTIES OF HT-DERIVED MATERIALS

basicity in $\mu\text{molCO}_2/\text{m}^2$), the catalysts show the following sequence: $\text{HTr3} > \text{HTr2} > \text{HTr4} > \text{HTO2} > \text{HTO3} > \text{HTO4}$ revealing a significant correlation between basicity and catalytic performance. The rehydration of catalyst HTO3 to obtain HTr3 led to a great enhancement of the amount of medium strength basic sites from 0.8 to 6 $\mu\text{mol}/\text{m}^2$. Since this catalyst exhibited the highest catalytic activity, the correlation between the amount of medium and strong-strength basic sites per square meter and the catalytic activity is demonstrated.

This basicity sequence also explains the behaviour of the calcined catalysts, which showed the following catalytic activity: $\text{HTO2} > \text{HTO3} > \text{HTO4}$. While catalyst HTO2 achieved total glycerol conversion after 35 h of reaction, catalyst HTO4 needed 60 h to reach the 80% of conversion. From these results the dependence between basic properties and catalytic activity of the catalysts clearly appears.

Catalyst HTr2 did not present a catalytic activity as high as could be expecting from the TPD- CO_2 analysis. A possible explanation can be found taking into account the TGA analysis which revealed the highest mass loss (43%) for this material. The water contained in the rehydrated catalysts can facilitate the migration of glycerol because of the great miscibility between water and glycerol. However, high levels of water in catalysts can cause a deactivation. Free water can even produce the hydrolysis of glycerol carbonate driving the equilibrium of the reaction again towards the formation of glycerol. This could be also an explanation to the induction period observed for the catalyst HTr2.

On the other hand, it should be remembered that the three hydroxyl groups of glycerol are susceptible of transesterification. Therefore, once the transesterification of the primary alcohol occurs, the intramolecular reaction between the secondary alcohol and the nearby carbonate group is favoured, thus producing GC. When the concentration of GC is high enough, the third free hydroxyl group reacts to produce a new transesterification between GC and the DEC leading to the formation of GDC. In terms of selectivity, two different products glycerol carbonate (GC) and glycerol dicarbonate (GDC) were obtained under the reaction conditions. The calcined catalyst HTO4 was the only one which did not yield GDC, obtaining only GC after 54 h of reaction (Entry 3, Table 2.3.4). By contrast, the catalyst HTr3 converted all the glycerol in 7 h with a yield of a 30% to GDC (Entry 5, Table 2.3.4). From the results displayed in Table 2.3.4, it seems that the catalysts more active were those that showed a higher conversion to glycerol dicarbonate and in a lower period of time.

The homogeneous catalyst K_2CO_3 was also tested under the same reaction conditions for comparative purposes. The number of Brønsted basic sites introduced into the homogenous reaction was comparable to the number of Brønsted basic sites found on the HTr4 sample. This catalyst presented a slightly higher activity than the rehydrated catalyst HTr4, giving a conversion of 97% after 6 hours of reaction. However, the maximum GDC achieved was only 53% (Entry 7, Table 2.3.4).

Table 2.3.4. Catalytic behaviour for all the catalysts tested in the transesterification of glycerol under standar conditions

Entry	Catalyst ^a	Reaction time (h)	Glycerol converted (%) ^b	Yield	
				GC (%) ^b	GDC (%) ^b
1	HTO2	32	96	9	87
2	HTO3	48	99	32	67
3	HTO4	50	76	76	--
4	HTr2	22	100	75	25
		26	100	57	43
5	HTr3	7	100	70	30
		26	100	20	80
6	HTr4	10	98	65	33
		26	100	31	69
7 ^c	K ₂ CO ₃	6	97	45	52
		10	98	54	44
		26	99	53	46
		12 ^d	100 ^d	66 ^d	34 ^d
8	HTr3 ^{d,e}	33 ^e	99 ^e	82 ^e	7 ^e

^aAll the catalysts were tested under the same reaction conditions (0.3 g of catalyst, Gly:DEC 1:17, 403 K and 1 atm).

^bConversion and yields were determined by GC-MS.

^cThe amount of K₂CO₃ used was comparable to the Brønsted basic sites of catalyst HTr4.

^dConversion and yields found after a second run.

^eConversion and yields found after a third run.

2.3. TUNABLE BASIC AND TEXTURAL PROPERTIES OF HT-DERIVED MATERIALS

Table 2.3.5. *Quantitative results obtained by EDX analysis*

Sample	Atomic ratio Mg/Al	Atomic ratio Al/Cl	Atomic ratio Al/F
HT4-CO3	4.12	--	--
HT4-Cl	3.96	1.15	--
HT4-F	4.08	--	0.79

vi. *Influence of the interlayer anion*

A representative sample (HT4-as) was employed to exchange different compensating anions (F^- , Cl^- , CO_3^{2-}) for comparative purposes. The incorporation of the different compensating anions was done by calcination of the as-synthesised sample and subsequent rehydration of the mixed oxide with a solution saturated with the corresponding anion under inert atmosphere. The presence of the different anions in such sample was confirmed by energy-dispersive X-ray spectroscopy (EDX). Several measurements were made in order to confirm the homogeneity of the samples. Nitrates were not detected in any sample. Quantitative results are given in Table 2.3.5.

It is interesting to note that an as-synthesised hydrotalcite without further activation such as HT4-CO3 showed a catalytic activity comparable to that of mixed oxides obtained by calcination at 723 K (Figure 2.3.6). Thus, catalyst HT4-CO3 achieved total glycerol conversion after 50 h of reaction while the mixed oxide HT04 did not lead to the total conversion of glycerol yielding an 80% of conversion after 60 h. This behaviour seems to indicate the importance of the type of basicity in this kind of transesterification reaction, being more active those catalysts which present Brönsted basicity since the anion CO_3^{2-} behaves as a Brönsted base.

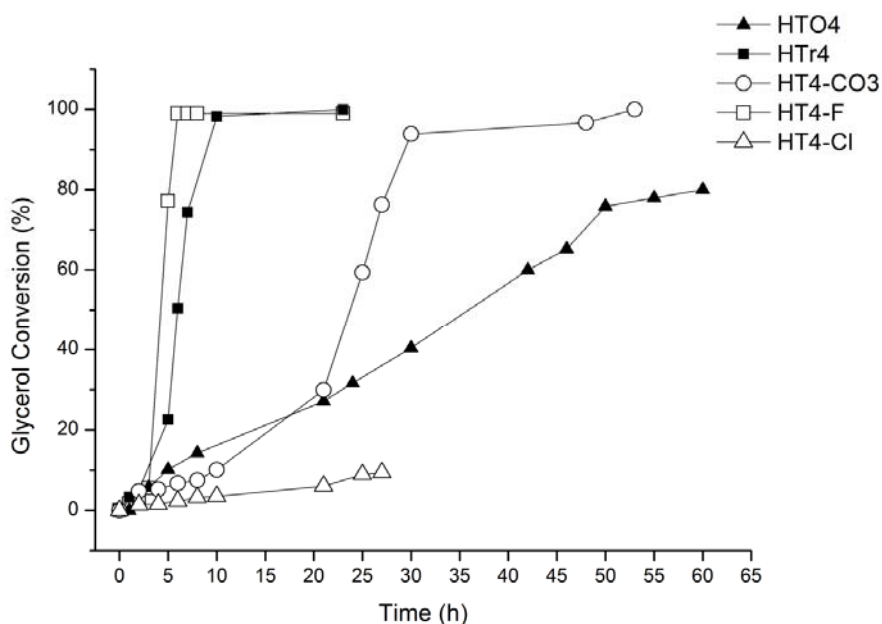


Figure 2.3.6. Effect of the compensating anion in the glycerol conversion at 403 K and standard reaction conditions.

In Figure 2.3.6 are displayed the catalytic profiles for the anion-exchanged hydrotalcites. The great catalytic activity showed by the catalyst containing fluorine as compensating anion can be pointed out. This catalyst (HT4-F) showed total glycerol conversion after 6 h of reaction compared to 10 h needed for catalyst HTr4. The fluorine anion seems to have a significant intrinsic basic character which can offer an additional advantageously basic catalyst as Choudhary and co-workers²⁹ reported previously.

A dramatic decrease in the catalytic activity was observed when chlorine was the interlayer anion. The catalyst HT4-Cl reached only 10% of glycerol conversion after 25 h of reaction. In that case, the presence of chlorine anions leads to the formation of strong acid sites in the hydrotalcite which inhibit its basic character.

The strength of these anion-exchanged HTs was analysed qualitatively by Hammett indicators (Table 2.3.6). Anion-exchanged hydrotalcites possess pK_{BH^+} values in the range $7.0 < pK_{BH^+} < 8.3$. The calcined catalyst (HTO4) and the rehydrated one (HTr4) showed stronger basicity (around $pK_{BH^+} = 15$) which is in line with the catalytic results obtained. The fluorine-exchanged hydrotalcite presented relatively weak basicity according to Hammett indicator measurements being in the same range that HT4-Cl and HT4-CO3. However, this sample was the most active in the transesterification of glycerol. Attempts to obtain basic site strength distributions by means of benzoic acid

2.3. TUNABLE BASIC AND TEXTURAL PROPERTIES OF HT-DERIVED MATERIALS

titration in the presence of Hammett indicators gave poorly reproducible results, due to the difficulty in accurately determining the end point.

Table 2.3.6. Results of Hammett indicator for calcined, rehydrated and anion-exchanged catalysts

Catalyst	Base strength (pK_{BH^+})
HTO4	$9.3 < pK_{BH^+} < 15$
HTr4	$9.3 < pK_{BH^+} < 15$
HT4-CO3	$7.0 < pK_{BH^+} < 8.3$
HT4-Cl	$7.0 < pK_{BH^+} < 8.3$
HT4-F	$7.0 < pK_{BH^+} < 8.3$

A TPD-CO₂ coupled MS analysis was made to clarify the great activity of catalyst HT4-F (Figure 2.3.7). The TPD-CO₂ analysis showed three different desorption peaks as showed the mixed oxides and the rehydrated hydrotalcites. The MS analysis demonstrated that these three peaks correspond to desorption of CO₂ from weak, medium and strong-strength basic sites. It is noteworthy that the amount of medium-strength basic sites (attributed to Brønsted basicity) is comparable to that found for the rehydrated catalyst HTr4. (Table 2.3.7)

In the TPD-CO₂ profile of HT4-F, the peaks shifted towards higher temperatures than peaks found in calcined catalyst HTO4 or the rehydrated one (HTr4). This results agree with the higher activity showed by catalyst HT4-F, but it was not possible to establish a correlation between TPD-CO₂ analysis of HT4-F and the basic strength found by using the Hammett method.

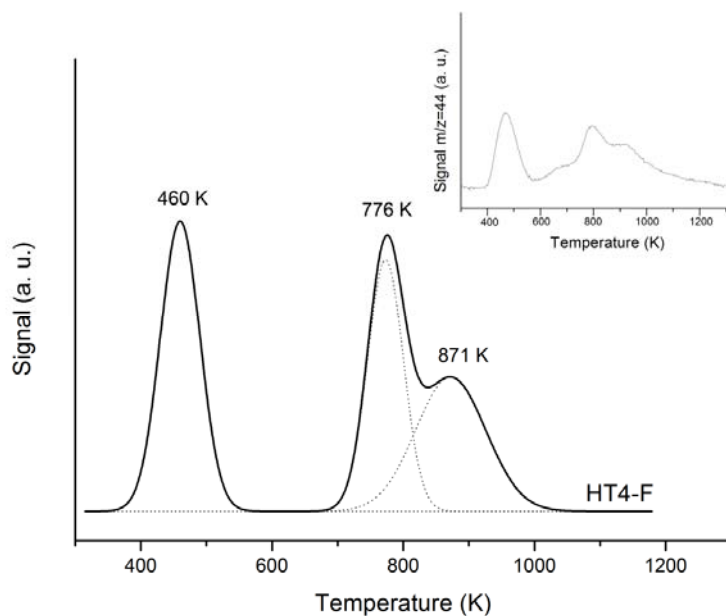


Figure 2.3.7. TPD-CO₂ profile of fluorine-exchanged catalyst (HT4-F). Insert: MS analysis.

Table 2.3.7. Comparison of the basic properties of the calcined, rehydrated and fluorine-exchanged catalysts

Sample	TPD analysis of adsorbed CO ₂			Total evolved CO ₂ (μmol·g ⁻¹)	Evolved CO ₂ (II+III) ^a (μmol·m ⁻²)
	Desorption peaks				
	I (≈ 450 K)	II (≈ 700 K)	III (≈ 800 K)		
HT04	94 (453)	19 (753)	61 (856)	174	0.4
HTr4	29 (437)	64 (701)	87 (832)	180	3.1
HT4-F	52 (460)	71 (776)	58 (871)	181	3.3

^aEvolved CO₂ from medium (II) and strong-strength (III) basic sites of catalysts. In brackets are given the temperature of maxima (K).

2.3. TUNABLE BASIC AND TEXTURAL PROPERTIES OF HT-DERIVED MATERIALS

vii. Reutilisation experiments

An important aspect of the heterogeneous catalysts is their recyclability. The reuse of catalysts HTO4 and HTr4 in the transesterification of glycerol has been reported previously by Álvarez *et al.*:¹⁴ these materials can be reused, but a small loss of activity was observed in each consecutive run.

The same trend was observed here for the best catalyst found (HTr3) which decreased in activity during the consecutive experiments. Total glycerol conversion was reached in the first run in 7 h while 12 h were needed to yield total conversion in second, and 33 h in the third run. Remarkable changes were also observed in the selectivity. Selectivity to the second transesterification product (glycerol dicarbonate, GDC) was higher in the first run and diminished progressively with every run. For instance, in the GDC obtained in the first run was a 30% after 7 h of reaction dropping to 7% in the third run after 33 h (Entry 8, Table 2.3.4).

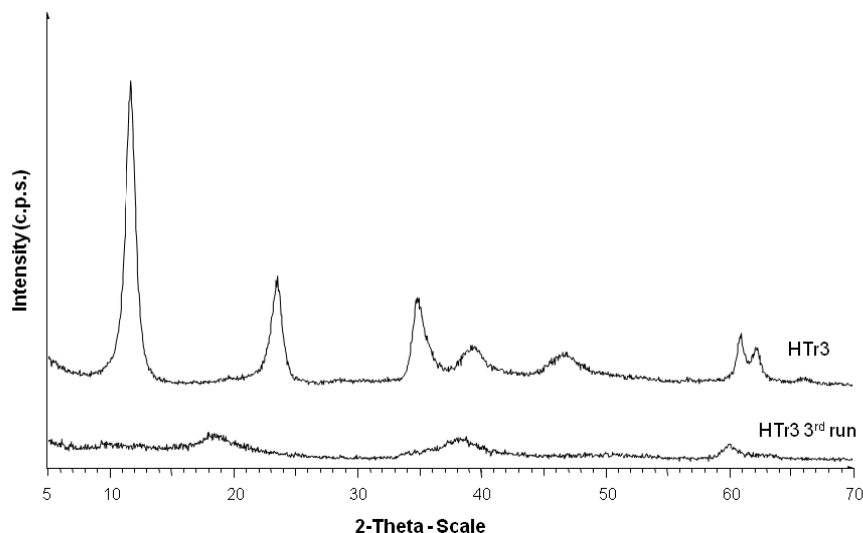


Figure 2.3.8. X-ray patterns for fresh and used catalyst HTr3.

The adsorption of reactants and products of reaction can be responsible of the deactivation of the catalyst. This poisoning of the catalyst surface prevents the accessibility of the OH⁻ centres leading to a loss of activity with every consecutive run. After three consecutive runs the catalyst was washed with ethanol and a new attempt was done to characterise the used catalyst by means of PXRD (Figure 2.3.8). The analysis revealed a loss of the crystalline structure of the original meixnerite-like phase after the third cycle. This modification of the solid is reminiscent of that observed upon calcination. Here the solid is not carbonated, but the TGA experiment shows that dehydration starts at about 100 °C. The reaction temperature of 130 °C is

then sufficient to provoke a significant dehydration, if we take into account that the reactor is swept by argon, and the reaction time relatively long. It can then be reasonably supposed that the dehydration of the catalyst surface during reaction is the cause of the decrease of catalytic activity.

The slower deactivation of the F-exchanged sample reported in Table 2.3.8 agrees with this hypothesis: this HT4-F sample is the most active and shows the lower deactivation since full conversion of glycerol is still observed at 6h of reaction in the fourth run. It can be seen on Table 2.3.2 that this sample shows the lower second loss, attributed to dehydroxylation of the surface. This can be accounted for by the substitution of part of OH by stable F anions, so that the bimolecular process of condensation of hydroxyls is unfavoured.

Table 2.3.8. *Catalytic properties of reused HT4-F catalyst*

Run	Reaction time (h)	Glycerol converted (%)	Yield	Yield
			GC (%)	GDC (%)
1	6	99	57	42
2	6	99	44	55
3	6	83	99	1
	7	99	94	5
4	6	87	100	--
	8	99	87	12
5	6	34	100	--
	9	97	95	2

2.3.4. Conclusions

Summarizing, we have prepared different hydrotalcite-like compounds with Mg/Al molar ratios between 2 and 4 which have been tested in the transesterification of glycerol with diethyl carbonate to obtain glycerol carbonates in a green and efficient method under soft conditions. The experimental results show that the type of basic centre has a large influence on the activity in the heterogeneous transesterification

2.3. TUNABLE BASIC AND TEXTURAL PROPERTIES OF HT-DERIVED MATERIALS

reaction. In addition, the absorption capacity of the Brønsted heterogeneous catalyst favours the subsequent transesterification of the glycerol carbonate.

Large amounts of water lead to a certain deactivation provoking an induction period in the first time of reaction as observed with catalyst HTr2. Catalyst HTr3 was the best catalyst and could be recycled a few times. The basicity of the catalysts can also be tuned by anion exchange. Thus, catalyst HT4-F was one of the most active in the transesterification of glycerol. Moreover, it has been demonstrated that this sort of reactions (transesterification reactions) do not require a great basicity, since a non-activated hydrotalcite behaving as a Brønsted base such as HT4-CO3 has a catalytic activity comparable to that found in calcined hydrotalcites. Thus it is concluded that Mg/Al mixed oxide catalysts and rehydrated catalysts are promising candidates for the transesterification reaction and would be able to replace homogeneous catalysts that have similar activity. It is however observed that the meixnerite active phase showed a poor mechanical-strength, since the solid changes with every consecutive run due to the strong affinity between the surface of the catalyst and the products of the reaction. This opens a path to a possible stabilisation of catalytic activity.

Reference

1. M.J. Climent, A. Corma, P. De Frutos, S. Iborra, M. Noy, A. Velty, P. Concepción, *J. Catal.*, 269 (2010) 140.
2. Y. Zheng, X. Chen and Y. Shen, *Chem. Rev.*, 108 (2008) 5253.
3. D. Herculat, A. Eggers, A. Strube, J. Reinhard, DE101108855A1 (2002).
4. G. Rokicki, P. Rakoczy, P. Parzuchowski, M. Sobiecki, *Green Chem.*, 7 (2005) 29.
5. J. B. Bell, V. A. Currier, J. D. Malkemus, US Pat. 2 915 529, 1959.
6. C. Vieville, J.W. Yoo, S. Pelet, Z. Mouloungui, *Catal. Lett.*, 56(4) (1999) 245.
7. M. Aresta, A. Dibenedetto, F. Nocito, C. Pastore, *J. Mol Catal. A: Chem.*, 257 (2006) 149.
8. J.W. Yoo, Z. Mouloungui, *Stud. Surf. Sci. Catal.*, 146 (2003) 757.
9. Y.V.S. Rao, D.E. De Vos, P. Jacobs, *Angew. Chem. Int. Ed. Engl.*, 36 (1997) 2661.
10. F. Figueras, *Topics in Catalysis*, 29, (2004).
11. F. Zhang, X. Xiang, F. Li, X. Duan, *Catal Surv Asia*, 12 (2008) 253.
12. G. Centi, S. Perathoner, *Microporous and Mesoporous Materials*, 107 (2008) 3.
13. J.L. Shumaker, C. Crofcheck, S.A. Tackett, E. Santillan-Jimenez, T. Morgan, Y. Ji, M. Crocker, T. J. Toops, *Appl. Catal. B: Environmental*, 82 (2008) 120.
14. M.G. Álvarez, A.M. Segarra, S. Contreras, J.E. Sueiras, F. Medina and F. Figueras, *Chem. Eng. J.*, 161 (2010) 340.
15. P. Tundo and M. Selva, *Acc. Chem. Research*, 35(9) (2002) 706.
16. A. Takagaki, K. Iwatani, S. Nishimura and K. Ebitani, *Green Chem.*, 12 (2010) 578.
17. Corma, S.B. Abd Hamid, S. Iborra, A. Velty, *J. Catal.* 234 (2005) 340.
18. B.F. Sels, D.E. De Vos, P.A. Jacobs, *Catal. Rev.* 43 (2001) 443.
19. A.L. McKenzie, C.T. Fishel, R.J. Davis, *J. Catal.* 138 (1992) 547.
20. J.I. Di Cosimo, V.K. Diez, M. Xu, E. Iglesia, C.R. Apesteguia, *J. Catal.*, 178 (1998) 499.
21. K.K. Rao, M. Gravelle, J.S. Valente, F. Figueras, *J. Catal.*, 173 (1998) 115.
22. J. Roelofs, A. J. van Dillen, K. P. de Jong, *Catal.Today* 60 (2000) 297.
23. S. Kannan, R.V. Jasra, *J. Mater. Chem.*, 10 (2000) 2311.

2.3. TUNABLE BASIC AND TEXTURAL PROPERTIES OF HT-DERIVED MATERIALS

24. S. K. Sharma, P. K. Kushwaha, V. K. Srivastava, S. D. Bhatt, R. V. Jasra, *Ind. Eng. Chem. Res.*, **46** (2007) 4856.
25. D. Kishore, S. Kannan, *App. Catal. A*, **270** (2004) 227.
26. R.J. Chimentao, S. Abelló, F. Medina, J. Llorca, J.E. Sueiras, Y. Cesteros, P. Salagre, *J. Catal.*, **252** (2007) 249.
27. F. Prinetto, G. Ghiotti, R. Durand, D. Tichit, *J. Phys. Chem. B*, **104** (2000) 11117.
28. S. Abelló, F. Medina, D. Tichit, J. Pérez-Ramírez, Y. Cesteros, P. Salagre, and J.E. Sueiras, *Chem. Commun.* (2005) 1453.
29. B.M. Choudary, M.L. Kantam, V. Neeraja, K.K. Rao, F. Figueras, L. Delmotte, *Green Chem.*, **3** (2001) 257.
30. T. Sate, H. Fujita, T. Endo and M. Shimada, *React. Solids*, **5** (1988) 219.
31. A.S. Bookin and V.I. Drits, *Clays Clay Miner.*, **41** (1993) 551.
32. F. Cavani, F. Trifirò, A. Vaccari, *Catal. Today*, **11** (1991) 173-301.
33. M. Gazzano, W. Kagunya, D. Matteuzzi and A. Vaccari, *J. Phys. Chem. B*, **101** (1997) 4514.
34. D. Tichit, M.N. Bennani, F. Figueras and J.R. Ruiz, *Langmuir*, **14** (1998) 2086.
35. S. Miyata, *Clays & Clay Miner.* **28** (1980) 50-6.
36. S. Abelló, F. Medina, D. Tichit, J. Pérez Ramirez, J. E. Sueiras, P. Salagre, Y. Cesteros, *Appl. Catal. B*, **70** (2007) 577.
37. P. Kustrowski, D. Sulkowska, L. Chmielarz, R. Dziembaj, *Appl. Catal.: A*, **302** (2006) 317.
38. S.K. Sharma, P.K. Kushwaha, V.K. Srivastava, S.D. Bhatt, R.V. Jasra, *Ind. Eng. Chem. Res.*, **46** (2007) 4856.
39. E. Kanazaki, *Inorg. Chem.*, **73** (1998) 2588.
40. H.A. Prescott, Z.J. Li, E. Kemnitz, A. Trunchke, J. Deutsch, H. Lieske and A. Auroux, *J. Catal.*, **234** (2005) 119.
41. J. Sanchez Valente, F. Figueras, M. Gravelle, P. Kumbhar, J. Lopez and J. -P. Besse, *J. Catal.* **189** (2000) 370.
42. R. Phillipp, K. Fujimoto, *J. Phys. Chem.*, **96** (1992) 9035.
43. C. Morterra, G. Ghiotti, F. Boccuzzi, S. Coluccia, *J. Catal.*, **51** (1978) 299.
44. G. Wu, X. Wang, Y. Sun, *App. Catal. A*, **377** (2010) 107.
45. D.G. Cantrell, L.J. Gillie, A. F. Lee, K. Wilson, *App. Catal. A*, **287** (2005) 183.

46. W. Xie, H. Peng, L. Chen, *J. Mol. Catal.* 246 (2006) 24.

47. H. Zeng, Z. Feng, X. Deng Y. Li, *Fuel*, 87 (2008) 3071.

UNIVERSITAT ROVIRA I VIRGILI

HYDROTALCITE-LIKE COMPOUNDS FOR THE VALORISATION OF RENEWABLE FEEDSTOCKS

Mayra García Álvarez

Dipòsit Legal: T. 724-2012

CHAPTER 3

SUPPORTED HYDROTALCITE-LIKE MATERIALS FOR TRANSESTERIFICATION OF GLYCEROL

Article:

From glycerol to glycerol carbonate: Transesterification over hydrotalcites supported on carbon nanofibers as highly active heterogeneous catalysts.

Mayra G. Álvarez, Anne M. Frey, Harry J. Bitter, Anna M. Segarra, Krjin P. de Jong and Francesc Medina.

(To be submitted)

Article:

Synthesis of glycerol carbonates by transesterification of glycerol in a continuous system using supported hydrotalcites as catalysts.

Mayra G. Álvarez, Martina Pliskova, Anna M. Segarra, Francesc Medina and François Figueras.

(Published in Applied Catalysis B: Environmental, 113-114 (2012) 212-220)

UNIVERSITAT ROVIRA I VIRGILI

HYDROTALCITE-LIKE COMPOUNDS FOR THE VALORISATION OF RENEWABLE FEEDSTOCKS

Mayra García Álvarez

Dipòsit Legal: T. 724-2012

CHAPTER 3

SUPPORTED HYDROTALCITE-LIKE MATERIALS FOR TRANSESTERIFICATION OF GLYCEROL

3.1. INTRODUCTION

As described during this work, the catalytic properties of HTs make full use of the inherent properties of these materials. These properties include: (1) a wide range of choice of M^{II} and M^{III} (and even M^{IV}) cations; (2) an unlimited combination of M^{II} and M^{III} with two or more types; (3) a free selection of anions; and (4) a nearly homogeneous distribution of cations in the brucite-like layers and anions in the interlayer spacing. Thus in principle, the catalytic activity of hydrotalcite-like compounds can be well controlled by adjusting these properties.

Recent studies have shown that the actual catalytic active sites in HTs are located at the edge of the platelets.¹ Generally, the number of exposed edge active sites is limited by the lateral size of the HT platelets and decrease with increasing the particle size. So that solid base catalyst composed of nanometer size particles should have more active sites on the surface than those of large particles, thus enhancing the catalytic activity. Therefore, new synthesis approaches of HTs have been developed focused on the control of particle size in order to maximize the number of active sites.^{2,3} Several approaches have been reported by using ultrasound during synthesis⁴ or reconstruction.² The resulting materials showed a significant increase in the activity in several base catalysed reactions, such as aldol condensations or isomerisation reactions. However, for nanometer sized catalyst particles there are considerable difficulties in separating and reclaiming the catalyst at the end of the reaction in liquid systems. An effective solution to this problem is to select an appropriate material to support and disperse HT particles. Recently, Othman *et al.*⁵

3.1. INTRODUCTION

have reported the synthesis of MgAl-HT coated on commercial zeolites to improve the adsorption of CO₂. In situ growth of MgAl-HT films over anodic aluminium oxide/aluminium has been reported by Lü *et al.*⁶ These materials showed to be more efficient in aldol condensation than their powdered analogous HT. More recently, it has been reported the in situ crystallisation of HTs in mesoporous structures, such as SBA-15.⁷ The resulted HT showed a crystallite size of about 9 nm, since the HT crystallised into the pore channels of the mesoporous structure. High active catalysts in Claisen-Schmidt condensation were prepared by formation of HT crystals inside the porous of a mesoporous carbon (CMK-41).⁸ Carbon nanotubes (CNTs) have also been used as support for HT's assembly.⁹ In this line, Winter *et al.*¹⁰ have reported carbon nanofibers-supported hydrotalcites with crystallite size of 20 nm. The resulting activated catalyst showed a high activity in the self-condensation of acetone and in the condensation of citral with acetone compared to that showed by the analogue bulk. So the increase in catalytic activity seems to be related to the small particle size of the hydrotalcites materials.

Based in this claims, in this chapter is reported the catalytic behaviour of hydrotalcite-supported materials in the transesterification of glycerol with diethyl carbonate. Two different types of supported materials were studied: firstly hydrotalcites supported on CNFs for the transesterification of glycerol in a batch reactor, and secondly hydrotalcites supported on α - and γ -Al₂O₃ particles with controlled size to be used in the transesterification of glycerol by using a continuous system.

Reference

1. J.C.A.A. Roelofs, A.J. van Dillen, K.P. de Jong, *Catal. Today*, **60** (2000) 297.
2. S. Abelló, F. Medina, D. Tichit, J. Pérez-Ramírez, Y. Cesteros, P.Salagre, J.E. Sueiras, *Chem. Commun.* (2005) 1453.
3. F. Winter, V. Koot, A. J. van Dillen, J. W. Geus, K. P. de Jong, *J. Catal.*, **236** (2005) 91.
4. X. Xie, X. Ren, J. Li, X. Hu, Z. Wang, *J. Nat. Gas Chem*, **15** (2006) 100
5. M.R. Othman, N.M. Rasid, W.J.N. Fernando, *Chem. Eng. Sci.*, **61** (2006) 1555.
6. Z. Lü, F. Zhang, X. Lei, L. Yang, S. Xu, X. Duan, *Chem. Eng. Sci.*, **63** (2008) 4055.
7. L. Li, J. Shi, *Chem. Commun.* (2008) 996.
8. A. Dubey, *Green Chem.*, **9** (2007) 424.
9. H. Wang, X. Xiang, F. Li, *AIChE J.*, **56** (2010) 768.
10. F. Winter, A. J. Van Dillen and K. P. de Jong, *Chem. Commun.* (2005) 3977.

3.2. FROM GLYCEROL TO GLYCEROL CARBONATE: TRANSESTERIFICATION OVER HYDROTALCITES SUPPORTED ON CARBON NANOFIBERS AS HIGHLY ACTIVE HETEROGENEOUS CATALYSTS

3.2.1. Introduction

Glycerol is produced in large quantities as a by-product of the biodiesel production and after several refining processes glycerol of industrial and pharmaceutical degree is obtained. Its commercialisation increases the profitability of biodiesel. However, the increased glycerol supply, due to the rising trend of biodiesel production, is pushing its price down. Thus, it is relevant to assure new commercialisation channels of glycerol by exploring alternative strategies for transforming it into more valuable products. Several conversion processes are described in the literature transforming glycerol into value-added products,¹ such as: ketomalonic acid by selective oxidation, fuels oxygenate by etherification^{2,3} or by acetylation⁴, propyleneglycol by hydrogenolysis, acrolein by dehydration,⁵ highly branched polymers by esterification, synthesis gas by reforming.^{6,7} Glycerol carbonate is one of the glycerol derivatives with increasing interest in the chemical industry⁸⁻¹² and is an useful compound with a large potential as a novel component of gas-separation membranes¹³ or biolubricant. Glycerol carbonate can be used for the synthesis of new functionalised polymers that might have interesting new applications such as polyesters, polycarbonates or polyurethanes. Likewise, it may be used in the synthesis of intermediates such as glycidol¹⁴ or as solvent for coatings, cosmetics, personal care, detergents...

Among others, transesterification of glycerol with a dialkyl carbonate to obtain glycerol carbonate is one of the simplest methods. Transesterification reactions can be carried out both in basic and acidic media; however, the transesterification of glycerol with dimethyl carbonate by using heterogeneous acidic catalysts is extremely low.¹⁵ We have previously reported the results of an exploratory study focussed on the synthesis of glycerol carbonate by the transesterification of glycerol with diethyl carbonate using basic heterogeneous catalysts based on Mg/Al hydrotalcite-like compounds.¹⁶ The results showed that Mg/Al mixed oxides and its rehydrated forms are efficient and reusable catalysts for the transesterification reaction, being able to replace homogeneous catalysts, such as K_2CO_3 , showing similar activity. Moreover, the non-toxicity, biodegradability and cleaner production process of diethyl carbonate (DEC) make it as a green reagent to be used as carbonylating agent.¹⁷ Along the same research lines, Takagaki *et al.* showed that an uncalcined hydrotalcite containing a hydromagnesite phase efficiently catalyzes glycerol carbonate synthesis from glycerol and DEC using DMF as solvent.¹⁸

3.2. FROM GLYCEROL TO GLYCEROL CARBONATE

Hydrotalcites (HT) are anionic clays which have the general formula $[M_n^{2+}M_m^{3+}(\text{OH})_{2(n+m)}]^{m+} A_{m/n}^{x-} \cdot y\text{H}_2\text{O}$, where M^{2+} and M^{3+} denote a divalent and a trivalent cation, respectively, and A^x is a charge compensating anion. This structure consist of brucite-like layers $[\text{Mg}(\text{OH})_2]$ in which magnesium cations are in the centre of octahedrons and hydroxyl groups are in its vertices and are connected forming layers. In HT, some divalent cations are substituted by trivalent cations introducing a positive charge, which is balanced by anions located in the interlayer. Additionally, crystallisation water molecules are also found in the interlayer. Changing the synthesis conditions can vary the lateral size of the layers and the degree of stacking.¹⁹

The controlled decomposition of hydrotalcite-like compounds leads to a well disperse and high surface areas mixture of their oxides which exhibit Lewis basicity and can be used as catalysts or catalytic supports in a great variety of reactions.^{12,20,21} The acid-base properties of calcined hydrotalcites can be modulated by changing the calcination temperature, the nature and amount of structural cations and also of the anions which are compensating the positive charge, as well as the preparative method.^{13,19,20} The mixture of the generated oxides after the calcinations of hydrotalcites shows a characteristic “memory effect”, so that can recover its original structure when contacting with water vapour or when immersed in liquid water, in absence of anions, converting the starting hydroxycarbonate to its topotactic rehydrated hydroxide. These rehydrated materials contain Brønsted basic sites^{22,23} due to the presence of OH^- as compensating anions in the interlayer space. This makes them useful for a wide number of base-catalysed reactions such as Knoevenagel and Claisen-Smith condensations,^{16,24,25} Michael additions or transesterification reactions.^{27,28}

Roelofs *et al.*²⁹ have stated that the active sites are likely located at the edges of the platelets, representing only a minor part of the Brønsted-sites in the hydrotalcite. Several attempts have been made to increase the number of active sites,^{23,30,31} however the exposed edge area is limited by the lateral size of HT crystallites. The size can be varied by using different synthesis methods and aging temperatures²³ or by applying ultrasound during synthesis or rehydration.^{29,30} On the other hand, the deposition of hydrotalcite nanolayers of 20 nm on carbon nanofibers gives place to supported catalysts 10 times more actives in the condensation of acetone than those obtained by conventional methods due to the higher amount of accessible sites.^{32,33} Based in these results, in this paper we report a study of the performance of these carbon nanofibers supported hydrotalcites (after heat treatment and calcination-rehydration) in the transesterification of glycerol with diethyl carbonate and the comparison with that of unsupported hydrotalcites. The influence of the reconstruction method (liquid-phase and gas-phase rehydration) was also investigated.

3.2.2. Experimental

i. Catalysts preparation

Hydrotalcite supported on CNF (Mg/Al = 2) was prepared as follows: magnesium and aluminium (with a molar ratio 2:1) was introduced into 5 g of oxidised carbon nanofibers (prepared as described elsewhere^{32,33}) by incipient wetness impregnation of an aqueous solution of the corresponding nitrates (0.7 mL/g) in such a way that a loading of 12 wt% of HT was obtained. The material was kept at room temperature for 1 h for equilibration and then was dried at 393 K for 2 h in static air. A second impregnation step with a base solution (containing 8.3 M NaOH and 0.56 M Na₂CO₃) was performed. The resulted material was aged for 18 h at 333 K in a water saturated N₂ atmosphere, followed by washing with deionised water (3 x 20 mL). Finally, the sample was dried at 393 K for 12 h and sieved to a fraction of 20-150 micron.

For comparative reasons, an unsupported hydrotalcite with a Mg/Al molar ratio of 2 was prepared by coprecipitation of magnesium and aluminium nitrates at a constant pH as described below. The appropriate amounts of Mg(NO₃)₂·6H₂O and Al(NO₃)₃·9H₂O were dissolved in 150 cm³ of distilled water and added dropwise into a glass vessel which initially contained 200 cm³ of deionised water. The pH was controlled by adding a 2M NaOH solution and was kept at 10. Both solutions were mixed under vigorous stirring and the suspension was stirred overnight at room temperature. The precipitated solid was filtered and washed several times with water and dried at 383 K to yield the parent hydrotalcite.

Activation of the Mg/Al supported hydrotalcite (HT-CNF) was performed by either thermal decomposition in Ar by heating at 10 K/min up to 773 K (denoted below as HT-CNFc) for 3 h or calcination followed by rehydration under inert atmosphere in either liquid or gas phase. For rehydration in liquid phase, 0.3 g of HT-CNFc sample were dispersed into 10 mL of deionised and decarbonated water and stirred over 24 h at room temperature. The catalyst was separated by centrifugation, washed with ethanol and dried at 100 °C under inert atmosphere. The sample was denoted as HT-CNFrl. The rehydration in gas phase was performed as follows. The as-synthesised (HT-CNF) sample was heated under an Ar flow to 723 K with a rate of 10 K/min for 3 h. Then, the sample was rehydrated by passing through the sample at room temperature during 72 h a flow of argon (100 mL/min) saturated with decarbonated water. This sample was denoted as HT-CNFrg.

The bulk hydrotalcite was activated by either thermal decomposition or thermal decomposition followed by rehydration in liquid phase as previously described. The obtained samples were denoted as HTc and HTr, respectively.

3.2. FROM GLYCEROL TO GLYCEROL CARBONATE

ii. *Characterisation*

Mg and Al elemental chemical analyses of the bulk samples were obtained by ICP analysis using a ICP-Spectro Arcos before the samples were dissolved in HNO₃. Specific surface areas were determined by nitrogen adsorption at 77 K using a Quadrasorb SI equipment. Samples were previously degassed in situ at 393 K under vacuum. Surface areas were calculated using the Brunauer-Emmet-Teller (BET) methods over a p/p_0 range where a linear relationship was maintained. X-ray diffraction (XRD) powder patterns were collected on a Siemens EM-10110BU diffractometer model D5000 fitted with a Cu K α (1.541 Å) radiation source. Data were recorded over a 2θ range of 5-70° with an angular step of 0.05° at 6s/step which resulted in a scan rate of 0.5°/min. Patterns were identified using files from the Joint Committee on Powder Diffraction Standards (JCPDS).

Thermogravimetric analysis (TGA) curves were recorded in a TGA7 thermogravimetric analyzer apparatus from room temperature to 1173K, at a heating rate of 5 K/min.

TEM images were obtained with a JEOL 1011 TEM operating at 80 kV. Samples were dispersed in ethanol and supported on a copper grid.

iii. *Standard batch catalytic transesterification reaction*

Glycerol (99%) and diethyl carbonate (DEC) (99.5%, GC grade) were purchased from Aldrich and used without any further purification. Ethanol (98%) from Aldrich was used as a solvent to characterize the products obtained. Transesterification reactions were performed in a three-neck round-bottomed flask equipped with a condenser. Typically, the flasks were charged with an excess of DEC (38.95 g) and glycerol (1.85 g). Freshly activated catalyst (0.30 g) was added and the experiment started with mechanical stirring under argon at 403 K. Stirring was continued until the completion of the reaction. Aliquots were periodically withdrawn, filtered and quantified by GC analysis equipped with a FID detector. This was performed on a Shimadzu GC (QP 2010) with a Zebron ZW-WAX capillary column.

iv. *Recycling experiments*

We investigated the reuse of the catalysts in the transesterification reaction of glycerol with DEC under the same reaction conditions that were used for the standard transesterification reaction. The reaction mixture was removed with a syringe equipped with a microfilter when the reaction had finished, leaving the catalyst in the smallest possible amount of liquid. The reaction mixture was then washed twice with DEC at 403 K. After that, a new charge of reactants was added to the used catalyst and the next run was performed.

3.2.3. Results and discussion

i. Characterisation of the catalysts

To confirm the Mg/Al molar ratio of bulk hydrotalcites, ICP analysis of samples was performed. The as-synthesised and rehydrated samples, HTas and HTr, presented Mg/Al molar ratios very close to that used in solution during the preparation with the values 2.09 and 2.05, respectively.

Figure 3.2.1 shows the normalised PXRD patterns of the supported materials at different stage of the synthesis as well as after their use in the catalytic reaction. All the samples presented diffraction lines due to the presence of hydrotalcite and the CNF support. The most intense line at $2\theta \approx 27^\circ$ corresponds to the diffraction of the CNF (graphite, JCPDS 01-075-1621). The plane (003) of hydrotalcite can be distinguished at angles $2\theta \approx 12^\circ$ and presents higher broadening than that presented by the pure hydrotalcite. This indicates that the crystallite size in the supported hydrotalcite is smaller than that of the pure hydrotalcite. After calcination at 723 K and subsequent rehydration in absence of CO_2 , the original layered structure was recovered, because of the well-known “memory effect”³⁴ where the original nitrate and carbonate anions have been replaced by Brønsted OH^- sites. The diffraction planes displayed by HT-CNF were also observed in the rehydrated samples. It was noticeable the peak broadening produced in the (003) plane for rehydrated samples compared with the HT-CNF sample, especially for the samples rehydrated in liquid phase (HT-CNFrl). Moreover, the relative intensity of the characteristic peaks of HT with respect to the most intense graphite reflection ($2\theta \approx 27^\circ$) was decreased. This fact is indicative of a loss of crystallinity.

The line broadening is even more pronounceable in used samples (Figure 3.2.1 d and e, respectively) indicating a smaller crystallite size than fresh catalysts along the (003) plane.

Representative TEM micrographs of synthesised and rehydrated samples (HT-CNFas, HT-CNFrl and HT-CNFrg, respectively) are given in Figure 3.2.2. TEM analysis of HT-CNF revealed well distributed small hexagonal HT crystallites present on the carbon nanofibers and it was not observed isolated hydrotalcite formations separated of the fibers. Some differences in morphology were observed for the sample rehydrated in liquid phase (HT-CNFrl) and a growth of the HT crystals was observed. It seems that rehydration in liquid phase favours the dissolution/recrystallisation processes produced during the rehydration of the mixed oxides. At this stage, the HT particles can migrate over the fibers and recrystallise to form larger particles. So, this sample presented agglomerations of HT crystals. This behaviour has not been observed in that sample rehydrated in gas phase.

3.2. FROM GLYCEROL TO GLYCEROL CARBONATE

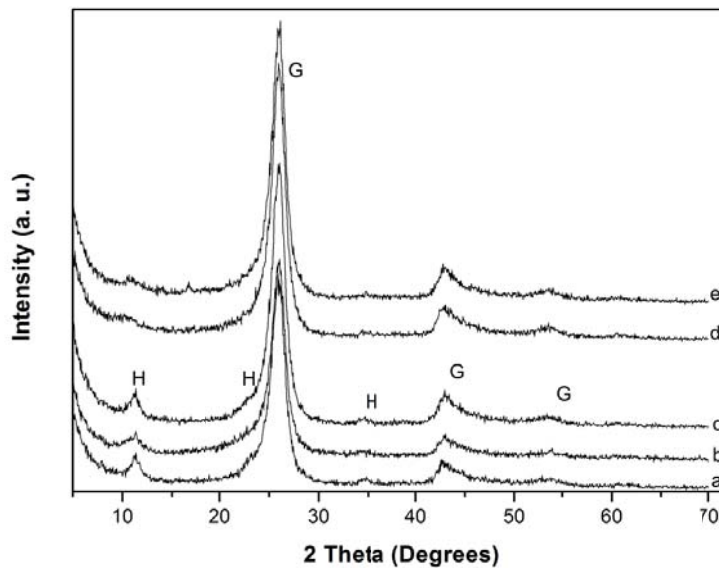


Figure 3.2.1. X-ray diffraction patterns of a) HT-CNFs; b) HT-CNFrl; c) HT-CNFrg; d) HT-CNFrl after 1 run and e) HT-CNFrg after 1 run. (H) represents the hydrotalcite phase and (G) represents the graphite phase.

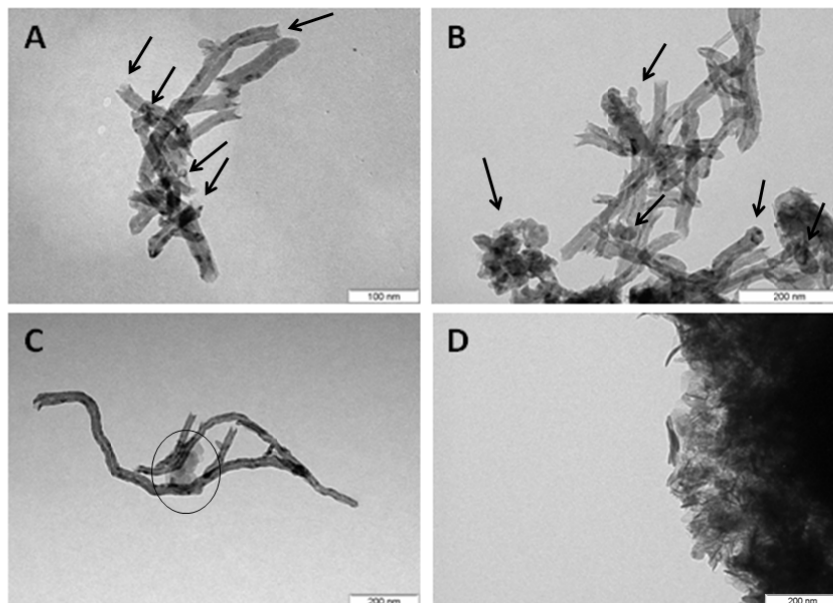


Figure 3.2.2. TEM images of A) HT-CNFs; B) HT-CNFrg; C) and D) HT-CNFrl.

The results of thermogravimetric analysis (TGA) of the supported samples HT-CNF, HT-CNF_{rl} and HT-CNF_{rg} are displayed in Figure 3.2.3. The supported hydrotalcites presented two weight loss steps during the decomposition in N₂ atmosphere. First, the removal of physisorbed and interlayer water is produced at temperatures up to 473-483 K. Then, the dehydroxylation of the layers and the decarbonation of the as-synthesised sample or dehydroxylation of the interlayer hydroxyl anions of rehydrated samples are produced above 573 K.^{21,35} This pattern of decomposition is rather specific for hydrotalcites. The first weight loss was greater in the sample rehydrated in liquid phase than in the sample rehydrated in gas-phase, which suggests that the former has more adsorbed water molecules.

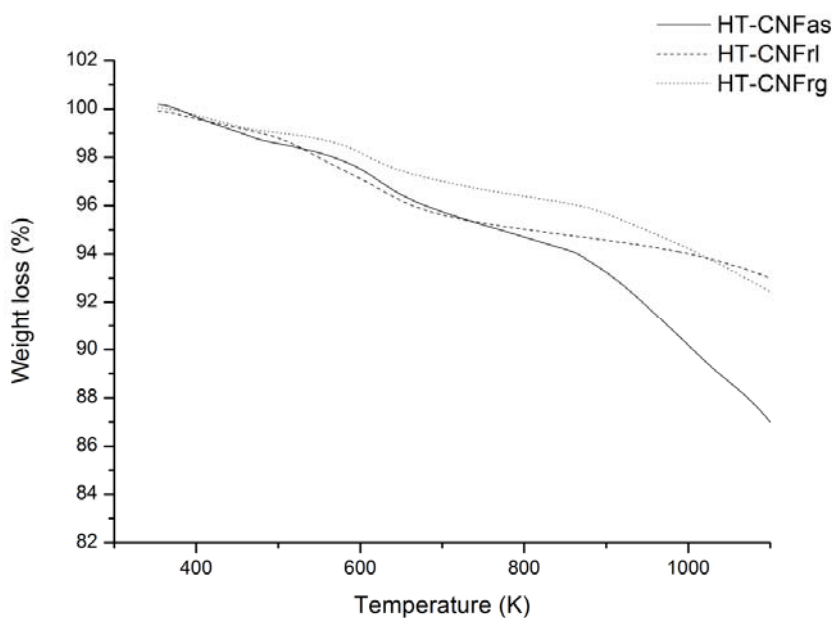


Figure 3.2.3. Thermogravimetric analyses of supported hydrotalcites HT-CNFas, HT-CNFrl and HT-CNFrg.

TGA analyses of supported HT in O₂ were performed to calculate the loading of hydrotalcite on the CNF support (Table 3.2.1). From the TGA results in N₂ and O₂ a loading of 12% of hydrotalcite was calculated in HT-CNF and in both rehydrated forms (HT-CNF_{rl} and HT-CNF_{rg}).

3.2. FROM GLYCEROL TO GLYCEROL CARBONATE

Table 3.2.1. *Physico-chemical properties of the different materials*

Catalyst	S _{BET} (m ² ·g ⁻¹)	Pore volume (cm ³ ·g ⁻¹)	HT loading (wt%) ^a
CNF	190	0.45	--
HT-CNFas	172	0.33	12
HT-CNFc	175	0.34	--
HT-CNFrl	173	0.35	12
HT-CNFrg	164	0.34	12
HT-CNFc _{used}	167	0.33	--
HT-CNFrl _{used}	166	0.35	--
HT-CNFrg _{used}	159	0.34	--

^aCalculated by TGA

Adsorption of N₂ was used to measure the specific surface area, pore volume and pore distribution of the pure and supported hydrotalcites. Results are summarised in Table 3.2.1. The adsorption-desorption isotherms of supported samples at 77.2 K confirm the presence of mesopores and the absence of micropores. The BET specific surface area of the supported samples is relatively high; however, a significant decrease in surface area and pore volume in supported HT (HT-CNF, HT-CNFrl and HT-CNFrg) with respect to that measured in CNF was observed. This is indicative of a partially filled of the fibers with HT. The rehydrated supported HTs present the same textural properties of the original HT-CNFas material so the specific surface area and pore volume was maintained after the calcination-rehydration treatment of HT-CNF.

The BET specific surface area for the bulk hydrotalcite was in accordance with those reported in the literature.³⁵

ii. *Transesterification of glycerol*

The transesterification of glycerol with diethyl carbonate over HT-CNF samples and unsupported hydrotalcites was performed. The possibility of diffusional limitations was estimated computing the Thiele modulus modified by Weisz.³⁶

$$\Phi = vR^2/(DeffC_0)$$

where v is the rate (mol s⁻¹ g⁻¹), R the radius of the catalyst particles (here 0.075 mm), C_0 the concentration of glycerol (5 × 10⁻⁴ mol ml⁻¹), and $Deff$ the diffusion coefficient (taken as 10⁻⁴ cm² s⁻¹). The Φ value is about 0.2 which is similar to that estimated by Davis *et al.*³⁷ for the transesterification of tributyrin with methanol with bulk hydrotalcites ($\Phi = 0.3$). Diffusion limits the overall process when $\Phi = 1$, therefore the effects of mass transfer did not limit the process.

The transesterification reaction of glycerol with DEC was investigated using the calcined and rehydrated samples from supported and unsupported hydrotalcite-like materials as catalysts.

Transesterification was performed at 403 K under a small flow of Ar with a molar excess of DEC/glycerol (17:1) to shift the reaction equilibrium towards the products. The catalytic properties were determined by measuring the glycerol conversion versus time.

Figure 3.2.4 shows the results of the catalytic performance using activated supported and pure hydrotalcites (Insert in Figure 3.2.4). A high activity for glycerol transesterification was found for the supported catalyst, especially the calcined one (HT-CNFc) in comparison with that observed for bulk activated hydrotalcites. The bulk calcined HT showed higher initial rate than that showed by the rehydrated catalyst: $15 \cdot 10^{-2}$ and $3 \cdot 10^{-2}$ mmol Glyg⁻¹cat·h⁻¹, respectively (Table 3.2.2). The glycerol conversion seems to occur with an induction period in this bulk HTs being this effect more pronounced in the rehydrated catalyst. This behaviour may be due to the great hydrophilic character of the hydrotalcite surface in the rehydrated form. After this initial period, the glycerol conversion increased greatly to form a plateau at total glycerol conversion from 22 h of reaction.

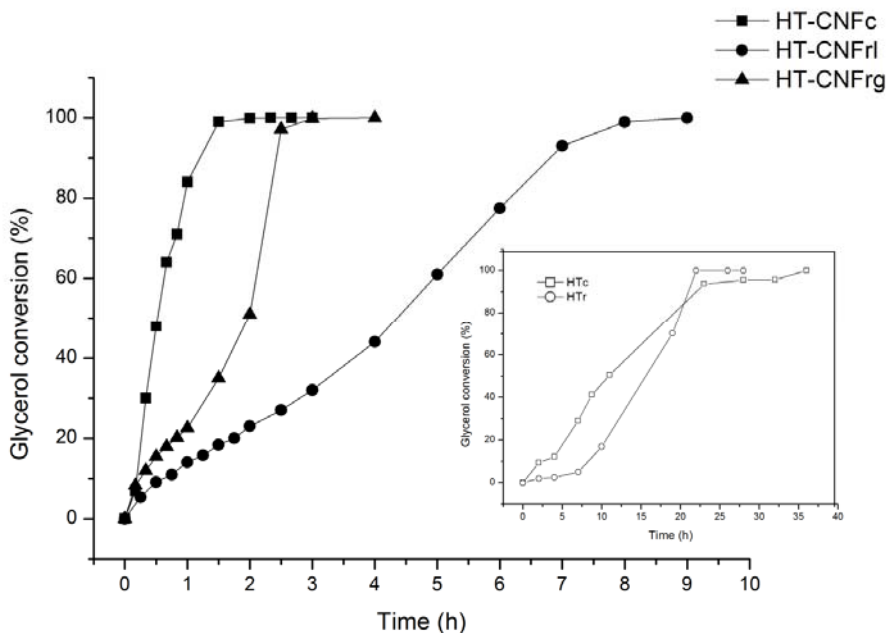


Figure 3.2.4. Catalytic behaviour of the different catalysts at 403 K and a glycerol : DEC molar ratio 1:17. Insert: Catalytic behaviour of bulk hydrotalcites under the same standard conditions.

3.2. FROM GLYCEROL TO GLYCEROL CARBONATE

Table 3.2.2. Initial reaction rates for transesterification of glycerol with DEC with the HT catalysts under the same standard conditions

Catalyst	Initial rate (mmol Gly·g ⁻¹ cat·h ⁻¹)	Initial rate (mmol Gly·g ⁻¹ HT·h ⁻¹)
HTc	18·10 ⁻²	18·10 ⁻²
HTr	3·10 ⁻²	3·10 ⁻²
HT-CNFc	6	53
HT-CNFrl	0.4	3
HT-CNFrg	0.8	7

All the activated supported materials (decomposed and rehydrated catalysts) were active for the transesterification of glycerol with diethyl carbonate and they presented much higher catalytic activity than bulk HTs. The best catalytic performance was found for HT-CNFc catalyst with an initial rate of 53 mmol_{gly} g⁻¹HT h⁻¹. On the other hand, rehydrated catalyst, HT-CNFrl, showed a noteworthy lesser activity with an initial rate of 4 mmol_{gly} g⁻¹HT h⁻¹ and 8 h were necessary to achieve total glycerol conversion compared to that 1.5 h necessary in the case of the calcined catalyst (HT-CNFc) (Table 3.2.3.). Moreover, the consecutive transesterification of glycerol carbonate to yield glycerol dicarbonate occurred in a very low percentage (around 3% of glycerol dicarbonate after 8 h of reaction), being the catalyst less active the more selective to the first product of transesterification, i.e. glycerol carbonate. After the rehydration treatment in liquid phase, ICP analysis of the rehydration water was made to test the possibility of HT leaching during the reconstruction process. The results showed the absence of significant amounts of Mg and/or Al in the liquid phase, thus indicating the stability of the catalyst during the rehydration. However, based on the TEM micrographs, hydrotalcite particles seem to migrate and sinter in a high degree when rehydrated in liquid phase, producing larger HT crystals located on the edge of the fibers.

Table 3.2.3. Catalytic behaviour of the different materials tested in the transesterification of glycerol under standard conditions

Entry	Catalyst ^a	Reaction time (h)	Glycerol converted (%) ^b	Yield GC (%) ^b	Yield GDC (%) ^b
1	HTc	32	96	65	31
2	HTr	22	100	75	25
3	CNF	8	–	–	–
4	HT-CNFc	2	100	58	42
5	HT-CNFrl	8	99	96	3
6	HT-CNFrg	3	100	79	21
7	HT-CNFc ^{c,d}	5 ^c 7 ^d	99 ^c 99 ^d	47 ^c 87 ^d	52 ^c 12 ^d

^aAll the catalysts were tested under the same reaction conditions (0.3 g of catalyst, Gly:DEC 1:17, 403 K and 1 atm).

^bConversion and yields were determined by GC-FID.

^cConversion and yields found after a second run.

^dConversion and yields found after a third run.

To test the influence of the hydrothermal treatment, rehydration in gas phase of the calcined catalyst was performed (named HT-CNFrg). For that purpose, the as-synthesised sample was heated under an Ar flow to 723 K with a rate of 10 K/min for 3 h. Then, the sample was rehydrated by passing an argon flow (100 mL/min) saturated with water, through the sample at room temperature for 72 h. This rehydrated sample was used without further treatment (i.e. drying). HT-CNFrg also exhibited lower initial activity in the transesterification of glycerol than HT-CNFc catalyst; however, the initial rate is twice that showed by catalyst rehydrated in liquid phase (HT-CNFrl) and total glycerol conversion was observed after 3 h of reaction. The greater activity of HT-CNFrg with respect to HT-CNFrl is also reflected in the increased selectivity to the second product of condensation ($\approx 21\%$ after 3 h of reaction). The enhancement in activity in HT-CNFrg catalyst may be attributed to the higher amount of water contained in that sample rehydrated in liquid phase (HT-CNFrl) as indicated by TGA analysis. This excess of water in HT-CNFrl catalyst leads to

3.2. FROM GLYCEROL TO GLYCEROL CARBONATE

a certain decrease of the activity probably due to a strong interaction between glycerol and the catalysts because of the higher hydrophilic character of the catalyst. Consequently, water can hinder the reactants adsorption (mainly for diethyl carbonate), thus limiting the catalyst activity. Moreover, free water can even produce the hydrolysis of glycerol carbonate driving the equilibrium of the reaction again towards the formation of glycerol. Thus, hydrophobicity presented by calcined catalysts due to the CNF support may favour the transesterification of glycerol.

The activity of this kind of catalysts was previously studied by Winter *et al.*^{33,34} in the catalytic acetone self-condensation reaction, showing that the rehydrated hydrotalcites were the most active for both the bulk and the supported materials. Tichit *et al.*²² previously observed the same behaviour for MgAl hydrotalcites, being the rehydrated ones much more active and selective than their parent mixed oxides. We can conclude that the difference in activity between calcined and rehydrated catalysts depend on the type of reaction and/or the reactants involved. Comparing the activity of the supported materials in the transesterification of glycerol with DEC, it was observed that the calcined catalyst is more active than the rehydrated ones. Moreover, a trend was observed: higher amount of water in the catalyst led to a lower catalytic activity. However, the opposite behaviour was found in the aldolisation of acetone being those rehydrated catalysts the most active. In the case of transesterification of glycerol, higher amounts of water in the supported catalysts have shown to produce a negative effect on the catalytic activity. This could be due to a strong competence for the active basic sites which become less accessible, since while glycerol is highly soluble in water DEC is not soluble at all. Consequently, high excess of DEC respect to glycerol is needed to carry out the transesterification reaction. This effect is not produced in the self-condensation of acetone, since reactants are soluble in water and non competence is produced.

Studies previously performed in our group³⁸ showed that Brønsted basicity presented by rehydrated hydrotalcites is more favourable for this kind of reactions than Lewis basicity (presented in the parent mixed oxides), but they also noted an abnormal low activity for that sample containing high amounts of water (HTr2) observing an induction period in the first time of reaction (as shown in insert in Figure 3.2.4). So, despite to Brønsted basicity have shown to be favourable for this kind of reactions an excess in water led to a certain deactivation producing a decrease in the initial rate.

The characterisation by PXRD of the used supported catalysts (Figure 3.2.1 d and e) showed a small change in the structure marked by the line broadening of the (003) plane of the HT. This could be due to the possibility of a slight exfoliation of the HT layers during the reaction due to the presence of glycerol and mechanical stirring. On the other hand, the N₂ physisorption analyses of the used samples showed that the specific surface area and the pore volume remain almost identical.

The performance of carbon nanofibers (CNF) was also investigated in the transesterification of glycerol with diethyl carbonate and has been found that they did not display any activity.

iii. *Stability of the catalysts.*

An important aspect of the heterogeneous catalysts is their stability or reusability in batch reactors. The most stability was observed for the HT-CNFc sample. In several runs and after removing the reaction mixture and washing, a slight loss of activity in every consecutive run was observed. Total glycerol conversion was reached in the first run in 90 min, dropping to 85% and 80% for the second and the third run, respectively (Figure 3.2.5). However, remarkable changes were observed in the selectivity. The selectivity to the second product of transesterification (glycerol dicarbonate, GDC) was higher in the first run and diminished abruptly with every run until no glycerol dicarbonate is obtained in the third run. This change in selectivity is indicative of some deactivation of the catalyst and could be attributed to a strong adsorption of side products or a loss of HT phase from the HT-CNF samples during the reaction.

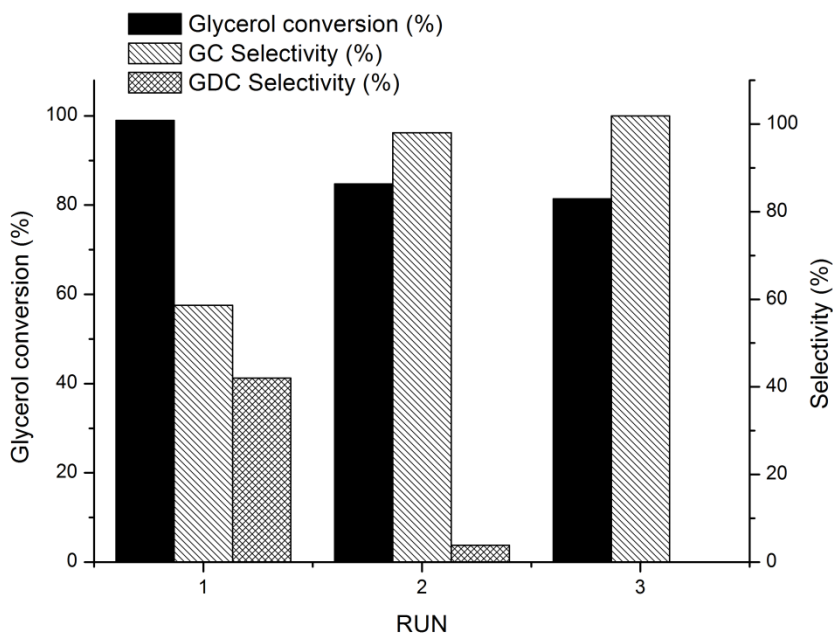


Figure 3.2.5. Catalytic performance of HT-CNFc catalyst after 90 minutes of reaction in three consecutive runs under standard reaction conditions.

One experiment was performed in order to see if some HT phase is dissolved during the reaction and to check the activity of these HT phase that could have been segregated from the HT-CNF catalyst. For this purpose, after 60 minutes of reaction, the HT-CNFc catalyst was removed from the reactor. As illustrated by the reaction

3.2. FROM GLYCEROL TO GLYCEROL CARBONATE

profile in Figure 3.2.6, the conversion of glycerol was stopped after the removal of the catalyst. Moreover, the composition of the products did not change. These results confirm that there was not catalytic contribution in homogeneous phase due to a possible leaching of HT. Moreover, no traces of Mg or Al were detected in the liquid phase at the end of this experiment. Furthermore, BET surface areas, as well as pore distribution of the catalyst remained practically identical after the transesterification reaction indicating the absence of pore blockage by fouling. These results indicate that the main cause of deactivation is due to a strong adsorption of some products on the surface by poisoning of the catalyst.

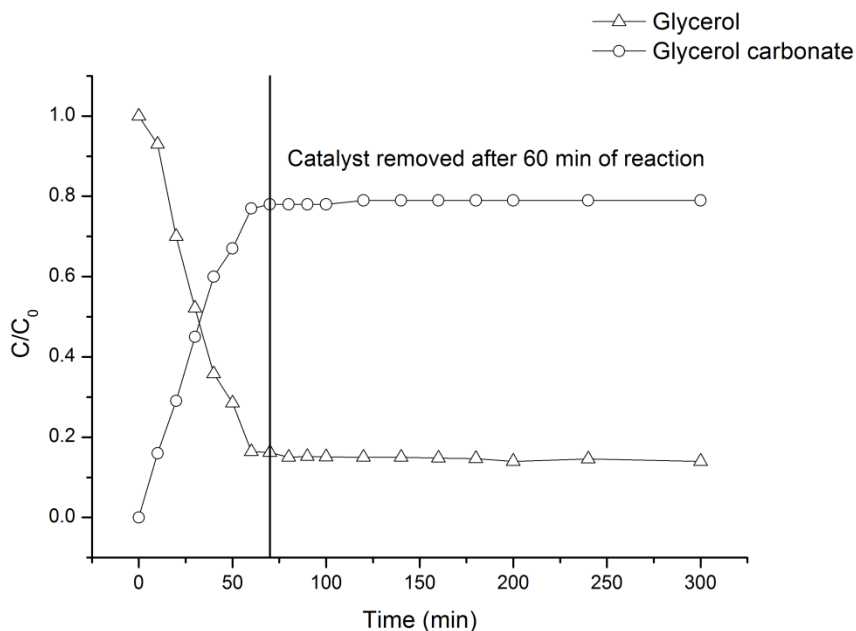


Figure 3.2.6. Transesterification profiles for HT-CNFc and removing of catalyst. Reaction was performed at 403 K and with a glycerol : DEC molar ratio 1:17.

3.2.4. Conclusions

Activated hydrotalcites supported on carbon nanofibers have been tested in the transesterification of glycerol with diethyl carbonate to obtain glycerol carbonate under soft conditions. These materials exhibited much greater catalytic activity in the transesterification of glycerol with DEC than bulk activated hydrotalcites. In particular, HT-CNFc showed a catalytic activity almost 300 times higher than that showed by bulk catalyst (HTc).

Large amounts of water in rehydrated samples provoked certain deactivation of the catalyst and a high induction period was observed in the case of rehydrated

hydrotalcite HTr. Moreover, it was found that the catalyst rehydrated in gas phase (HT-CNFr_g) revealed a catalytic activity higher than the catalyst rehydrated in liquid phase. Thus, the reconstruction method of the hydrotalcite has a great influence on the catalytic behaviour of the final catalyst. The greater catalytic activity of the calcined supported catalyst HT-CNF_c agrees with this hypothesis. The low-hydration degree of the mixed oxide together with the hydrophobicity of the CNF support led to the enhancement of the transesterification reaction.

Thus it is concluded that HT supported on carbon nanofibers are promising candidates for the transesterification reaction and would be able to replace homogeneous catalysts which present similar or lower performance under the same catalytic conditions.¹⁹ Moreover, calcined supported catalyst (HT-CNF_c) was able to be reused in three consecutive runs without significant loss of activity showing a considerable mechanical strength of the material. It is however observed that the rehydrated active phase showed a poorer mechanical-strength, since the solid slightly changes after the reaction due to the strong affinity between the surface of the catalyst and the products of the reaction.

3.2. FROM GLYCEROL TO GLYCEROL CARBONATE

Reference

1. M. Pagliaro, R. Ciriminna, H. Kimura, M. Rossi, C. Della Pina, *Angew. Chem. Int. Ed.* **46** (2007) 4434.
2. K. Klepáčová, D. Mravec, M. Bajus, *Appl. Catal. A: Gen.* **294** (2005) 141.
3. J. Barrault, J.M. Clacens, Y. Pouilloux, *Topics in Catal.* **27** (2004) 137.
4. J.A. Melero, R. Van Grieken, G. Morales, M. Paniagua, *Energy and Fuels* **21** (2007) 1782.
5. S.H. Chai, H.P. Wang, Y. Liang, B.Q. Xu, *J. Catal.* **250** (2007) 342.
6. A. Corma, G.W. Huber, L. Sauvanaud, P. O'Connor, *J. Catal.* **250** (2007) 307.
7. R.R. Soares, D.A. Simonetti, J.A. Dumesic, *Angew. Chem. Int. Ed.* **45** (2006) 3982.
8. M. Bandres, A. Deswartvaegher, C.P. De, Patent WO2007/080172.
9. M. Notari, F. Rivetty, Patent WO2004/052874.
10. D. Herault, A. Eggers, A. Strube, J. Reinhardt, Patent DE 10110855.
11. Traupe, P. Maurer, M. Moeller, S. Yung, M. Hallmann, A. Natsch, Patent DE 10323703.
12. A. Bher, J. Eilting, K. Irawadi, J. Leschinski, F. Lindner, *Green Chem.*, **10** (2008) 13.
13. A.S. Kovvali, K.K. Sikar, *Ind. Eng. Chem. Res.*, **41** (2002) 2287.
14. Z. Mouloungui, J. W. Yoo, C. A. Gachen, A. Gaset and G. Vermeersch, EP0739888.
15. J.R. Ochoa-Gómez, O. Gómez-Jiménez-Abesraturi, B. Maestro-Madurga, A. Pesquera-Rodríguez, C. Ramírez-López, L. Lorenzo-Ibarreta, J. Torrecilla-Soria, M.C. Villarán-Velasco, *Appl. Catal. A*, **366** (2009) 315.
16. M.G. Álvarez, A.M. Segarra, S. Contreras, J.E. Sueiras, F. Medina and F. Figueras, *Chem. Eng. J.*, **161** (2010) 340.
17. P. Tundo and M. Selva, *Acc. Chem. Research*, **35(9)** (2002) 706.
18. A. Takagaki, K. Iwatani, S. Nishimura and K. Ebitani, *Green Chem.*, **12** (2010) 578.
19. W.T. Reichle, *Solid State Ionics*, **22** (1986) 135.
20. *Layered Double Hydroxides*", Eds. X. Duan, D.G. Evans, Springer, Germany (2006).

21. V. Rives, Ed., *Layered Double Hydroxides: Present and Future*”, Nova Sci. Pub., Inc., New York (2001), and references therein.
22. D.Tichit, M. Naciri Bennani, F. Figueras, R. Tessier and J. Kervennal, *Appl. Clay Sci.* **13** (1998) 401.
23. A. Guida, L.M. Hassane, D. Tichit, F. Figueras, P. Geneste, *Appl. Catal. A*, **164** (1997) 251.
24. M.L. Kantam, B.M. Choudary, C.V. Reddy, K.K. Rao, F. Figueras, *Chem. Comm.* **9** (1998) 1033.
25. M.J. Climent, A. Corma, S. Iborra, J. Primo, *J. Catal.* **151** (1995) 60.
26. B.M Choudary, M.L. Kantam, C.R. Reddy, K.K. Rao, F. Figueras, *J. Mol. Catal. A* **146** (1996) 279.
27. G.S. Macala, A.W. Robertson, C.L. Johnson, Z.B. Day, R.S. Lewis, M.G. White, A.V. Iretskii, P.C. Ford, *Catal. Lett.* **122** (2008) 205.
28. B. Veldurthy, J.M. Clacens, F. Figueras, *J. Catal.* **229** (2005) 237.
29. J.C.A.A. Roelofs, D.J. Lensveld, A.J. van Dillen, K.P. de Jong, *J. Catal.* **203** (2001) 184.
30. S. Abelló, F. Medina, D. Tichit, J. Pérez-Ramírez, Y. Cesteros, P.Salagre, J.E. Sueiras, *Chem. Commun.* (2005) 1453.
31. R.J. Chimentao, S. Abelló, F. Medina, J. Llorca, J.E. Sueiras, Y. Cesteros, P. Salagre, *J. Catal.*, **252** (2007) 249.
32. F. Winter, A. Jos van Dillen, K.P. de Jong, *Chem. Comm.*, (2005) 3977.
33. F. Winter, V. Koot, A.J. van Dillen, J.W. Geus, K.P. de Jong, *J. Catal.*, **236** (2005) 91.
34. S. Miyata, *Clays & Clay Miner.* **28** (1980) 50-6.
35. F. Cavani, F. Trifiro, A. Vaccari, *Catal. Today* **11** (1991) 173.
36. P.B. Weisz, *Science*, **179** (1973) 433.
37. Y. Xi, R.J. Davis, *J. Catal.*, **254** (2008) 190.
38. M.G. Álvarez, R.J. Chimentão, F. Figueras, F. Medina, *Appl. Clay Sci.*, (2012) doi:10.1016/j.clay.2012.02.004.

UNIVERSITAT ROVIRA I VIRGILI

HYDROTALCITE-LIKE COMPOUNDS FOR THE VALORISATION OF RENEWABLE FEEDSTOCKS

Mayra García Álvarez

Dipòsit Legal: T. 724-2012

3.3. SYNTHESIS OF GLYCEROL CARBONATES BY TRANSESTERIFICATION OF GLYCEROL IN A CONTINUOUS SYSTEM USING SUPPORTED HYDROTALCITES AS CATALYSTS

3.3.1. Introduction

During the last years, a growing interest has been noticed for the development of renewable alternative fuels such as bio-diesel, produced from vegetable oils by transesterification processes with methanol or ethanol. The high biodiesel production capacity in the European Union and USA could create a surplus of glycerol obtained as by-product in this process. The formation of this glycerol (about 100 g/kg of bio-diesel)¹ represents a considerable technical and economic burden since it is not fully exploited on the market. Therefore, it is especially important to explore new applications for this product as well as alternative strategies for transforming it into new suitable products. A great number of publications have been reported in this field, highlighting the immense activity in the chemistry of glycerol.² Several important chemicals can be obtained from glycerol via oxidation, esterification, etherification, acetalisation, dehydrogenation, polymerisation and so on. Glycerol carbonate and its esters are most interesting derivatives of glycerol. They are relatively new materials in the chemical industry and, due to their properties (low toxicity, low flammability and low vapour pressure) have great potential as new component in gas-separation membranes, non-volatile solvents for dyes, lacquers, pharmaceuticals, detergents, adhesives, cosmetics, and biolubricants³ and for the synthesis of new functionalised polymers such as polyglycerol.⁴ Fuels also represent large scale applications, and Notari and Rivetti *et al.*⁵ recently reported that a mixture containing alkyl esters or fatty acids (bio-diesel) and one or more esters of fatty acids of glycerol carbonate (constituting between 10 and 40 percent of the weight) can be used as fuel.

Traditionally, glycerol carbonate has been synthesised by reaction between glycerol and phosgene,⁶ but due to the high toxicity of phosgene, alternative routes based on transesterification in basic media of dialkyl or alkylene carbonates have been explored. The current industrial synthesis of glycerol carbonate entails two steps:⁷ first ethylene oxide reacts with carbon dioxide to yield the cyclic ethylene carbonate which is further reacted with glycerol to give glycerol carbonate and ethylene glycol. This process involves the use of homogeneous basic catalysts such as sodium bicarbonate or sodium hydroxide introducing some drawbacks such as the neutralisation of the base as well as the recovery of the product by distillation under reduced pressure.

The improvement of the economic and environmental feasibility of the industrial synthesis of glycerol carbonate (i.e. reducing the number of steps and waste) entails the design of an optimised direct method for its production. Few references have

3.3. TRANSESTERIFICATION OF GLYCEROL IN A CONTINUOUS SYSTEM

been found in the literature concerning the production of glycerol carbonate using simplified methodologies. Vieville *et al.*⁸ obtained glycerol carbonate (up to 32% after 1 hour) by direct carbonation of glycerol in supercritical carbon dioxide in the presence of zeolites and ion exchange resins, using ethylene carbonate as co-reactant. Aresta *et al.* have recently reported the direct carboxylation of glycerol with carbon dioxide using tin complexes ($n\text{-Bu}_2\text{Sn}(\text{OCH}_3)_2$, $n\text{-Bu}_2\text{SnO}$ and $\text{Sn}(\text{OMe})_2$) as catalysts.⁹ However, the best glycerol conversion achieved after 15 hours of reaction was below 7%. Catalysts based on zinc, $\text{Zn}(\text{CH}_3\text{C}_6\text{H}_4\text{-SO}_3)_2$, were used by Yoo *et al.*¹⁰ to synthesize glycerol carbonate from glycerol and urea. In this case, the conversion achieved was 85% after 1 hour of reaction.

The non-toxicity, biodegradability and cleaner production process of alkyl carbonates such as dimethyl or diethyl carbonate (DMC or DEC, respectively) make them green reagents that prevent pollution at the source during synthesis.¹¹ Moreover, DEC including ethoxy and carbonyl groups can be used as an effective carbonylating and ethylating agent as well as a raw material for manufacturing polycarbonates.¹² Glycerol carbonate can be obtained via a transesterification reaction of DMC with glycerol using homogeneous catalysts such as $n\text{-Bu}_2\text{Sn}(\text{OCH}_3)_2$, resulting in a 65% conversion after 15 hours.⁹ The usual synthesis is performed using as catalyst large quantities of K_2CO_3 to produce either glycerol carbonate, glycerol dicarbonate or diglycerol tricarbonate depending on the reaction temperature and/or the amount of DMC added.⁴ Mouloungui *et al.*¹³ reported the synthesis of glycerol carbonate by reaction of glycerol on a cyclic organic carbonate in the presence of a solid catalyst consisting of an anionic, bi-carbonated or hydroxylated macroporous resin, or alkaline X- or Y-type zeolite. This reaction produces glycol as by product with a selectivity of about 15-30%.

We have recently reported the results of an exploratory study focussed on the synthesis of glycerol carbonate by the transesterification of glycerol with diethyl carbonate using heterogeneous catalysts based on hydrotalcite-like compounds.¹⁴ The results showed that Mg/Al mixed oxides and the rehydrated hydrotalcites are efficient and reusable catalysts for the transesterification reaction, being able to replace homogeneous catalysts, such as K_2CO_3 , which showed similar activity. Along the same research lines, Takagaki *et al.* showed that an uncalcined hydrotalcite containing a hydromagnesite phase efficiently catalyzes glycerol carbonate synthesis from glycerol and DEC using DMF as solvent.¹⁵ Climent *et al.* also recently reported that solids with well balanced acid-base pairs such as Zn/Al mixed oxides from hydrotalcite-like compounds are efficient catalysts for the transesterification of glycerol with ethylene carbonate or carbonylation of glycerol with urea.¹⁶

Hydrotalcite-like compounds (HTs) are anionic clays with the general formula $[\text{M}^{\text{II}}_{1-x}\text{M}^{\text{III}}_x(\text{OH})_2]^{x+} \text{A}^{n-x/n} n\text{H}_2\text{O}$, where M^{II} and M^{III} stand for a divalent and a trivalent cation, respectively, A is a charge-balancing anion and x the value of the stoichiometric coefficient ($x = \text{M}^{\text{II}} / (\text{M}^{\text{II}} + \text{M}^{\text{III}})$). HTs are usually prepared by co-precipitation from metal salts in alkaline media at constant pH followed by a hydrothermal treatment of the

precipitate. The usual protocol of activation for these materials is controlled thermal decomposition which leads to the formation of mixed oxides showing a good dispersion of metals, a large specific surface area and Lewis basic properties. The rehydration of calcined hydrotalcites under a CO₂ free atmosphere allows the layered structure to be recovered containing interlayer OH⁻ anions, which provides significant Brønsted basic properties.^{17,18}

Roelofs *et al.*¹⁹ proposed that the active sites participating in catalysis are located at the edge of the platelets. Thus, the number of accessible edge active sites is limited by the lateral size of the HT crystallites and increases with decreasing particle size. Consequently, several studies have been conducted to maximize the number of active sites by minimizing the lateral size of the HTs.^{20,21} This was achieved by using ultrasound during reconstruction^{20,22} or by preparing small HT platelets (≈ 20 nm) on carbon nanofibers.²³ The resulting catalysts showed a significant increase in catalytic activity in reactions such as self-condensation of acetone and in the condensation of citral with acetone. For practical applications, HTs have the inconvenience to be obtained in very small particle sizes, which can be used in batch reactors but not in continuous flow reactors due to the severe pressure drop.

In this work, particles of α - and γ -Al₂O₃ were used as supports for the synthesis of Mg/Al hydrotalcites by impregnation of Mg and Al precursor salts. After calcination and rehydration, catalysts consisting of HT dispersed on Al₂O₃ with Brønsted basic sites were obtained. The structure of these catalysts is reported. An exploratory study of their catalytic properties for the synthesis of glycerol carbonate has been performed in order to prove the possibility of using these catalysts in a continuous system.

3.3.2. Experimental

i. Materials

Particles of 0.2-0.3 mm of α -Al₂O₃ (10 m²/g) and γ -Al₂O₃ (115 m²/g) both from Norton were used as supports. The precursor salts, Mg(NO₃)₂·6H₂O (purity 99%) and Al(NO₃)₃·9H₂O (purity 98%), were purchased from Sigma-Aldrich.

ii. Catalysts preparation

In a typical procedure, 4 g of α - or γ -Al₂O₃ were impregnated with 4 mL of a solution containing the appropriate amount of magnesium and aluminum salts (1.6 mmol/g or 2.04 mmol/g of Mg(NO₃)₂·H₂O and 0.8 mmol/g or 0.5 mmol/g of Al(NO₃)₃·9H₂O) in deionised water. The impregnated alumina was dried in an oven at 373 K for 1 h and then calcined in a tubular quartz packed bed reactor at 723 K (heating rate: 10 K/min) flowing 30 mL/min of air. At this stage a solid referred as HTO α -alpha or gamma is obtained. The rehydration of the supported mixed oxides obtained after this treatment was performed in a closed 100 mL autoclave batch reactor at 473 K for 12 h (containing 5 g of solid and 40 g of decarbonated water) and gives samples

3.3. TRANSESTERIFICATION OF GLYCEROL IN A CONTINUOUS SYSTEM

referred as HTrx-alpha or gamma, where x denotes the Mg/Al molar ratio in solution (2 or 4).

iii. *Analysis and characterisation*

Specific surface areas of the samples were determined by nitrogen adsorption at 77 K using a Micromeritics ASAP 2000 equipment. Samples were previously degassed in situ at 393 K under vacuum for 5 h. Surface areas were calculated using the Brunauer-Emmet-Teller (BET) methods over a p/p_0 range where a linear relationship was maintained. X-ray diffraction (XRD) powder patterns were collected on a Siemens EM-10110BU diffractometer model D5000 fitted with a Cu $K\alpha$ (1.541 Å) radiation source. Data were recorded over a 2θ range of 5-70° with an angular step of 0.05° at 3 s/step which resulted in a scan rate of 1°/min. Patterns were identified using files from the Joint Committee on Powder Diffraction Standards (JCPDS).

The basicity measurements were obtained by temperature programmed desorption (TPD) of CO₂ on a Thermo Finnigan TPDRO 1100 equipped with a TCD detector. Typically, ca. 0.350 g of sample were placed in a tubular quartz reactor. The sample was pretreated with Ar at 353 K during 1 h and then cooled to room temperature and treated with a CO₂ flow (2.5% CO₂ in He). The desorption of CO₂ was measured by heating the sample from room temperature to 1073 K at a heating rate of 10 K/min in He flow, and water was trapped on magnesium perchlorate, in order to avoid interferences. The number of basic sites was calculated from the CO₂ peaks by deconvolution using the software of the equipment, and a calibration of the instrument using a known amount of CaCO₃.

iv. *Catalytic activity tests*

Glycerol (99%), diethyl carbonate (DEC) (99.5%, GC grade) and dimethyl sulphoxide (DMSO) as solvent (99%) were purchased from Aldrich and used without any further purification. Transesterification reaction was performed in a continuous system formed of a tubular quartz packed bed reactor, a furnace equipped with a temperature controller, a Gilson pump and an inlet for flowing 3 mL/min of Ar. The mixture of reactants, containing glycerol (1.85 g), DEC (38.95 g) and solvent (21.90 g) was fed into the pre-heated reactor containing 4g of fresh catalyst with a feed flow of 0.1, 0.05 or 0.025 mL/min.

The influence of the support, the type of solvent used as well as the amount of magnesium added and the activation form of catalysts were studied.

Samples were periodically collected and quantified by GC analysis equipped with a FID detector. This was performed on a Shimadzu GC-2010 with a Zebron ZW-WAX capillary column.

3.3.3. Results and discussion

i. Characterisation of the catalysts

PXRD patterns of alpha and gamma-supported samples are displayed on Figures 3.3.1 A and B. The patterns of the samples supported on α -Al₂O₃ (Fig. 3.3.1 A) show the peaks characteristic for corundum phase (JCPDS: 042-1468). Additional peaks were observed on rehydrated sample corresponding to (003) and (006) reflection planes of meixnerite phase (JCPDS: 22-700) obtained after rehydration of magnesium and aluminium mixed oxides. In addition, the sample HTr2-alpha developed new diffraction peaks identified as boehmite phase (JCPDS: 01-088-2112), attributed to the rehydration of part of the alumina which has not reacted to form hydrotalcite. Diffraction lines of boehmite (γ -AlO(OH)) and meixnerite were also clearly detected on rehydrated samples supported by γ -Al₂O₃ (Figure 1B) indicating that at least part of the γ -Al₂O₃ support was transformed into boehmite after the rehydration treatment. This sample also exhibits at $d=1.52$ nm the (110) reflexion of HT, which can be used to determine the a lattice parameter of HT on the support. The Al/Mg+Al ratio obtained from the Vegard's law is close to 0.3, as expected from the composition used in the synthesis. (Table 3.3.1) On the other hand, the catalyst prepared with higher amount of magnesium (HTr4-Alpha) presented a (110) reflexion at $d=1.527$ nm revealing the formation of a hydrotalcite with an Al/Mg+Al of approximately 0.3 instead of 0.2, as expected from the Mg/Al molar ratio in the solution. From this result, we can suppose that catalyst HTr4-Alpha contains an extra-phase of MgO(H) not detected by PXRD.

The transformation of γ -Al₂O₃ into a hydrated phase has already been described by other authors^{24,25} and can occur even at room temperature.²⁶ The hydrated species formed depend on variables such as pH of the media, temperature, pressure and others. The size of the particles of HT was computed from the Scherrer equation using the (003) line width. The results reported in Table 3.3.1, show the formation of particles in the nanometric range, with a smaller size when α -Al₂O₃ is the support. The average size obtained about 13.5 nm is comparable to that reported for HT on C nanofibers.²¹

The restructuring of the solid by hydration-dehydration may also involve physico-chemical changes in the support relative to the pore structure and surface acid-basic properties,^{25, 27} that can affect the catalytic properties such as activity, selectivity or stability during time on stream. The specific surface area and textural parameters of the supports and catalysts are reported in Table 3.3.1. As was seen in PXRD analysis, the hydrothermal treatment of the catalyst produced structural changes in the support, making the material more crystalline and increasing the crystallite size; consequently a notable decrease in specific surface area, more marked in catalysts supported on γ -Al₂O₃, is observed. The final solid shows an average pore size of about 6-7 nm, in the range of mesopores.

3.3. TRANSESTERIFICATION OF GLYCEROL IN A CONTINUOUS SYSTEM

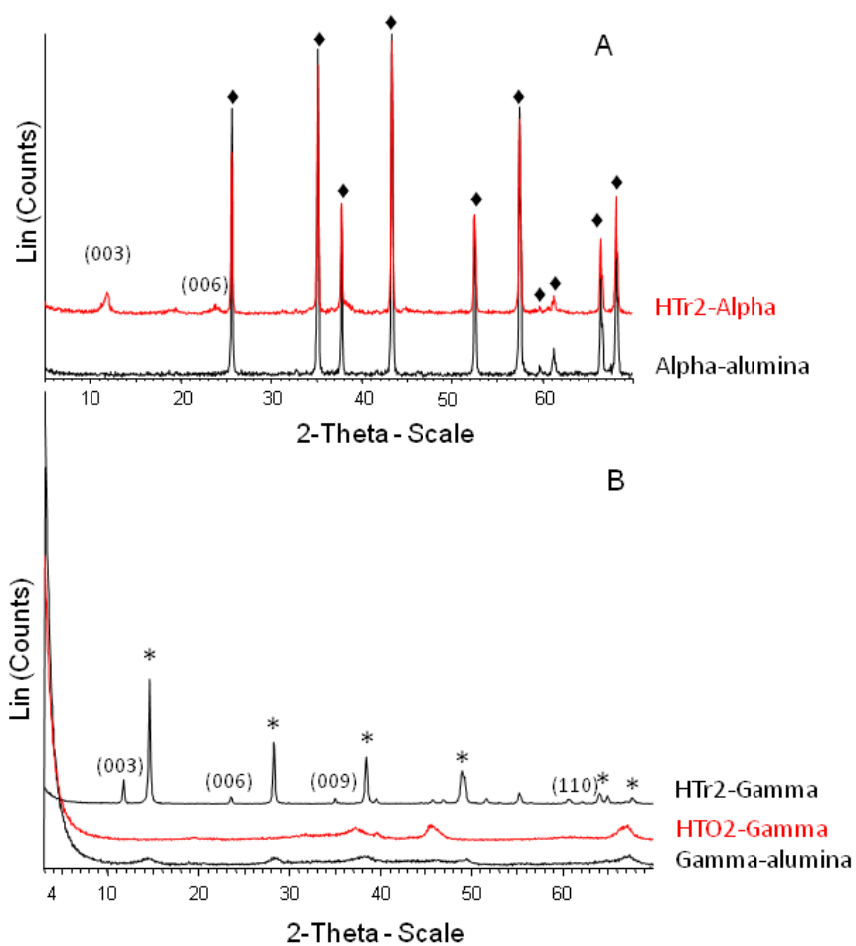


Figure 3.3.1. PXRD diffractograms of: A) Alpha-alumina supported catalysts and B) Gamma-alumina supported catalysts. (♦) Corundum phase; (*) Boehmite phase (γ - $\text{AlO}(\text{OH})$). (hkl) indexed diffraction lines from meixnerite.

Table 3.3.1. BET specific surface area, textural properties and XRD characterisation of catalysts and supports

Catalyst	BET surface area (m ² /g)	Pore volume ^a (cm ³ /g)	Average pore diameter ^b (nm)	XRD analysis		
				Phase ^c	HT Crist. size ^d (nm)	HT (Al/Mg+Al) ^e
α -Al ₂ O ₃	14	–	–	Corundum	–	–
HTO2-Alpha	15	–	–	Periclase + corundum	–	–
HTO4-Alpha	15	–	–	Periclase + corundum	–	–
HTr2-Alpha	17	–	–	Meixnerite + boehmite + corundum	13.5	0.3
HTr4-Alpha	23	–	–	Meixnerite + corundum	14.9	0.3
γ -Al ₂ O ₃	246	0.47	7.59	–	–	–
HTO2-Gamma	226	0.37	6.57	Periclase	–	–
HTO4-Gamma	200	0.35	6.93	Periclase	–	–
HTr2-Gamma	64	0.25	15.91	Meixnerite + boehmite	21.8	0.3
HT4r-Gamma	139	0.29	8.17	Meixnerite + boehmite	20.2	–

^aDetermined from the nitrogen adsorbed volume at p/p₀=0.984.

^bDetermined from the maximum of BJH pore size distribution.

^cObserved by XRD analysis.

^dCalculated with Scherrer equation using LaB₃ as patron.

^eCalculated from (110) reflexion by using the Vegard's law.

3.3. TRANSESTERIFICATION OF GLYCEROL IN A CONTINUOUS SYSTEM

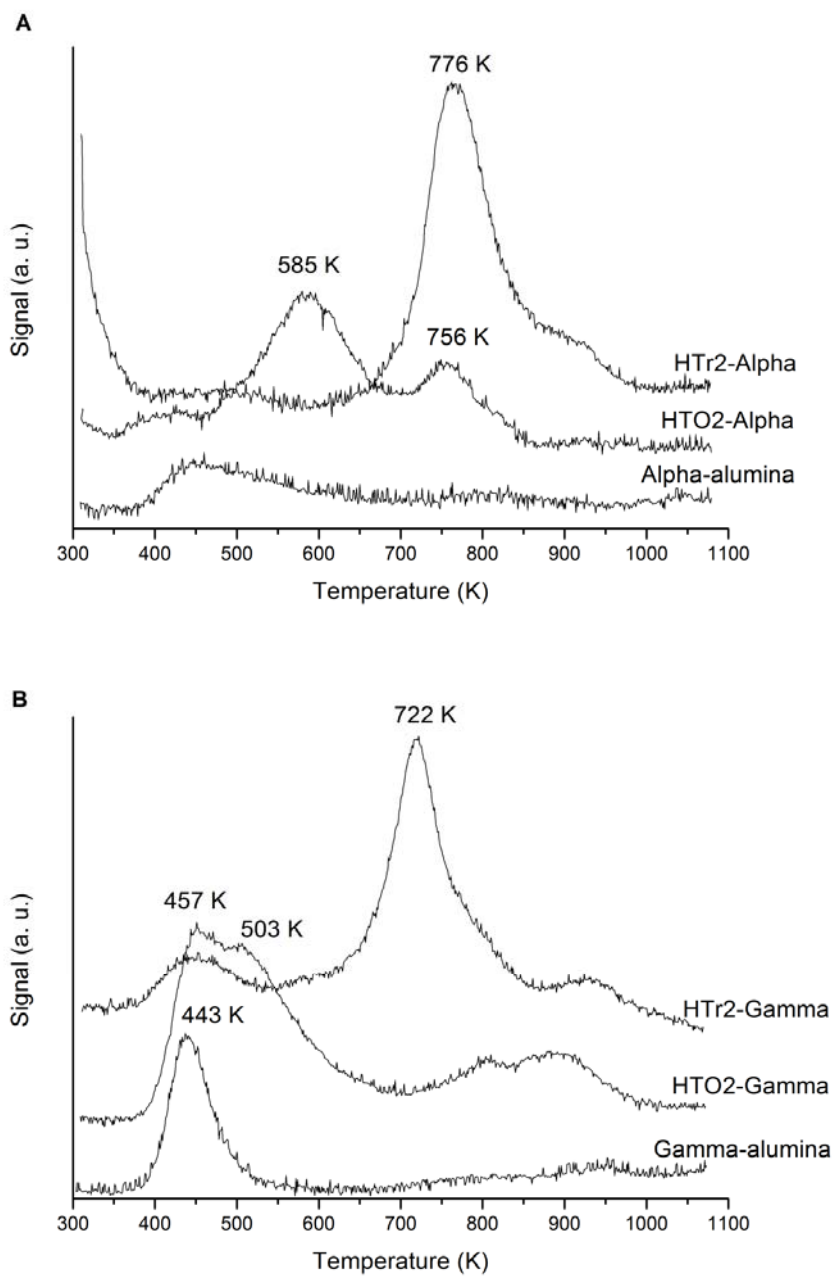


Figure 3.3.2. TPD-CO₂ profiles of: A) catalysts supported onto alpha-alumina and B) catalysts supported onto gamma-alumina.

The basicity of the support, supported mixed oxides and hydrothermally treated catalysts was measured by TPD-CO₂ and the basic strength could be assigned according to the temperature at which peaks appeared (Figure 3.3.2). The number of basic sites was estimated by deconvolution and integration of these peaks (Table 3.3.2).

Both alpha and gamma supported catalysts showed similar TPD-CO₂ profiles. Hydrated catalysts presented an intense peak around 775 K which can be assigned to the decomposition of bicarbonate species, formed by adsorption of CO₂ on the Brønsted basic sites of the rehydrated hydrotalcites.²¹ Calcined catalyst supported on alpha alumina also presented a weak desorption at this temperature, indicating a lower amount of Brønsted basic sites on the surface of mixed oxides. A second peak around 900 K is observed on both the calcined and hydrated samples and could be ascribed to strong Lewis basic sites, i.e. O²⁻ linked to coordinatively unsaturated Mg species (corner or edges).

Gamma supported samples presented low temperature peaks between 443 K and 458 K, more intense on the calcined sample, which can be assigned to an adsorption on Lewis sites identified to oxygens linked to Al cations, since pure γ -Al₂O₃ presented the same desorption peak. When γ -Al₂O₃ is used as support, the desorption peaks are shifted towards lower temperatures compared to those observed for HT/ α -Al₂O₃. This change in basic strength is more marked on calcined samples, suggesting a high interaction of mixed oxides on the γ -Al₂O₃ support. The temperature corresponding to the desorption of CO₂ observed on these supported HT is higher than that reported for bulk HT: in that case the peak of CO₂ was observed at 600-700K^{28,29}, compared to >700K here. This effect is due in part to the higher rate of increase of temperature in the TPD (10K/min here compared to 5K/min) which shifts the peaks up to 723 K, as reported by Valente *et al.*³⁰

3.3. TRANSESTERIFICATION OF GLYCEROL IN A CONTINUOUS SYSTEM

Table 3.3.2. Results of basic properties for the samples

Sample	TPD analysis of adsorbed CO ₂				Total evolved CO ₂ (μmol·g ⁻¹)
	Desorption peaks				
	<500 K	500-600 K	650-850 K	>850 K	
α-Al ₂ O ₃	5 (436) ^a	—	—	—	5
HT02-Alpha	—	39 (585)	19 (756)	—	58
HT04-Alpha	—	33 (579)	27 (743)	—	60
HTr2-Alpha	—	—	62 (776)	17 (882)	79
HTr4-Alpha	—	—	59 (749)	9 (880)	68
γ-Al ₂ O ₃	35 (443)	—	—	—	35
HT02-Gamma	53 (457)	50 (513)	—	19 (880)	122
HTr2-Gamma	9 (458)	—	128 (729)	9 (898)	146

^a Temperature of maximum (K)

Table 3.3.2 shows that the strong basicity is introduced onto alumina by the addition of HT, and that a rather similar number of basic sites is measured for either calcined or rehydrated catalysts. On bulk samples, the determination of basicities using calorimetric adsorption of CO₂³¹ showed a lower number of sites and a lower heat of adsorption for rehydrated samples. On smaller particles, the small difference observed here shows that the equilibrium of CO₂ between the bulk and the surface is fast at the temperature of 353 K used for the adsorption, leading to the same amount adsorbed on calcined and rehydrated samples. The main difference is then the higher number of Brønsted basic sites on the rehydrated samples.

ii. Catalytic Activity

An exploratory study of the transesterification of glycerol with DEC was made in order to check whether a continuous flow reactor could be used, with these calcined/hydrated materials as catalysts. The reaction was performed at a constant temperature (403 K) and the mixture of reactants, containing glycerol (1.85 g), DEC (38.95 g) and solvent was fed into the pre-heated reactor (containing 4g of fresh catalyst). The dependence of parameters such as solvent, feed flow rate, support and hydration of catalysts was studied.

a. Effect of the solvent and feed flow rate

The selection of the solvent is an important aspect to consider in the design of an experiment. The main function of the solvent is the solubilisation of the reactants and the products. However, the presence of a solvent in the media can modify aspects of the reaction such as yield and selectivity. Since the reactants are strongly polar (glycerol) and aprotic (dimethyl carbonate), three different aprotic polar solvents: dimethyl sulphoxide (DMSO), dimethyl formamide (DMF) and dimethyl acetamide (DMA), were tested in the continuous reaction in order to find the best solution.

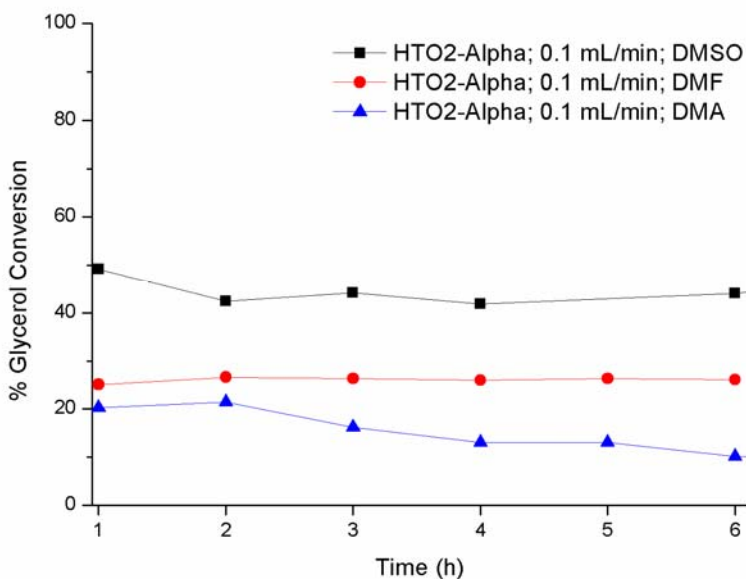


Figure 3.3.3. Glycerol conversion found for catalyst HTO2-Alpha for the three different solvents tested at 403 K and a fixed feed flow of 0.1 mL/min.

Figure 3.3.3 reports the glycerol conversion for the different solvents. A significant effect of the solvent was observed, with the highest conversion close to 50% found for dimethyl sulphoxide (DMSO), falling to 30% or 20% for dimethyl formamide (DMF) or dimethyl acetamide (DMA), respectively.

The properties of these solvents are displayed on Table 3.3.3. The glycerol conversion is correlated to the polarity of the solvent, and increases with an increase in polarity measured by the dipolar moment or dielectric constant values. This is in accordance with literature reports^{32,33} in which a higher catalytic activity for hydrotalcite-like compounds with solvents with higher polarity has been observed.

3.3. TRANSESTERIFICATION OF GLYCEROL IN A CONTINUOUS SYSTEM

This could be due to a better desorption of the products from the hydrophilic surface of the catalyst.

Table 3.3.3. *Properties of the tested solvents*

Solvent	pKa	Polarity	Boiling point (K)	Dielectric constant	Dipole moment	Glycerol Conversion (%)
DMSO	35	7.2	462	46.68	4.1	50
DMF	--	6.4	426	36.71	3.86	30
DMA	--	6.5	439	37.78	3.72	20

Three different flow rates were tested (Figure 3.3.4) using DMSO as solvent. The conversion increases proportionally with the contact time up to 20 min⁻¹ (flow 0.05 mL.min⁻¹), and total conversion is reached at the lower flow. This result proves that the rate is not controlled by extra-particle mass transfer. The rate computed from these results is 5 10⁻⁸ mol.s⁻¹g⁻¹. The possibility of diffusional limitations can be estimated computing the Thiele modulus modified by Weisz.³⁴

$$\varphi = vR^2/(DeffC_0)$$

where v is the rate (mol s g⁻¹), R the radius of the catalyst grains (here 0.01 cm), C_0 the concentration of glycerol (3 × 10⁻⁴ mol.ml⁻¹), and $Deff$ the diffusion coefficient (taken as 10⁻⁴ cm² s⁻¹) the φ value is about 0.02. Diffusion limits the overall process when $\varphi = 1$, therefore intraparticle diffusion does not limit the process. The variation of selectivities as a function of conversion (insert of Fig.4) shows that DGC is formed from GC in a consecutive reaction.

b. Effect of the support and hydration of catalysts

Catalysts were activated by calcination (called HTO2-Alpha or HTO2-Gamma) or by hydration of the calcined catalysts (called HTr2-Alpha or HTr2-Gamma). The following conditions were used for all the catalysts: a feed flow of 0.05 mL/min, a temperature of 403 K and DMSO as solvent. The pure supports, α -Al₂O₃ or γ -Al₂O₃, presented no catalytic activity at all.

Figure 3.3.5 shows the catalytic behaviour for calcined catalysts. Two different products, glycerol carbonate (GC) and glycerol dicarbonate (GDC), were obtained under these reaction conditions (Scheme 3.3.1). The primary alcohols are presumably more reactive than the secondary alcohol, however, once the

transesterification of the primary alcohol occurs, the intramolecular reaction between the secondary alcohol and the nearby carbonate group is favoured, thus producing GC. Finally, the transesterification reaction between GC and the DEC leads to the formation of GDC.

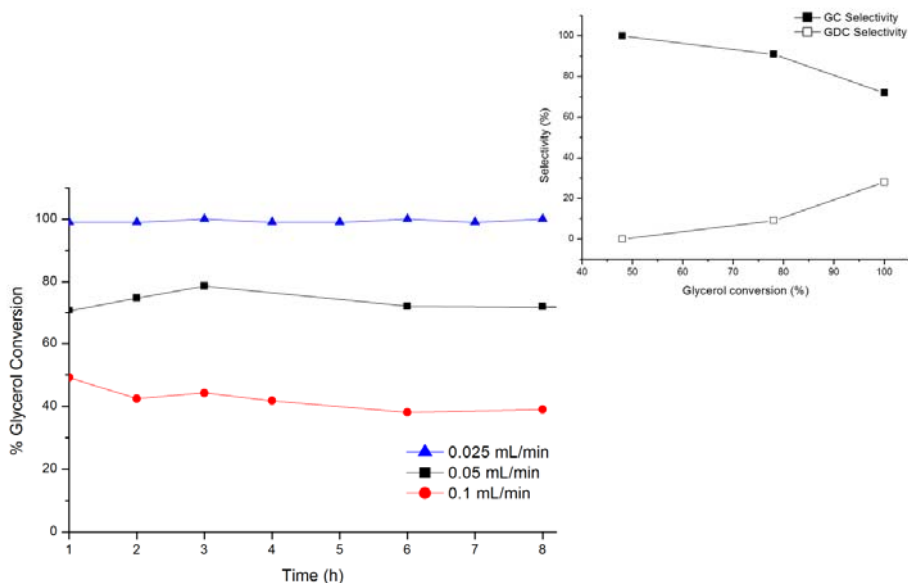
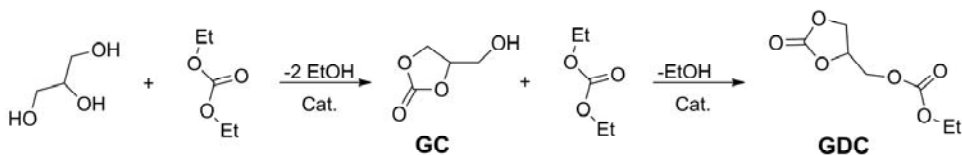


Figure 3.3.4. Results of the variation in HTO2-Alpha catalyst performance for the transesterification of glycerol with diethyl carbonate at 403 K by varying the feed flows. Insert: variation of the selectivity to glycerol carbonate and glycerol dicarbonate with the conversion.

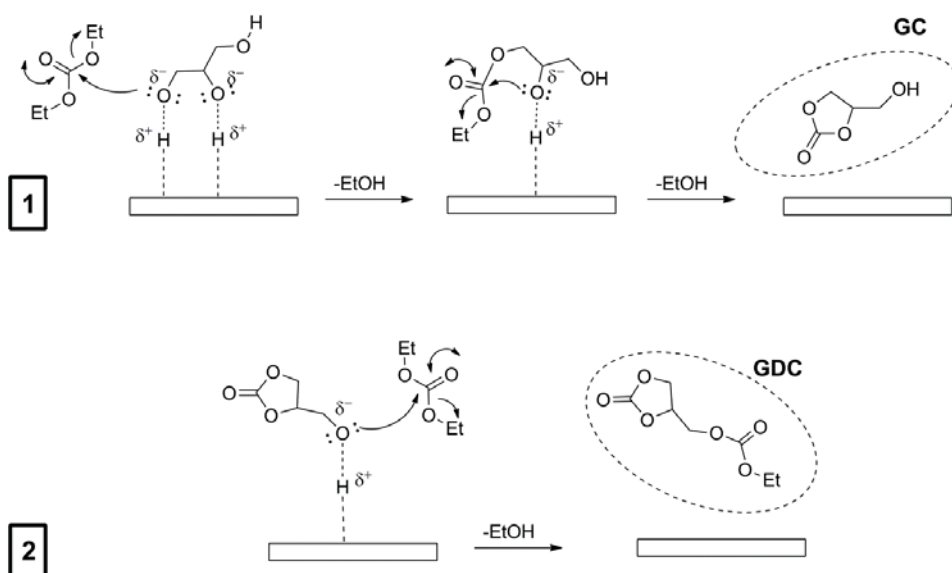


Scheme 3.3.1. Consecutive transesterification reaction of glycerol with DEC.

A possible reaction mechanism is proposed in scheme 3.3.2. First, glycerol is coordinated as a bidentate ligand to the catalyst surface by hydrogen bonds activating the oxygen atoms as nucleophiles. This bidentate coordination is proposed

3.3. TRANSESTERIFICATION OF GLYCEROL IN A CONTINUOUS SYSTEM

due to the absence of mono-transesterification products. The oxygen of the primary alcohol attacks the carbonylic carbon atom of diethyl carbonate producing the liberation of an ethanol molecule. Then, the oxygen atom of the secondary hydroxyl group attacks the carbonylic carbon atom again in an intramolecular transesterification, which is favoured due to the stable geometry of the five member cycle formed. A second molecule of ethanol is generated and glycerol carbonate is desorbed from the surface of the catalyst. When the concentration of glycerol carbonate is high enough, it is coordinated to the surface of the catalyst by its free hydroxyl group which acts as a nucleophile producing a new transesterification leading to the formation of glycerol dicarbonate and a new molecule of ethanol.



Scheme 3.3.2. Proposal of mechanism of hydrotalcite-catalysed transesterification of glycerol with DEC.

For calcined catalysts, the results of Figure 3.3.5 show that the catalytic activity of the samples supported on alpha alumina is higher than that of the samples supported on gamma alumina. Catalyst HTO2-Alpha reached 78% conversion of glycerol, constant as a function of time, whereas HTO2-Gamma achieved only a 20% of conversion. This result is in line with the lower strength of basic centers showed by the calcined sample supported on gamma-alumina, as revealed by the TPD-CO₂ analysis. The higher selectivity of HTO2-Alpha to GDC can be accounted for by the higher conversion.

The catalytic activity was improved when the catalysts were rehydrated (Figure 3.3.6). Both supported alpha and gamma alumina catalysts then reach total glycerol

conversion. If we take into account the similar number of basic sites between calcined and hydrated samples (Table 3.3.2) onto a same support and the differences in surface area for catalysts supported on gamma and alpha alumina, the rehydrated catalysts show definitively better catalytic properties than the calcined ones. This suggests that the presence of Brønsted basic sites is an important factor that induces a better catalytic performance in the transesterification of glycerol, as has been observed in literature.^{14,35}

At a comparable conversion of about 90%, both rehydrated catalysts, HTr2-Alpha and HTr2-Gamma, led to the formation of GC and GDC, but the maximum amount of GDC achieved by HTr2-Gamma catalyst (2.6%) was rather low compared to that obtained on HTr2-Alpha (40.8%). The selectivity to GDC decreased with time of stream on both catalysts: HTr2-Alpha yielded about 40% of GDC in the first hours of reaction dropping to 23.6% of GDC after 8 h, while HTr2-Gamma yielded only 2.6% of GDC in the first hours of stream, decreasing rapidly to obtain pure GC. This deactivation is more marked on HTr2-Gamma and affects only the glycerol conversion, while the sample HTr2-Alpha maintained a total conversion during all the experiment, with a selectivity to GC close to 70%. The consecutive scheme of this reaction is formally analog to a rake scheme:^{36,37} in this scheme, at a given conversion level, the selectivity to GDC is determined by the ratio rate of reaction/rate of desorption of GC. The rate of desorption of GC is controlled by the basicity of the surface, and therefore the selectivity to GDC should be higher when the basic strength increases. This effect accounts for the higher selectivity of HTr2-Alpha for GDC, in agreement with the results of TPD.

Catalysts supported on gamma-alumina (HTr2-Gamma and HTr2-Gamma) showed lower conversions than catalysts supported on alpha-alumina despite their higher surface area. The BET surface area of the pure $\gamma\text{-Al}_2\text{O}_3$ was 246 m^2/g and the pore volume and pore diameter were 0.47 cm^3/g and 7.59 nm, respectively. After impregnation of nitrates, BET surface area and pore volume of rehydrated catalysts decreased remarkably (Table 3.3.1), however the average pore diameter increased. This behaviour is more marked in catalyst HTr2-Gamma than HTr4-Gamma. Thus, the effect of the support is clearly evident on catalytic activity, being the catalysts supported on $\alpha\text{-Al}_2\text{O}_3$ more active and stable.

Deactivation can be provoked for instance by the hydrolysis of diethylcarbonate producing an acid moiety which would block the basic sites. This reaction involving water is expected to be facilitated on hydrated catalysts. The fact that the catalyst supported by α -alumina are more stable than those supported by γ -alumina can be related to their high surface area, with a higher retention of water compared to α -alumina of low surface area.

3.3. TRANSESTERIFICATION OF GLYCEROL IN A CONTINUOUS SYSTEM

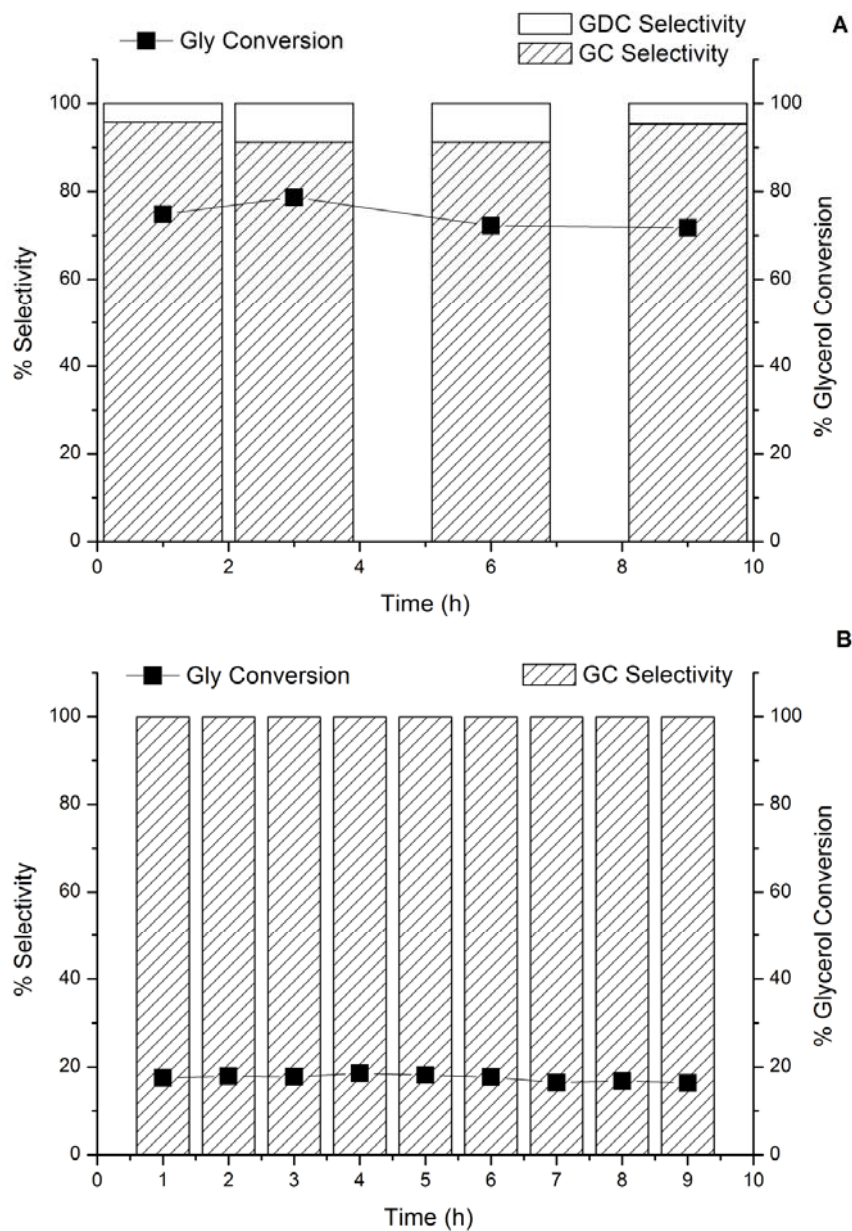


Figure 3.3.5. Catalytic behaviour (conversion and selectivity) of calcined catalysts at 403 K and a feed flow of 0.05 mL/min. A) HTO2-Alpha and B) HTO2-Gamma.

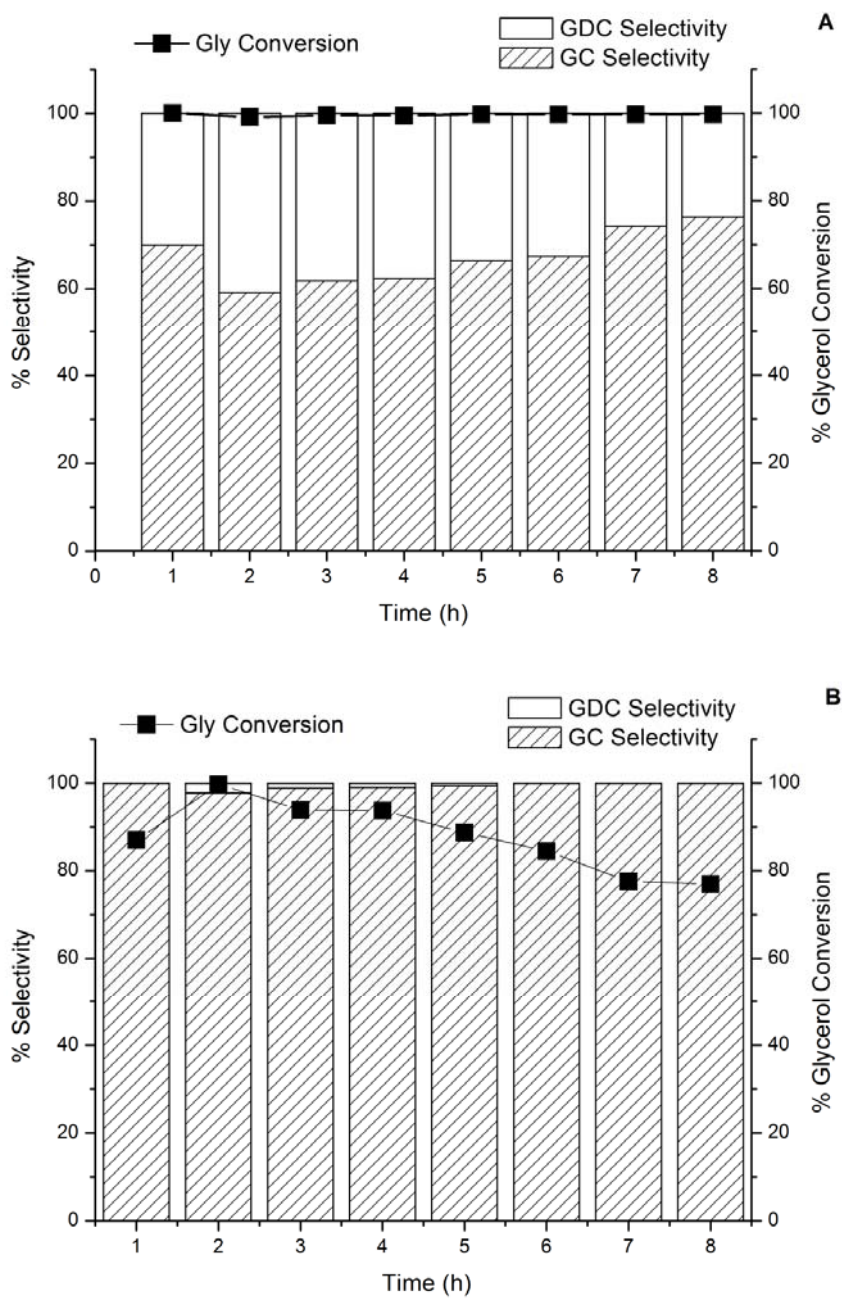


Figure 3.3.6. Catalytic activity for rehydrated catalysts at 403 K and a feed flow of 0.05 mL/min. A) HTr2-Alpha and B) HTr2-Gamma.

3.3. TRANSESTERIFICATION OF GLYCEROL IN A CONTINUOUS SYSTEM

c. *Effect of the amount of magnesium*

It is well known that the ratio Mg/Al is an important factor in the catalytic activity of HTs. Indeed other authors have reported an increase of the activity of HT for transesterification reactions when the Mg content increased.^{38,39}

In order to check the influence of the amount of magnesium contained in catalysts in the catalytic activity, two new catalysts were synthesised by impregnation of particles of $\alpha\text{-Al}_2\text{O}_3$ with a magnesium and aluminum nitrate solution with a Mg/Al molar ratio of 4 instead of 2. As reported above the Mg/Al ratio in the hydrotalcites phase is indeed practically constant. Catalysts were activated by calcination and rehydration of calcined materials as done in previous catalyst. The amounts of CO_2 adsorbed by these solids are reported in Table 3.3.2: they are rather close to those observed with the other preparations.

Figure 3.3.7 A shows the catalytic behaviour of the calcined catalyst, HTO4-Alpha. The catalyst presented total glycerol conversion during all the experiment (8 h) and the selectivity to GDC was maintained almost constant (around a 20%). When the catalyst was rehydrated (Figure 3.3.7 B), total glycerol conversion was also achieved, but after 8 h on stream a small deactivation occurred manifested by both a loss of glycerol conversion and a loss of the secondary product of transesterification (GDC). The glycerol conversion dropped to 88% after 9 hours and the selectivity towards GDC initially 20% dropped and the reaction became completely selective to the product of the primary product of transesterification, GC.

Table 3.3.4 reports the different catalytic behaviours of the catalysts with higher content in magnesium compared to the previous ones. Calcined catalysts showed a higher glycerol conversion and a higher selectivity to glycerol dicarbonate at the expenses of glycerol carbonate, with increasing magnesium content. All the points of this Table 3.3.4 are reported on a graph selectivity versus conversion (Figure 3.3.8), and fit the same curve, showing that the selectivity to GC is determined by the conversion. On the other hand, the conversion is roughly proportional to the amount of CO_2 adsorbed (insert in Figure 3.3.8). 90% selectivity to glycerol carbonate can be reached at about 80% conversion using these catalysts showing a good stability as a function of time.

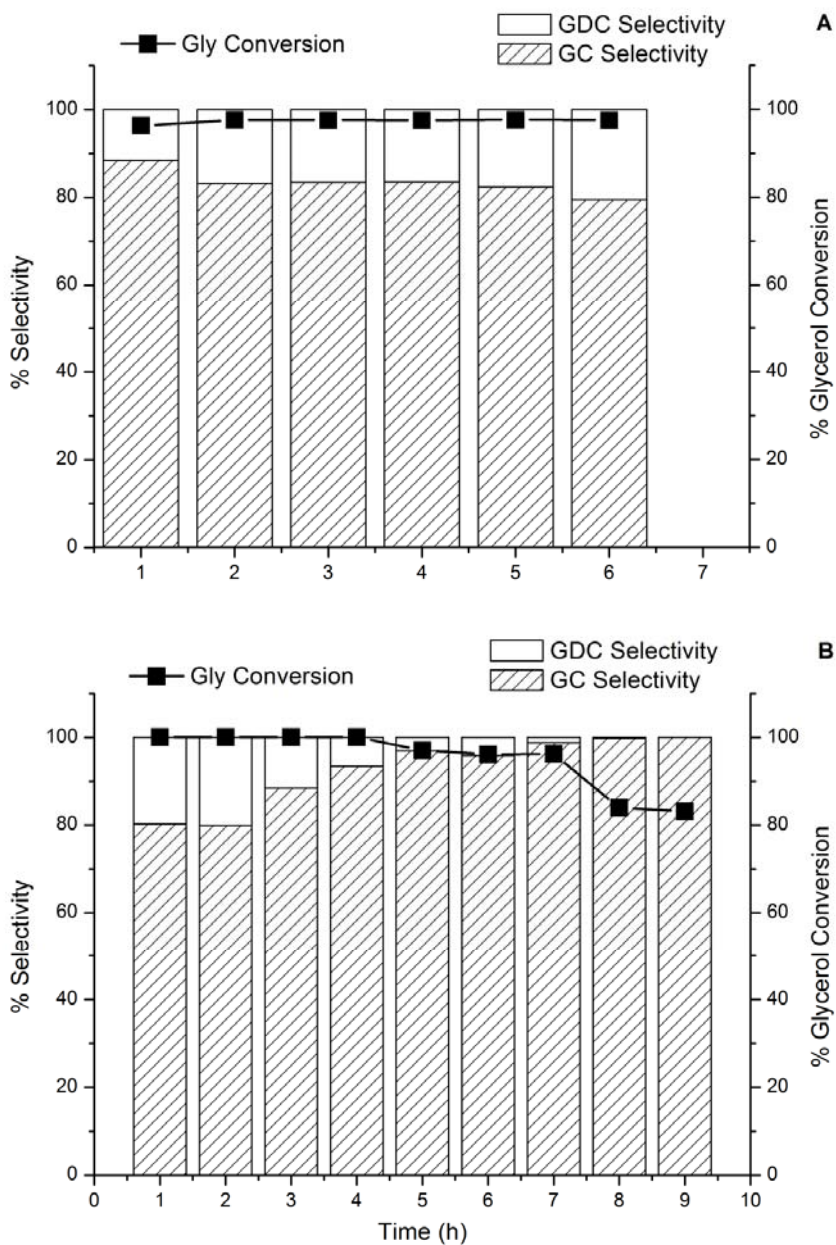


Figure 3.3.7. Catalytic activity for catalysts with higher Mg content at 403 K and a feed flow of 0.05 mL/min.: A) calcined catalyst, HTO4-Alpha and B) rehydrated catalyst, HTR4-Alpha.

3.3. TRANSESTERIFICATION OF GLYCEROL IN A CONTINUOUS SYSTEM

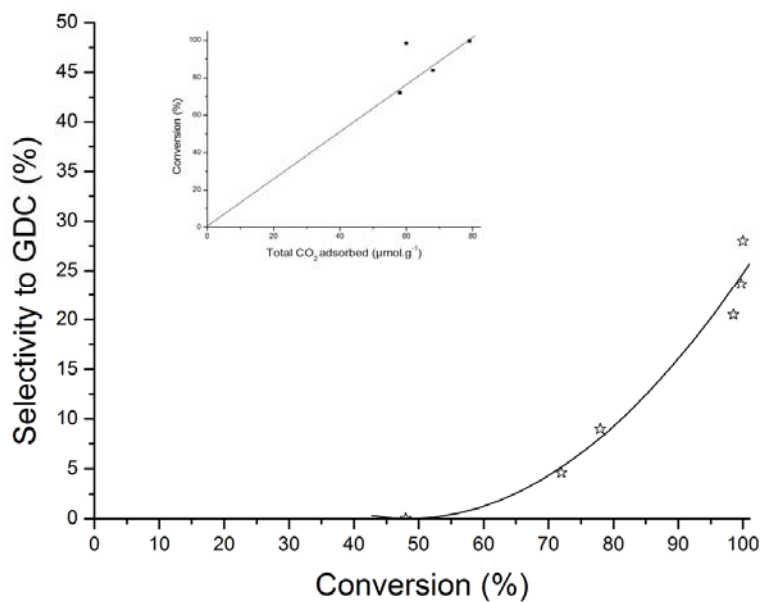


Figure 3.3.8. Selectivities of the catalysts supported on α -alumina as a function of the conversion. Insert: variation of the conversion with the amount of CO_2 adsorbed.

Table 3.3.4. Catalytic behaviour of catalysts with different Mg/Al molar ratio

Catalyst	Mg/Al molar ratio ^a	% Glycerol Conversion ^b	% GC Selectivity ^b	% GDC Selectivity ^b
HTO2-Alpha	2	72	95.4	4.6
HTO4-Alpha	4	98.5	79.5	20.5
HTr2-Alpha	2	99.7	76.4	23.6
HTr4-Alpha	4	83.9	100	--
HTO2-Gamma	2	20	100	--
HTr2-Gamma	2	80	100	--

^aNominal value.

^bAfter 8 hours of continuous stream

3.3.4. Conclusions

In conclusion, we have developed an efficient method for the obtention of hydrotalcites supported on α -Al₂O₃ or γ -Al₂O₃. These solids can be activated like bulk HT by calcinations and further rehydration. Due to their better mechanical properties, these solids can be used in a continuous flow reactor. They are active for the conversion of glycerol into glycerol carbonate and glycerol dicarbonate.

Due to the immiscibility of glycerol and diethyl carbonate, the reaction was carried out using a solvent to favour the flow of reactants through the catalytic system. Different polar solvents were evaluated in the glycerol transesterification, among which dimethyl sulphoxide (DMSO) is the most favourable.

The experimental results show that the type of basic centre has a significant influence on the activity in the transesterification reaction. Thus, catalysts which present Brønsted basicity (rehydrated catalysts) showed better performances than calcined samples which present mainly Lewis basic sites. In addition, the stronger adsorption at the Brønsted sites favours the consecutive transesterification of the glycerol carbonate. Moreover, it has been observed that the most active catalysts lead to a higher yield of GDC produced at the expenses of glycerol carbonate.

An increase in the magnesium content in the catalyst led to a higher glycerol conversion and higher yield of GDC, however catalyst HTr4-Alpha showed lower stability than catalyst HTr2-Alpha, probably due to the presence of an extra-phase of MgO(H) in the catalyst.

On the other hand, the support effect on catalytic properties is clearly evident, the catalysts supported on α -Al₂O₃ being more active. This higher activity is accounted for by the stronger basicity of hydrotalcites supported onto α -Al₂O₃ due to the weak interaction between the hydrotalcite and the support, evidenced by TPD of CO₂.

Thus, it is concluded that hydrotalcite-type compounds are promising candidates for the continuous transesterification reaction, being possible substitutes of homogeneous catalysts used for this propose and opening the possibility of processes in continuous reactors.

3.3. TRANSESTERIFICATION OF GLYCEROL IN A CONTINUOUS SYSTEM

Reference

1. D. Fabbri, V. Benovi, M. Notari and F. Rivetti, *Fuel*, **86** (2007) 690.
2. Y. Zheng, X. Chen and Y. Shen, *Chem. Rev.*, **108** (2008) 5253.
3. D. Herault, A. Eggers, A. Strube and J. Reinhard, DE101108855A1 (2002).
4. G. Rokicki, P. Rakoczy, P. Parzuchowski and M. Sobiecki, *Green Chem.*, **7** (2005) 529.
5. Notari and F. Rivetti, to Polimeri Europa, US20050261144 (2005).
6. A.G. Shaikh and S. Sivaran, *Chem. Rev.*, **96** (1996) 951.
7. A. Behr, J. Eilting, K. Irawadi, J. Leschinski and F. Lindner, *Green Chem.* **10** (2008) 13.
8. C. Vieville, J.W. Yoo, S. Pelet and Z. Mouloungui, *Catal. Lett.*, **56(4)** (1999) 245.
9. M. Aresta, A. Dibenedetto, F. Nocito and C. Pastore, *J. Mol Catal. A: Chem.*, **257** (2006) 149.
10. J.W. Yoo and Z. Mouloungui, *Stud. Surf. Sci. Catal.*, **146** (2003) 757.
11. P. Tundo and M. Selva, *Acc. Chem. Research*, **35(9)** (2002) 706.
12. D. Wang, B. Yang, X. Zhai and L. Zhou, *Fuel Process. Technol.* **88** (2007) 807.
13. Z. Mouloungui, J. W. Yoo, C. A. Gachen, A. Gaset and G. Vermeersch, EP0739888.
14. M.G. Álvarez, A.M. Segarra, S. Contreras, J.E. Sueiras, F. Medina and F. Figueras, *Chem. Eng. J.*, **161** (2010) 340.
15. A. Takagaki, K. Iwatani, S. Nishimura and K. Ebitani, *Green Chem.*, **12** (2010) 578.
16. M.J. Climent, A. Corma, P. De Frutos, S. Iborra, M. Noy, A. Velty, P. Concepción, *J. Catal.*, **269** (2010) 140.
17. R. Tessier, D. Tichit, F. Figueras and J. Kervenal, FR2729137, 1995.
18. D.Tichit, M. Naciri Bennani, F. Figueras, R. Tessier and J. Kervenal, *Appl. Clay Sci.* **13** (1998) 401.
19. J.C.A.A. Roelofs, A.J. van Dillen, K.P. de Jong, *Catal. Today*, **60** (2000) 297.
20. S. Abelló, F. Medina, D. Tichit, J. Pérez-Ramírez, Y. Cesteros, P.Salagre, J.E. Sueiras, *Chem. Commun.* (2005) 1453.

21. F. Winter, V. Koot, A. J. van Dillen, J. W. Geus, K. P. de Jong, *J. Catal.*, **236** (2005) 91.
22. M.J. Climent, A. Corma, S. Iborra, K. Epping, A. Velty, *J. Catal.*, **225** (2004) 316.
23. F. Winter, A.J. van Dillen, K.P. de Jong, *Chem. Commun.* (2005) 3977.
24. H. Ly, Y. Xu, C. Gao, Y. Zhao, *Catal. Today*, doi:10.1016/j.cattod.2010.07.015
25. L. Yun-Cheng, X. Lan, X. Feng, W. Zhan-Wen, W. Fei, *Appl. Surf. Sci.*, **253** (2006) 766.
26. G. Lefèvre, M. Duc, P. Lepeut, R. Caplain, M. Fédoroff, *Langmuir*, **18** (2002) 7530.
27. X. Yang, Z. Sun, D. Wang, W. Forsling, *J. Colloid and Interface Sci.*, **308** (2007) 395.
28. D. Tichit, M.H. Lhouty, A. Guida, B. Chiche, F. Figueras, A. Auroux, E. Garrone, *J. Catal.*, **151**(1995) 50.
29. S. Abello, F. Medina, D. Tichit, J. Perez-Ramirez, J. C. Groen, J. E. Sueiras, P. Salagre, Y. Cesteros, *Chem. Eur. J.*, **11** (2005) 728.
30. J. Sanchez Valente, J. Prince, A.M. Maubert, L. Lartundo-Rojas, P. Ángel, G. Ferrat, J.G. Hernández, E. Lopez-Salinas, *J. Phys. Chem. C*, **113** (2009) 5547.
31. J. Sanchez Valente, F. Figueras, M. Gravelle, P. Kumbhar, J. Lopez and J. -P. Besse, *J. Catal.* **189** (2000) 370.
32. D. Tichit, D. Lutic, B. Coq, R. Durand and R. Teissier, *J. Catal.*, **219** (2003) 167.
33. D. Kishore and S. Kannan, *J. Molec. Catal. A.*, **223** (2004) 225.
34. P.B. Weisz, *Science*, **179** (1973) 433.
35. A. Corma, S.B.A. Hamid, S. Iborra and A. Velty, *J. Catal.*, **234** (2005) 340.
36. J.M. Tatibouët, J.E. Germain, C.R. Acad. Sci., Paris 289 (II) (1979) 305.
37. M. Cozzolino, R. Tesser, M. Di Serio, P. D'Onofrio, E. Santacesaria, *Catalysis Today*, **128** (2007) 191.
38. D.G. Cantrell, L.G. Gillie, A.F. Lee and K. Wilson, *Appl. Catal. A: Gen.*, **287** (2005) 183.

3.3. TRANSESTERIFICATION OF GLYCEROL IN A CONTINUOUS SYSTEM

39. H. Zeng, Z. Feng, X. Deng, Y. Li, *Fuel*, **87** (2008) 3071.

CHAPTER 4

STUDY OF THE ULTRASOUND TREATMENT EFFECT ON LAYERED DOUBLE HYDROXIDES

Article:

Structure evolution of layered double hydroxides activated by induced reconstruction

Mayra G. Álvarez, Ricardo J. Chimentao, Noelia Barrabés, Karin Föttinger, Francesc Gispe-Guirado, Evgeny Klemeynov, Didier Tichit and Francesc Medina.

(To be submitted to Microporous and Mesoporous Materials)

UNIVERSITAT ROVIRA I VIRGILI

HYDROTALCITE-LIKE COMPOUNDS FOR THE VALORISATION OF RENEWABLE FEEDSTOCKS

Mayra García Álvarez

Dipòsit Legal: T. 724-2012

CHAPTER 4

STUDY OF THE ULTRASOUND TREATMENT EFFECT ON LAYERED DOUBLE HYDROXIDES

4.1. INTRODUCTION

Miyata¹ was the first in describing the reconstruction of the calcined hydrotalcites by hydration. This unique property, known as structural memory effect, allows preparing several LDHs containing different anions, oxoanions or organic anions, such as dyes.

The calcination conditions (temperature, rate and duration) are important parameters determining the structure recovery, which also strongly depends on the composition of the parent LDH. For example, mixed oxides from Ni-based LDHs are much more difficult to reconstruct than those from Mg or Zn-based LDHs. The thermal behaviour of this kind of materials is characterised by three main steps (Figure 4.1.1). First, physisorbed and interlayer water is lost (up to 523 K). In a second step, the structure collapses and the removal of the hydroxyl groups from the layers is produced (523 -750 K). In this step, the LDH is converted in a mixed oxide, which can be reconstructed into the original LDH by contacting with water. In a third step, this mixed oxide can be transformed into a metastable phase by calcination at higher temperatures (ca. 1023 K). If a mixed oxide is introduced in deionised and decarbonated water under inert atmosphere, hydroxyl groups will be incorporated as compensating anions into the structure. This property has widely been used to prepare Brønsted basic solids which are highly efficient in several catalytic reactions as discussed in previous chapters.

4.1. INTRODUCTION

Although the efficiency of this kind of materials has been demonstrated in several catalytic reactions, the identification of the actual active sites presents a considerable challenge.

Catalytic activity is often ascribed to the presence of defect surface sites²⁻⁴ and several efforts have been done to produce materials presenting structural defects to enhance the catalytic activity.⁵ Other studies show, however, that active sites are located on the ordered array of hydroxyl sites on the basal surface rather than on defect sites associated with the edges.⁶

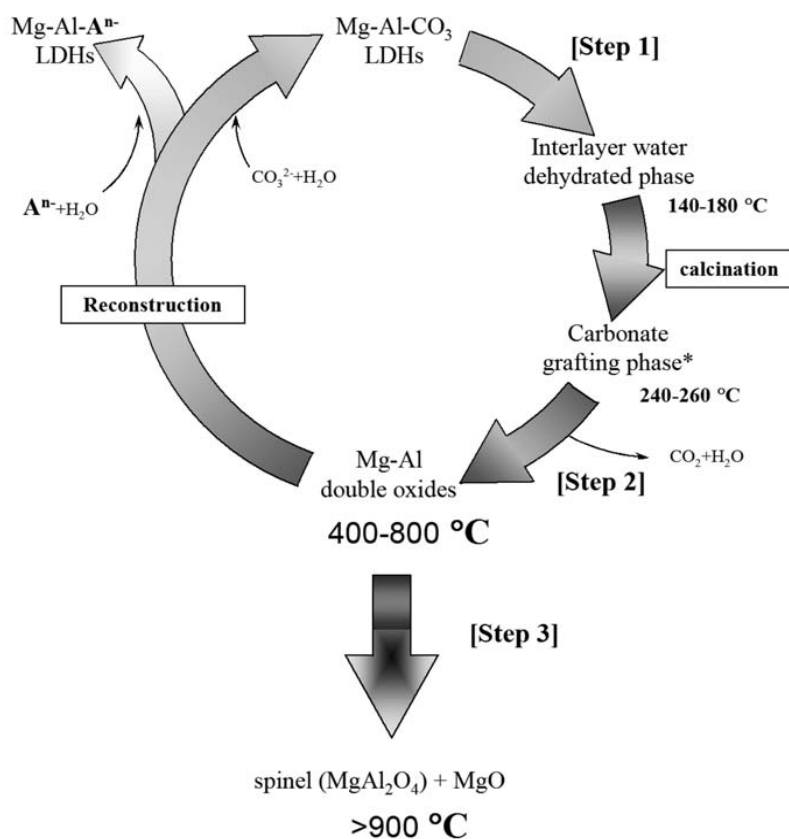


Figure 4.1.1. Decomposition-reconstruction cycle of a MgAl-LDH. Taken from ref. 7.

By means of ultrasound techniques, we can alter the crystallisation processes of the materials and widen the application areas of the obtained materials. Ultrasound has attracted much attention during the last years in the synthesis of organic and inorganic materials. It is widely recognised that the effects caused by ultrasound can be mainly attributed to:

- 1) Rapid movement of fluids due to variation of sonic pressure, which accelerates mass transfer.
- 2) Formation and collapse of microbubbles (cavitation phenomena) creating localised high pressure and high temperature conditions.
- 3) Micro-streaming, in which a large amount of vibrational energy is applied to small volumes with little heating.⁸

Several studies show that sonication enhances and/or alter the dissolution processes, chemical reactions and nucleation and growth of precipitates in some inorganic powder synthesis.⁹⁻¹¹ For instance, Kooli *et al.*¹² studied the use of ultrasound to promote anion exchange in LDHs. They noted the possibility that ultrasound may improve the crystal quality of the LDH.

The comprehension of the LDHs properties as well as of the structure and the reactivity of the decomposed and reconstructed materials used as catalysts is an important target which requires understanding of the crystal chemistry. For that reason, in this chapter it is shown the study of the ultrasound treatment effect on layered double hydroxides.

4.1. INTRODUCTION

REFERENCE

1. S. Miyata, *Clays Clay Miner.*, 28 (1980) 50.
2. J.C.A.A. Roelofs, D.J. Lensveld, A.J. van Dillen, K.P. de Jong, *J. Catal.*, 203 (2001) 184.
3. F. Winter, X. Xia, B.P.C. Hereijgers, J.H. Bitter, A.J. van Dillen, M. Muhler, K.P. de Jong, *J. Phys. Chem. B*, 110 (2006) 9211.
4. D.H. Wells, W.N. Delgass, K.T. Thomson, *J. Am. Chem. Soc.*, 126 (2004) 2956.
5. R.J. Chimentao, S. Abelló, F. Medina, J. Llorca, J.E. Sueiras, Y. Cesteros, P. Salagre, *J. Catal.*, 252 (2007) 249.
6. X. Lei, F. Zhang, L. Yang, X. Guo, Y. Tian, S. Fu, F. Li, D.G. Evans, X. Duan, *Am. Inst. Chem. Eng.*, 53 (2007) 932.
7. C. Forano, T. Hibino, F. Leroux, C. Taviot-Gueho, *Handbook of Clay Science* (Ed. F. Bergaya, B.K.G. Theng, G. Lagaly) (2006) 1053.
8. T.J. Mason, *The Royal Society of Chemistry* (1990) 157.
9. Y. Fang, D.K. Agrawal, D.M. Roy, P.W. Brown, *J. Mater. Res.*, 7 (1992) 2294.
10. H. Jiasang, K.K. Agrawa, Y. Fang, R. Roy, *J. Mater. Sci.*, 28 (1993) 5297.
11. N. Enomoto, H.L. Choi, N. Katsumoto, Z. Nakagawa, *Trans. Mater. Res. Soc. Japan*, 14A (1994) 777.
12. F. Kooli, W. Jones, V. Rives, M.A. Ulibarri, *J. Mater. Sci. Lett.*, 16 (1997) 27.

4.2. STRUCTURE EVOLUTION OF LAYERED DOUBLE HYDROXIDES ACTIVATED BY INDUCED RECONSTRUCTION

4.2.1. Introduction

Layered double hydroxides (LDHs), also known as hydrotalcites (HTs) have attracted considerable attention in the past few years due to their potential uses as adsorbents, anion scavengers, catalysts, catalysts precursors or catalysts supports. LDHs have the general formula $[M^{II}_{1-x}M^{III}_x(OH)_2]^{x+} A^{n-}_{x/n} nH_2O$, where M^{II} and M^{III} stand for a divalent and a trivalent cation octahedrally coordinated with hydroxyl groups sharing edges to form brucite-like layers. These edge-sharing octahedral units form infinite layers with the hydroxyl ions sitting perpendicular to the plane of the layers.¹ In LDHs, a fraction of the divalent cations in the brucite lattice is isomorphically substituted by trivalent cations such that the layers acquire a positive charge, which is balanced by intercalation of anions between the layers (represented as A^{n-} in the general formula). Crystallisation water molecules are also found in the interlayer space.

The thermal decomposition of LDHs leads to mixed metal oxides, which are characterised by high specific surface areas, homogeneous dispersion of metals and unique acid–base properties, which presumably exposes strong Lewis base sites.^{2,3,4} The basic properties of these sites depend on the nature and ratio of the metallic cations in the layers.⁵ These mixed oxides are able to recover the original layered structure by treatment with water. Interestingly, the reconstruction of decomposed Mg–Al hydrotalcite by rehydration at room temperature has been reported to enhance the catalytic activity.⁶ During the rehydration in an inert atmosphere, the brucite-like layers are reformed and the charge-compensating anions are replaced by hydroxyl anions, thus forming Brønsted base sites, however this process results in an important decrease in specific surface area of the material respect to the corresponding mixed oxide.⁷

The crystallinity and textural properties of hydrotalcites are essential features for them to be utilised as catalysts^{8,9} and may be affected by various experimental parameters which determine the supersaturation of the synthesis medium such as pH and temperature of preparation, concentration of used solutions, flow rate during addition of reactants, hydrodynamic conditions in the reactor and/or post synthesis operations (e.g. an ageing of obtained precipitate). The crystal quality of LDHs affects their surface properties and the activity trend.¹⁰ Since hydrothermal treatment generally increases crystallinity, the application of ultrasound assisted rehydration on hydrotalcites has been reported as an effective method which permits the synthesis of materials with different surface characteristics leading to important differences in terms of catalytic activity.¹¹ In addition, the change in the nature of the cations in the layers, the M^{2+}/M^{3+} molar ratio, the nature of the compensating anions or the activation methodology can modify the acid–base properties of these catalysts.^{6,12}

4.2. STRUCTURE EVOLUTION OF LDH ACTIVATED BY INDUCED RECONSTRUCTION

Therefore, the comprehension of the LDHs properties as well as of the structure and the reactivity of the decomposed and reconstructed materials used as catalysts requires understanding of their crystal chemistry.

This work is focused on the investigation of the reconstruction capability of ZnAl and ZnMgAl calcined LDHs. For this purpose, we applied mechanical stirring and ultrasonication during rehydration of ZnAl and ZnMgAl LDHs to study the effect produced in the crystallinity of the materials as well as in the textural and acid-base properties.

The obtained samples were characterised by several physico-chemical techniques including powder X-Ray diffraction methods such as Rietveld refinement and XASF spectroscopy, to study the crystallinity of the materials. The elucidation of the characteristics of the reconstructed samples is of fundamental importance in studies of these materials as catalysts. Here, the carbonylation of glycerol with urea has been selected as catalytic test to identify the influence of crystalline, textural and acid-base properties of the reconstructed samples on the catalytic properties.

4.2.2. Experimental

i. Preparation of the samples

The parent ZnAl and ZnMgAl HTs with a M^{2+}/M^{3+} molar ratio of 2 were obtained according to the standard co-precipitation method¹ as follows. The appropriate amounts of $Zn(NO_3)_2 \cdot 6H_2O$, $Mg(NO_3)_2 \cdot 6H_2O$ and $Al(NO_3)_3 \cdot 9H_2O$ were dissolved in 150 cm³ of distilled water and added dropwise into a glass vessel which initially contained 200 cm³ of deionised water. The pH was controlled by adding a 2M NaOH + 1M Na₂CO₃ solution and was kept at 10. Both solutions were mixed under vigorous stirring. The suspension was stirred overnight at room temperature. The precipitated solid was filtered and washed several times with hot deionised water and dried at 383 K to yield the as-synthesised hydrotalcite (labelled from now as HT1as for ZnAl-HT and HT2as for ZnMgAl-HT). The solid was calcined in air by heating at 10 K/min up to 723 K over 5 hours to obtain the corresponding mixed oxides (HT1c and HT2c). These mixed oxides were rehydrated in liquid phase at room temperature under mechanical stirring and sonication for various time periods under an inert atmosphere to maximise the accessibility of the OH⁻ groups.^{11,13} The samples are denoted as HT1RMx or HT2RUSx (where HT1 and HT2 correspond to ZnAl and ZnMgAl HTs, respectively and x refers to the time of hydrothermal treatment in hours).

ii. Characterisation of the samples

Zn, Mg and Al elemental chemical analyses were obtained by induced coupled plasma (ICP) after dissolution of the samples in HNO₃. Specific surface areas were determined by nitrogen adsorption at 77 K using a Micromeritics ASAP 2000 equipment. Samples were previously degassed in situ at 393 K under vacuum.

Surface areas were calculated using the Brunauer-Emmet-Teller (BET) methods over a p/p_0 range where a linear relationship was maintained. XRD measurements were made in transmission mode using a Bruker-AXS D8-Discover diffractometer with a vertical theta-theta goniometer and a Vantec linear detector. Monochromatic Cu_k radiation was obtained from a copper X-ray tube operated at 40 kV and 40 mA and a Ge monochromator. Data were recorded over a 2θ range of $5\text{-}70^\circ$ with an angular step of 0.008° at 4.5 s/step. Patterns were identified using files from the ICDD (International Centre for Diffraction Data).

Hydrotalcite samples present a marked anisotropic peak broadening due to the crystal structure itself: stacking faults and disorder. The conventional profile fitting consider that the peak width for a phase changes as a function of 2θ angle according to the Cagliotti¹⁴ expression:

$$\text{FWHM}_{\text{hkl}}^2 = U \tan^2 \theta + V \tan \theta + W$$

Where FWHM_{hkl} is the full width at half maximum of a hkl reflection and U, V and W are parameters to be refined in a diffractogram. Due to the anisotropic peak broadening in hydrotalcites, it is necessary to estimate the FWHM separately for reflections that belong to (00l), (0kl), (h0l) or (hkl) family. In the present case, the anisotropic crystallite size broadening was corrected with the Spherical Harmonics approach.

The profile fitting was performed in two steps. First, the cell parameters and the peak width were fitted. After that, the FWHM of each reflection was obtained together with their Miller indices. The contribution of the diffractometer to the peak width was considered by analysing the LaB_6 SRM 660a.

The second step involved the introduction of the structure¹⁵ into the profile analysis, the Rietveld analysis itself. The Spherical Harmonics approach was used again to correct the anisotropic broadening but at this stage all the parameters (a total of 10 independent parameters) were fixed from the values fitted in the previous step. The cell parameters and the general atomic coordinates for all atoms (except H) were refined. The isotropic temperature factors for groups of atoms were also refined. The occupation site was fixed according to the chemical analysis.

All the diffractogram fittings were performed by means of the program TOPAS¹⁶ working under the programming mode (launch mode) with local routines.

The estimation of the weight fractions of the different phases co-existing in the sample was calculated with the Rietveld method according to the well-known relationship:¹⁷

$$W_p = S_p \rho_p V_p^2 / \sum_{i=1}^n S_i \rho_i V_i^2$$

4.2. STRUCTURE EVOLUTION OF LDH ACTIVATED BY INDUCED RECONSTRUCTION

where W is the weight fraction, ρ is the crystal density, V is the unit cell volume and S is the refinable scale factor for phase p in a mixture of n phases.

X-ray absorption spectra (XAFS) were recorded at the BM25 beam line (SpLine) of the ESRF synchrotron (Grenoble, France). The spectra were acquired in transmission mode using a Specac infrared-transmission cell equipped with Kapton windows. The samples were diluted in a cellulose powder and pressed to form wafers with 13-mm diameter. The mass of sample in the wafers was optimised to maximise the signal-to-noise ratio in the ionisation chambers. The wafer was placed in a stainless steel holder directly to make the analysis. The experiment was performed at room temperature under a constant flow of Ar.

For energy calibration, a standard Zn foil was introduced before samples. Typical EXAFS spectra of Zn K edge were recorded from 9500 to 10200 eV, with a variable step energy value, with a minimum 0.5-eV step across the XANES region. XANES region data were normalised and derived analytically using standard algorithms (software FEFFIT). EXAFS spectra were analysed using Horae,¹⁸ IFEFF¹⁹ and FEFF6²⁰ software packages. The absorption spectra were normalised and converted into k -space. Data in the range of k from 2 to 9 Å⁻¹ were Fourier-transformed and fitted in R -space.

The basicity-acidity measurements were obtained by temperature programmed desorption (TPD) of CO₂ or NH₃ on a Thermo Finnigan TPDRO 1100 equipped with a TCD detector. Typically, ca. 0.150 g of sample were placed in a tubular quartz reactor. The sample was pretreated with Ar at 353 K during 1 h and then cooled to room temperature and treated with a CO₂ or a NH₃ flow (3% CO₂ in He or 5% NH₃ in He, respectively). The desorption of CO₂ was measured by heating the sample from room temperature to 1073 K at a heating rate of 10 K/min in He flow. Water was trapped on magnesium perchlorate. The number of basic sites was calculated from the CO₂ peaks by deconvolution using the software of the equipment, and a calibration of the instrument using a known amount of CaCO₃. On the other hand, the desorption of NH₃ was measured by heating the samples from room temperature to 973 K at a heating rate of 20 K/min under He flow. In this case, water was trapped on soda lime. The number of acid sites was calculated by calibration of the equipment using pulses of a known amount of NH₃. Thermogravimetric analysis (TGA) curves were recorded in a Labsys/Setaran TG thermo balance apparatus from room temperature to 1173K, at a heating rate of 10 K/min.

The carbonylation of glycerol with urea was performed in a 50 mL round-bottomed flask at 423 K under low pressure (≈ 0.4 bar) and magnetic stirring (500 r.p.m.). Typically, glycerol was placed into the reactor and led to the reaction conditions before the urea (molar ratio glycerol/urea = 2) and the activated catalyst (10 wt% respect to glycerol) were added. The reaction was stopped after 5 h and then methanol was added as solvent to analyse the products. The samples were filtered and analysed by GC analysis equipped with a FID detector. This was performed on a Shimadzu GC (QP 2010) with a Zebron ZW-WAX capillary column.

4.2.3. Results and Discussion

The different LDH phases were characterised by X-ray diffraction. Figure 4.2.1 A shows the normalised XRD patterns of the prepared LDHs and some differences have been observed among the as-synthesised sample and the reconstructed ones. Note that XRD patterns for all the samples show sharp and intense (00l) reflections; however, the basal reflections in the parent material (HT1as) are broader than those presented by the hydrothermally treated samples. Moreover, the reflections found at intermediate angles become sharper when ultrasound is applied. The sharpness and symmetry of the (0kl) reflections of the hydrothermally treated LDHs evidence their better crystallinity and probably these samples present a very low stacking fault density. On the other hand, new peaks in the mid- 2θ region ($2\theta \approx 32^\circ$ and $2\theta \approx 37^\circ$) were found corresponding to ZnO phase (Zincite ICDD: 89-0510). The hydrothermally treated samples presented (00l) peaks slightly shifted to higher 2θ angles compared to the as-synthesised sample (HT1as) probably due to a higher amount of crystallisation water molecules located into the interlayer of the later. The resulted diffraction patterns were refined by applying the Rietveld method (Figure 4.2.1 B) to get accurate information about structure of the samples. The corresponding structural data obtained by this method is reported in Table 4.2.1. The space group generally observed for this kind of compounds is R3m, so the cell parameter c is equal to $3d_{003}$. This cell parameter depends on the nature and charge of the interlamellar anions and the interaction between them and the layers as well as the presence and number of water molecules. The decrease in the a parameter may be related to the partial reactivity of Zn during rehydration to form a zinc oxide phase. This segregation of Zn provokes a decrease of the Zn/Al molar ratio in the HT phase and, consequently, the distance between adjacent cations (i.e., a parameter) decreases. The distances metal-oxygen reported in Table 4.2.1 are an average value obtained taking into account that both divalent and trivalent cations are located in the same positions. A slight increase of d_{M-OH} can be noted when ultrasound was applied; however, the d_{M-OH} is slightly lower in the sample rehydrated mechanically. These differences are also noticeable in the HO-OH distances. The $d_{(HO-OH)OH}$ was elongated when samples were submitted to ultrasound assisted treatment, respect to the as-synthesised sample (HT1as) and the mechanically rehydrated (HT1RM24). The increase HO-OH distance in sonicated samples indicates that the octahedral environment of the cations is more flattened and, consequently, the layer thickness decreases.^{21,22} The sample HT1RUS0.5, i.e. ultrasonicated during the shorter period of time, presented the higher $d_{(HO-OH)OH}$ and a HO-M-OH angle of 82.25° . Moreover, the layer-interlayer distance increases from the as-synthesised sample to the samples hydrothermally treated.

4.2. STRUCTURE EVOLUTION OF LDH ACTIVATED BY INDUCED RECONSTRUCTION

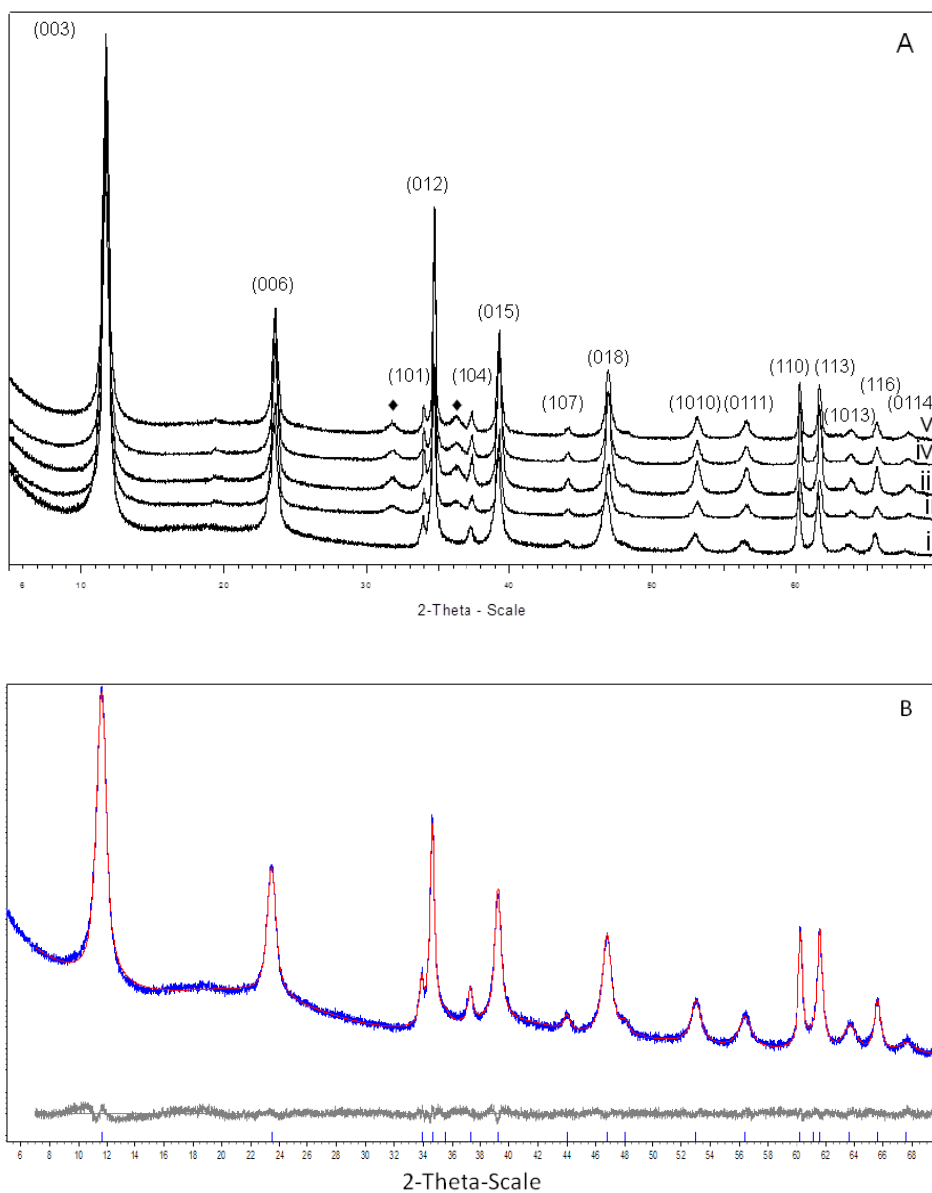


Figure 4.2.1. A) Normalised PXRD diffractograms for HT1 series: i) HT1as; ii) HT1RM24; iii) HT1RUS0.5; iv) HT1RUS2 and v) HT1RUS10. B) Rietveld refinement using the anisotropic peak broadening model for sample HT1as. Experimental diffractogram (blue), calculated (red) and difference (grey).

Table 4.2.1. Structural parameters (in Å) obtained by Rietveld refinements

Sample	a	c	d _(M-OH)	d _{(OH-OH)oh}	d _{(O-OH)ii}	Angle HO-M-OH	Layer thickness	R _{wp} ^a	nH ₂ O ^b	% ZnO
HT1as	3.0695(1)	22.716(1)	2.005(1)	2.582(4)	2.95(3)	80.14(9)	1.878(4)	5.85	0.75	–
HT1RM24	3.0649	22.6254(8)	1.995(1)	2.555(4)	3.18(1)	79.65(8)	1.844(4)	5.81	0.64	5.95 ± 0.12
HT1RUS0.5	3.0644	22.6309(5)	2.0342(8)	2.676(2)	3.05(9)	82.25(5)	2.007(2)	4.93	0.61	6.86 ± 0.12
HT1RUS2	3.0648	22.6488(6)	2.009(8)	2.601(3)	3.133(9)	80.64(6)	1.906(3)	5.44	0.61	7.35 ± 0.10
HT1RUS10	3.0650	22.6317(5)	2.0076(9)	2.593(3)	3.06(1)	80.47(7)	1.896(2)	5.30	0.62	8.39 ± 0.12

^aConventional Rietveld goodness of fit

^bCalculated by TGA

4.2. STRUCTURE EVOLUTION OF LDH ACTIVATED BY INDUCED RECONSTRUCTION

As a preliminary stage, useful information can be obtained by comparison of the full-width at half-maximum values (FWHM) for the different Bragg reflection families. The variation of FWHM with the (*hkl*) planes was plotted by means of the Williamson-Hall²³ plot. This plot is based on the assumption that the peak size broadening (FWHM_L) and the peak strain broadening (FWHM_e) change with the 2θ angle according to:

$$\text{FWHM}_L = K\lambda/L \cos \theta ; \text{FWHM}_e = C\varepsilon \tan \theta$$

In theory, the resulting peak width is the convolution product of FWHM_L and FWHM_e. However, the Williamson-Hall plot simplifies the problem by assuming that the resulting peak width is the sum of β_L and β_e. Then, the peak width obtained from the diffractogram (FWHM_{exp}) (after subtraction of the instrumental contribution) can be expressed as:

$$\text{FWHM}_{\text{exp}} \cos \theta = C\varepsilon \sin \theta + K\lambda/L$$

By plotting the FWHM_{exp} cos θ term against sin θ for each (*hkl*) reflection is obtained a distribution of points. The dependent term is related with the microstrain component (=Cε) while the independent one is related with the crystallite size (=Kλ/L). This type of representation is very useful for a quick view of the behaviour of different (*hkl*) families.

In the Williamson-Hall plots (Figure 4.2.2), the widths of (003) and (006) planes are almost identical for all the samples, therefore present a slope ≈ 0, indicating mainly size effects in the (00l) direction. The FWHM of the reflection (110) decrease from the as-synthesised sample (HT1as) to the hydrothermally treated, being these values lower on those samples treated with ultrasound. On the other hand, (h0l) and (0kl) reflections presented an increase in width with increasing the Miller index. Moreover, the family of planes are reasonable aligned. This effect could be an indicative of micro-strain, but due to the similar behaviour found for the (h0l), (0kl) and (11l) families it can be deduced that lattice strain is negligible and only size effects can be considered.²⁴ It noticeable the different slope presented by the alignment of the different families of planes in the different samples. It has been observed a decrease in the slope from the as-synthesised sample to the ultrasonicated treated ones.

The profile analysis also allows obtaining information about the stacking (calculated from the (00l) Bragg reflection) and crystallinity of the samples obtained.

The mean crystallite size for the different Bragg reflection was obtained from the integral breadth (β) by using the Double-Voigt Approach and applying the Scherrer equation:²⁵

$$\beta = \lambda/L \cos \theta$$

Where L is the volume weighted mean crystallite size. It was not considered the microstrain in the crystallite size estimation in order to simplify the problem. The

mean crystallite size estimation obtained for the different Bragg reflections is given in Table 4.2.2. The crystallite size calculated for the different families of planes increase with the hydrothermal treatment. The calculations confirmed smaller crystallite sizes in the parent material (HT1as) along the different directions.

Table 4.2.2. Mean crystallite size estimation (in Å) for the different hkl families

Sample	(00l)	(0kl)	(h0l)	(hkl)
HT1as	119(7)	392(3)	221	243(3)
HT1RM24	153 (6)	542(7)	301	285(3)
HT1RUS0.5	158(8)	594(5)	331	325(3)
HT1RUS2	166(1)	620(6)	361	327(4)
HT1RUS10	156 (7)	572(5)	351	316(3)

The refinement performed also provides information about the extra-phases coexisting in the samples. Thus, while the sample HT1as presented a pure LDH structure (with an empirical formula $Zn_{0.6682}Al_{0.3318}(OH)_2(CO_3^{2-})_{0.148} \cdot 0.75 H_2O$), the rehydrated samples showed a segregation of Zn^{2+} from the lamellar structure to form ZnO phase (zincite) due to dissolution-precipitation phenomena produced during the hydrothermal treatment which cannot be re-incorporated into the brucite-like layers. The weight % of the phases presented in the sample was estimated by using the Rietveld method. The total re-structuration of the mixed oxide was not achieved after the rehydration under mechanically stirring for 24 h and ≈ 6 wt% of ZnO was found. After this, the amount of ZnO increased with the increasing time of sonication of the sample indicating that the application of ultrasound favours the segregation of Zn^{2+} from the brucite-like layers and thus the formation of the ZnO. Extra-phases of Al were not detected by this technique.

Solid ^{27}Al NMR analyses of HT1as and the rehydrated ones confirmed that almost the totality of Al had an octahedral coordination. Aluminium octahedrally coordinated with OH groups showed a signal at about $\delta = 10$ ppm. The calcined sample (HT1c) showed moreover a signal centred on $\delta = 80$ ppm corresponding to Al tetrahedrally coordinated, which practically disappears after the hydrothermal treatment, as seen in Figure 4.2.3.

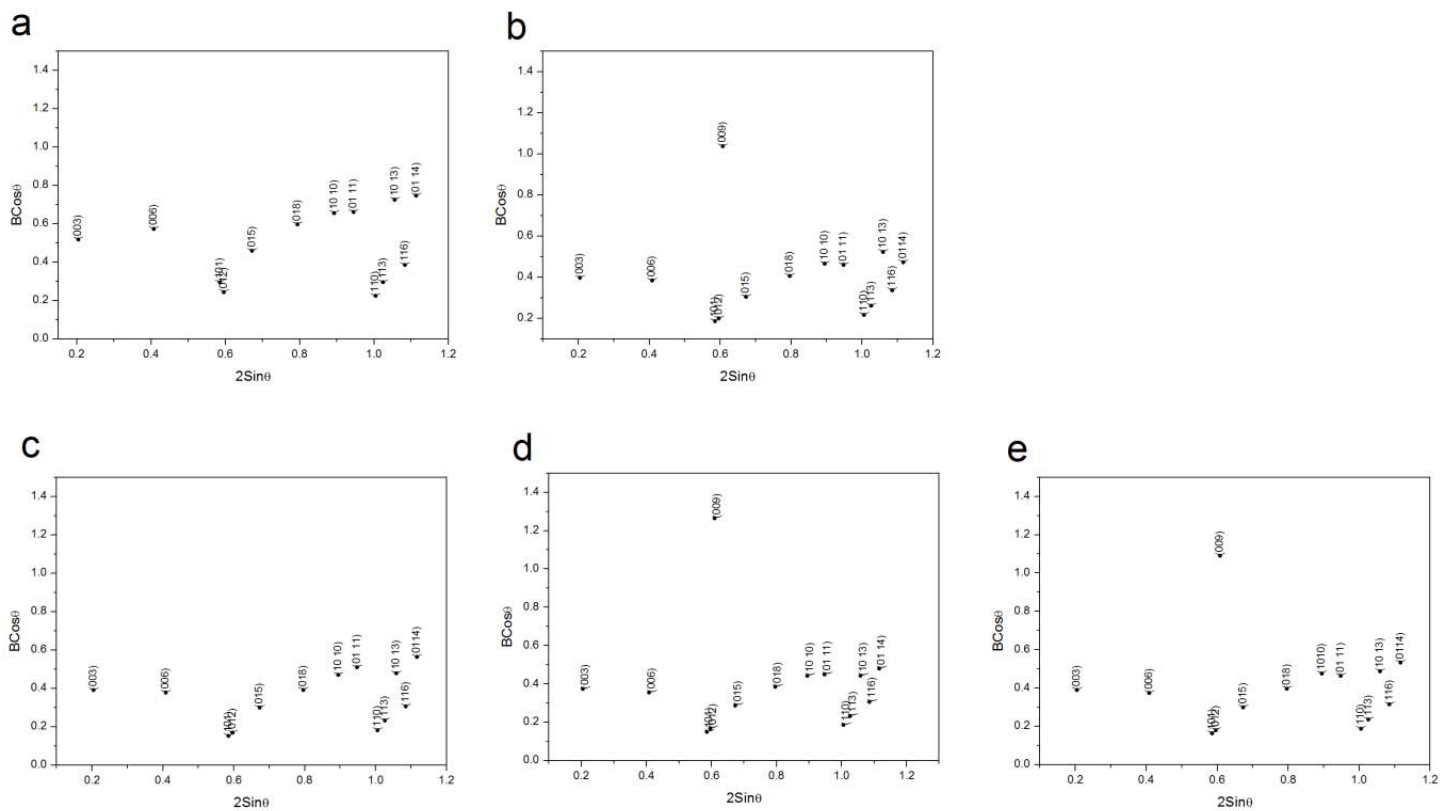


Figure 4.2.2. Williamson-Hall plots for HT1 series. a) HT1as; b) HT1RM24; c) HT1RUS0.5; d) HT1RUS2 and e) HT1RUS10.

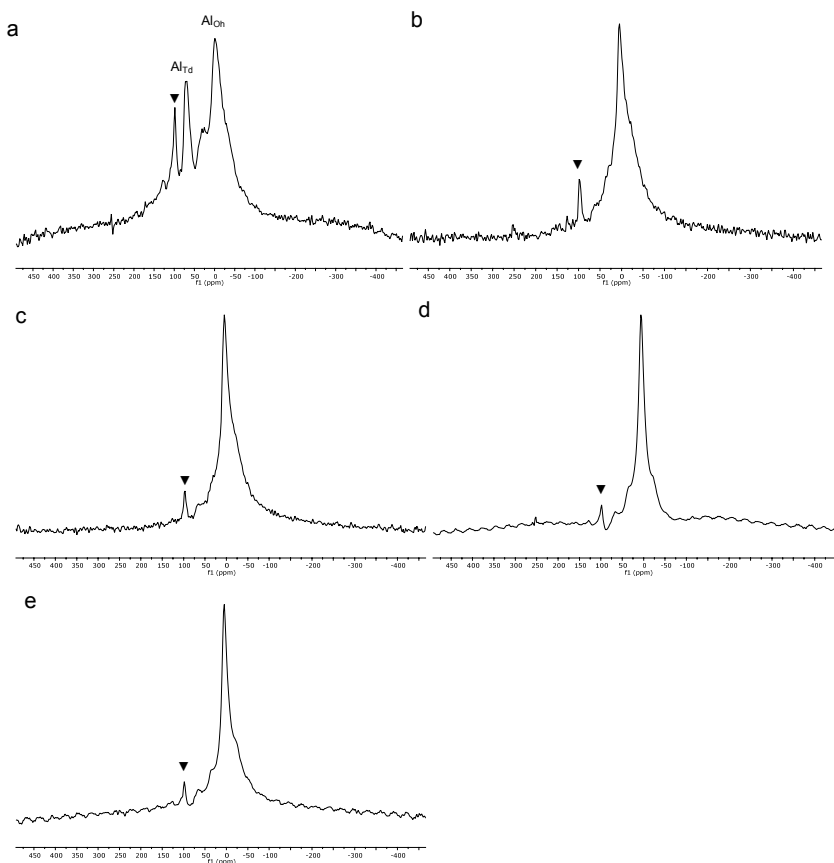


Figure 4.2.3. ^{27}Al NMR of the HT1 series. a) HT1c (calcined HT1as at 723 K) ; b) HT1RM24; c) HT1RUS0.5; d) HT1RUS2 and e) HT1RUS10. (▼) Attributed to spinning side bands.

Detailed local characterisation of the Zn environment was also studied by EXAFS spectroscopy. Changes in the XANES region at the Zn K-edge were observed for the different rehydrated samples (Figure 4.2.4). As a first glance, the Zn K-edge profiles resemble the one of the parent material when the hydrothermal treatment is applied, indicating a higher reconstruction degree of the material. However, complete reconstruction of the calcined hydrotalcite was not achieved as previously confirmed by Rietveld refinements, which indicated a certain amount of ZnO in the rehydrated samples.

4.2. STRUCTURE EVOLUTION OF LDH ACTIVATED BY INDUCED RECONSTRUCTION

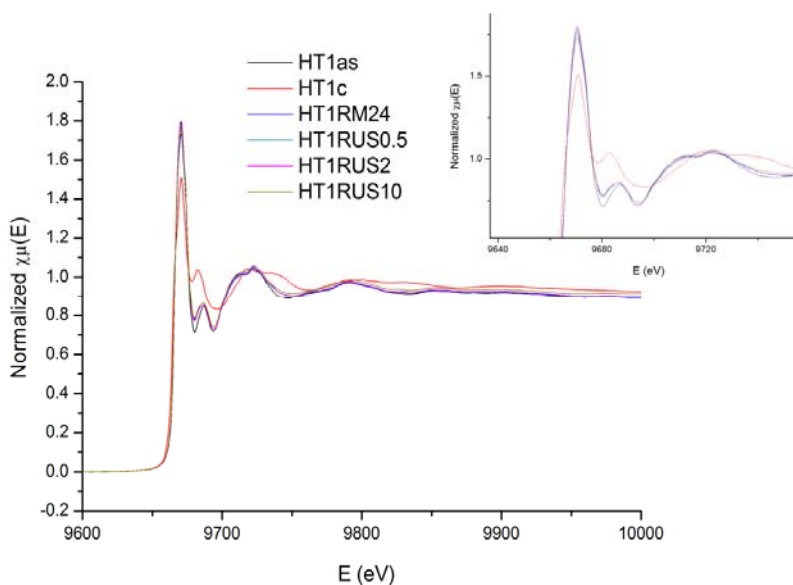


Figure 4.2.4. XANES spectra of ZnAl hydrotalcites (HT1 series) after the hydrothermal treatment at Zn *k*-edge.

The EXAFS spectra show similar distribution curves indicating that the local order around the Zn atoms remains unchanged after applying the different hydrothermal treatments (Figure 4.2.5). The first peak corresponds to the presence of oxygen atoms surrounding the cation (Zn). The results of the Zn-O distances are consistent with an octahedral environment of OH groups around the Zn²⁺ (Table 4.2.3).²⁶ Even though the Zn-O distance is expected to be 2.11 Å in an octahedral environment,²⁷ shorter Zn-O distances would also be expected (especially in Al rich HTs) due to the difference in ionic radii of the former cations Zn²⁺ ($r_{\text{Zn(II)}} = 0.740 \text{ \AA}$) and Al³⁺ ($r_{\text{Al(III)}} = 0.535 \text{ \AA}$).^{17,28} Results of the EXAFS data analysis presented in Table 3 are from fits considering single scattering of the entire spectrum. As an example, figure 6 shows the experimental and calculated Zn environment spectrum of sample HT1as. A good fit was obtained for all the spectra. The second shell is related to the presence of Al³⁺ or Zn²⁺ cations. Compounds with a trivalent rate $x = 0.33$ are suggested to be based on a structure composed by a divalent cation surrounded by three M³⁺ and three M²⁺ cations and six divalent cations surrounding a trivalent metal; i.e. for a Zn_{0.67}Al_{0.33}-HT, six Zn²⁺ are surrounding Al³⁺ centers while three Zn²⁺ and three Al³⁺ surround Zn²⁺ centers.^{29,30,31}

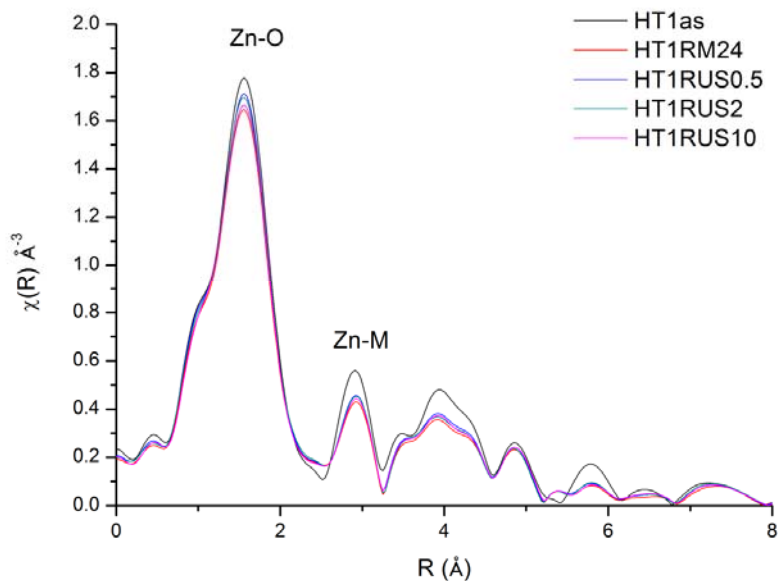


Figure 4.2.5. Zn *k*-edge Fourier transform of HT1 series. Distances are given without phase shift correction.

Zn²⁺ seems to conserve a six-fold coordination, since the distances Zn-O are higher than those bond lengths expected for a typical four-fold coordination (≈ 1.96 Å), although Zn-O distance slightly became shorter from 2.06 Å for the as-synthesised sample to 2.04 Å for the hydrothermally treated ones, probably due to the formation of zinc oxide during the rehydration. On the contrary, the Zn-Zn distance became longer from HT1as to rehydrated samples. No differences were found on Zn-O and Zn-Zn distances among samples submitted to ultrasound.

4.2. STRUCTURE EVOLUTION OF LDH ACTIVATED BY INDUCED RECONSTRUCTION

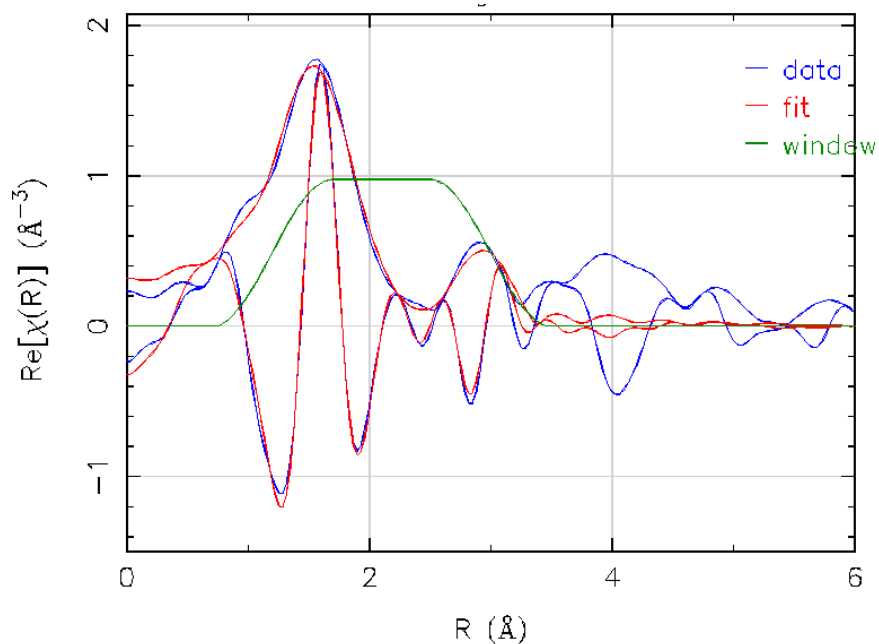


Figure 4.2.6. Experimental (blue) and calculated (red) Zn environmental radial distribution and EXAFS Fourier transform modulus for sample HT1as.

Table 4.2.3. Structural parameters (first two shells) of ZnAl-HT (HT1 series) obtained by EXAFS fitting. *N* represents the coordination number and σ^2 corresponds to the Debye-Waller factor

Sample	Bond	R (Å)	N	σ^2 (Å ²)
HT1as	Zn-O	2.06	6.0	0.01
	Zn-Al	3.03	3.0	0.02
	Zn-Zn	3.08	3.0	0.02
HT1RM24	Zn-O	2.04	5.3	0.01
	Zn-Al	3.03	2.5	0.02
	Zn-Zn	3.11	2.3	0.02
HT1RUS0.5	Zn-O	2.04	5.5	0.01
	Zn-Al	3.03	2.6	0.02
	Zn-Zn	3.11	2.5	0.02
HT1RUS2	Zn-O	2.04	5.5	0.01
	Zn-Al	3.03	2.6	0.02
	Zn-Zn	3.11	2.5	0.02
HT1RUS10	Zn-O	2.04	5.4	0.01
	Zn-Al	3.03	2.5	0.02
	Zn-Zn	3.11	2.4	0.02

Coordination numbers were calculated based on LDH sample Zn₂Al-CO₃: 6 Zn-O and Zn-Me (3Zn, 3Al) from ref. [26-28].

The specific surface area was measured in order to check the effect of the hydrothermal treatment and sonication in the textural properties of the samples. The S_{BET} of the samples, performed at liquid N_2 temperature (77 K), was observed to decrease with the hydrothermal treatment (Table 4.2.4). As expected, the calcined sample presented an increase in surface area and pore volume compared to the as-synthesised sample while the reconstructed samples presented a decrease in surface area.

The surface area of the parent hydrotalcite (HT1as) was found to be $64 \text{ m}^2/\text{g}$, decreasing to $44 \text{ m}^2/\text{g}$ for sample sonicated during the largest period of time (HTRUS10). The use of ultrasound did not lead to the increase of surface area as could be expected,^{11,13} but the opposite behaviour was found since surface area decrease from $51 \text{ m}^2/\text{g}$ in sample rehydrated mechanically (HT1RM24) to $45 \text{ m}^2/\text{g}$ for sample submitted at 0.5 h of ultrasonication (HT1RUS0.5), which is in agreement with the observed XRD and EXAFS data. These data are in agreement with those previously reported by Álvarez et al.^{32,33} who observed a decrease in surface area in MgAl-HTs despite the use of ultrasound. Furthermore, it should be noted that the surface area did not suffer modification at all among the samples submitted to ultrasound, independently of the time of treatment.

All the samples presented isotherms of type IV (Figure 4.2.7) according with the IUPAC classification, representing mesoporous materials with a strong interaction between the surface of the solid and the adsorbate³⁴ and no microporosity was observed in any sample. The samples presented a H1 type hysteresis, i.e. desorption started immediately after completion of adsorption.

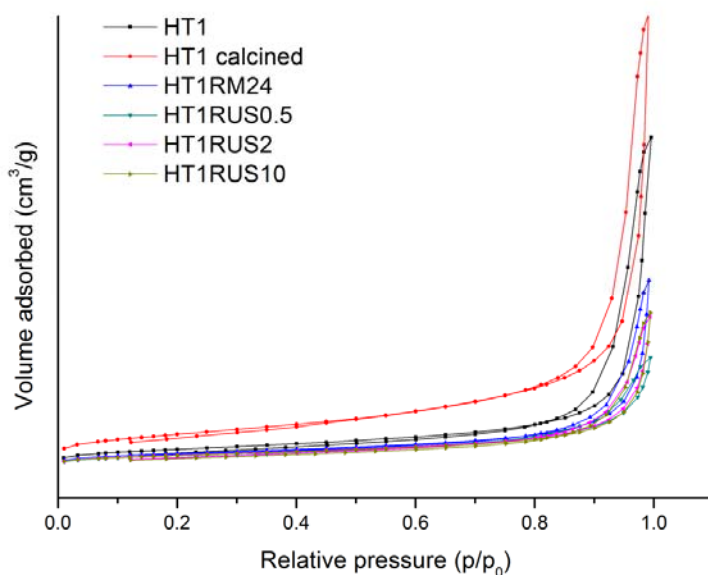


Figure 4.2.7. N_2 adsorption-desorption isotherms at 77 K of HT1 series.

4.2. STRUCTURE EVOLUTION OF LDH ACTIVATED BY INDUCED RECONSTRUCTION

The sample HT1as presented the higher specific surface area, as well as the higher pore volume and pore size. These values were observed to decrease when sample was mechanically rehydrated and decreased again when ultrasound was applied to the sample remaining almost constant with time of ultrasound applied (Table 4).

Table 4.2.4. Textural properties of ZnAl-HT (HT1 series) obtained by adsorption-desorption of N₂ at 77 K

Sample	BET surface area (m ² /g)	Pore volume (cm ³ /g)	Average pore diameter (Å)
HT1as	64	0.24	147
HT1RM24	51	0.13	99
HT1RUS0.5	45	0.10	87
HT1RUS2	45	0.11	99
HT1RUS10	44	0.11	96
HT1 calcined	111	0.32	115

The hydrothermal treatment conditions have influenced significantly the surface area of the rehydrated hydrotalcites. The textural properties of the hydrotalcites are related to the agglomeration of the particles and the particle size. The hydrothermal treatment and especially the application of ultrasound led to enhance the crystallinity of the material as seen by X-ray diffraction and EXAFS. This probably occurs because the ultrasound treatment enhances the solubility of the hydrotalcite phase generating particles in a wide distribution size. The smallest particles are thermodynamically unstable and tend to dissolve and vanish. The mass of these dissipating particles is available to grow the largest particles (less soluble) and coarsen the size distribution. So the small particles transfer their mass to the largest ones to produce a more metastable phase. This phenomenon is known as Ostwald ripening.^{35,36}

One of the most attractive features of hydrotalcites is their acid-base properties. Compared to their parent single metal oxides, hydrotalcites present acid-base pair sites of medium and strong-strength, which make this kind of compounds very desirable catalysts. The acid-base properties of the obtained HTs were studied by temperature programmed desorption (TPD) of CO₂ and NH₃. The measured amount of the desorbed probe molecules gives us information about the total concentration of surface active basic or acid sites. The data obtained are presented in Figure 4.2.8. It is show that the total basicity increases from the mixed oxide (obtained by calcination at 723 K of HT1as) to the rehydrated materials and reached a maximum for the catalyst HT1RUS10. The hydrothermal treatment led to an enhancement of the total number of basic sites (per mass unit) which are around three times higher in rehydrated samples than in the corresponding mixed oxide.

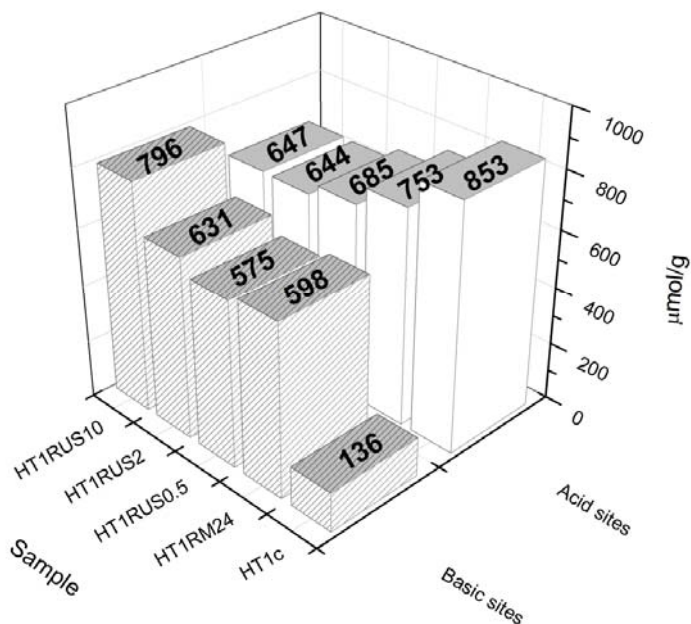


Figure 4.2.8. Total acidity and basicity of HT1 series samples determined by TPD of NH_3 and CO_2 .

TPD- CO_2 profiles show different adsorbed species (Figure 4.2.9 A). The strength of the basic sites may be assigned according to the temperature at which peaks appeared. The basic strength seems to decrease with the ultrasound treatment. The temperature of the maximum desorption rate of CO_2 was up to 20 K higher in sample rehydrated only mechanically than in sonicated samples. The CO_2 desorption of the calcined sample showed mainly one small peak at ≈ 500 K, while two main peaks at about 550 K (weak strength), 650 K (medium strength) were observed for the rehydrated samples. It is known that hydrotalcites present weak basic sites that originate from interlayer OH groups,^{3,37,38} thus these two main peaks can be ascribed to the decomposition of bicarbonate species formed by adsorption of CO_2 on the generated Brønsted basic sites as well as CO_2 desorbed from Zn-O and Al-O pairs. As a main difference, small peaks at higher temperatures (≈ 770 K) were observed in the samples submitted to ultrasound treatment, e.g. HT1RUS0.5, HT1RUS2 and HT1RUS10, with a contribution of approximately 10 % of the total CO_2 evolved. This peak was not observed for the sample rehydrated only mechanically (HT1RM24) and is attributed to strong Lewis basic sites which can be associated with unsaturated O^{2-} linked to Al. A Small peak at lower temperature was also distinguished in samples treated with ultrasound during larger periods of time, i.e. HT1RUS2 and HT2RUS10. It seems that the hydrothermal treatment and more specifically the

4.2. STRUCTURE EVOLUTION OF LDH ACTIVATED BY INDUCED RECONSTRUCTION

ultrasound-assisted rehydration induce changes in the population of the basic sites, which may affect the catalytic behaviour of these materials.

The opposite trend was found for the total concentration of acid sites which decreases from the mixed oxide (853 $\mu\text{mol/g}$) to the rehydrated samples, although changes in the concentration of acid sites have been found to be in a lower extent than those showed for the total concentration of basic sites. The amounts of desorbed NH_3 remain practically constant after the application of ultrasound and the maximum rate achieved was found for the calcined sample as could be expected due to the nature of the ZnO , essentially acid. The NH_3 TPD profiles are displayed in Figure 4.2.9 B. They extended in a 400 K-700 K temperature range and showed several overlapped components.

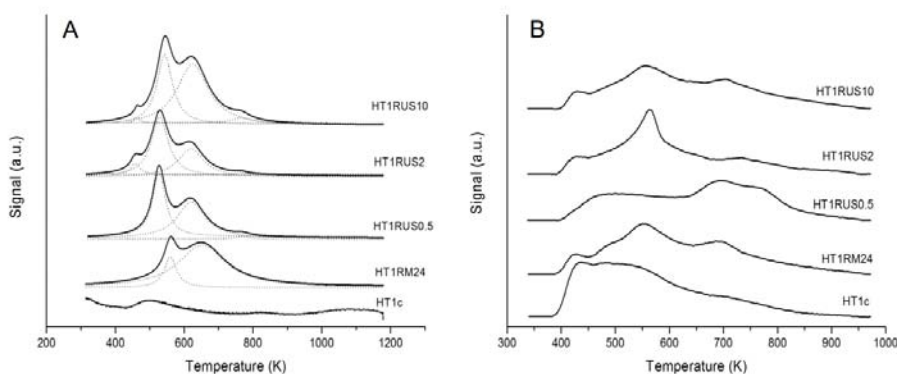


Figure 4.2.9. CO_2 (A) and NH_3 (B) desorption profiles obtained by temperature programmed desorption (TPD) for HT1 series.

i. Influence of the incorporation of a second divalent cation

A new series of hydrotalcites was prepared to study the effect of the incorporation of a second divalent cation (Mg^{2+}) to form a ternary HT. The new LDH phases ZnMgAl were prepared following the same procedure than that ZnAl LDHs. The ICP analysis confirmed the molar ratio $M^{(II)}/M^{(III)} = 2$ of the bulk, although higher proportion of Mg^{2+} than Zn^{2+} ions was found, obtaining a molar ratio $\text{Mg}^{2+}/\text{Al}^{3+} \approx 1.2$. The resulted diffraction patterns are displayed in Figure 4.2.10 A. Reflections can be indexed to the 3R polytype (space group R-3m). As a first glance, normalised diffractograms show less diffraction planes than those displayed by ZnAl hydrotalcites. Moreover, broader peaks are also observed. Any broadening of the diffraction peaks is indicative of structural disorder. The broadening of the (018) reflection and the well-resolved sharp (113) reflection in the pattern point toward the existence of stacking faults rather than turbostratic disorder in these samples.^{39,40} However, Rietveld refinements were also performed for these samples (Figure 4.2.10 B). The

corresponding data are reported in Table 4.2.5. The R_{wp} values for this refinement are higher than those obtained for the ZnAl LDHs, indicating the difficulty to accurately fitting the X-ray profiles even applying the spherical harmonics approach. The cell parameter a (representing the distance between two adjacent metals) is related to the ionic radius of cations. The experimental data are in agreement with the fact that the exchange of some Zn^{2+} by Mg^{2+} led to a decrease of the a cell parameter, since $r_{Mg(II)} = 0.66 \text{ \AA}$ is lower than $r_{Zn(II)} = 0.740 \text{ \AA}$. However, the hydrothermal treatment had not influence in the a parameter, since no changes were observed among all the HT2 samples.

The hydrothermal treatment did not have a marked correlation with the mean crystallite size and the different (hkl) families seem to be affected in different way.

From the crystallographic data, it is evident that ZnMgAl hydrotalcites present lower crystallinity degree than ZnAl hydrotalcites. Moreover, the background of these samples presented in the XRD is indicative of a certain amorphous phase. Moreover, it seems that the incorporation of magnesium as ternary cation led to the formation of more disordered materials. It can be expected that the formation of a hydrotalcite with cations of different size led to more distorted structures. On the other hand, the Mg^{2+} seems to stabilise the structure, since the ultrasound-assisted treatment did not lead to a segregation and crystallisation of ZnO as previously seem in ZnAl hydrotalcites. No magnesium or aluminium crystalline phases were detected by this technique.

The Zn K-edge EXAFS of the local layer structure were also analysed for these samples. The Fourier transform spectra are similar to that observed for HT1 samples. The EXAFS analysis confirmed that Zn^{2+} still have an octahedral environment of hydroxyl groups since the Zn-O distance was $d_{zn-o} = 2.06 \text{ \AA}$ (Table 4.2.5).

Table 4.2.5. Structural (in \AA) and textural parameters of HT2 series obtained by Rietveld refinement, EXAFS fitting and BET measurements.

Sample	a^a	c^a	R_{wp}	nH_2O^b	d_{Zn-O}^c	d_{Zn-Al}^c	d_{Zn-Zn}^c	BET surfaces area (m^2/g) ^d
HT2as	3.0527(1)	22.732(3)	7.35	0.59	2.06	3.03	3.16	95
HT2RM24	3.0532(1)	22.719(3)	6.32	0.55	2.05	2.98	3.16	84
HT2RUS0.5	3.0521(1)	22.686(3)	6.15	0.57	2.05	2.98	3.16	93
HT2RUS2	3.0517(1)	22.681(2)	6.77	0.55	2.05	2.98	3.16	92
HT2RUS10	3.0538(1)	22.730(2)	7.70	0.53	2.05	2.98	3.16	64

^aParameter obtained by Rietvel refinements.

^bCalculated by thermogravimetric analysis.

^cParameter obtained by EXAFS fitting.

^dCalculated by adsorption-desorption of N_2 at 77 K.

4.2. STRUCTURE EVOLUTION OF LDH ACTIVATED BY INDUCED RECONSTRUCTION

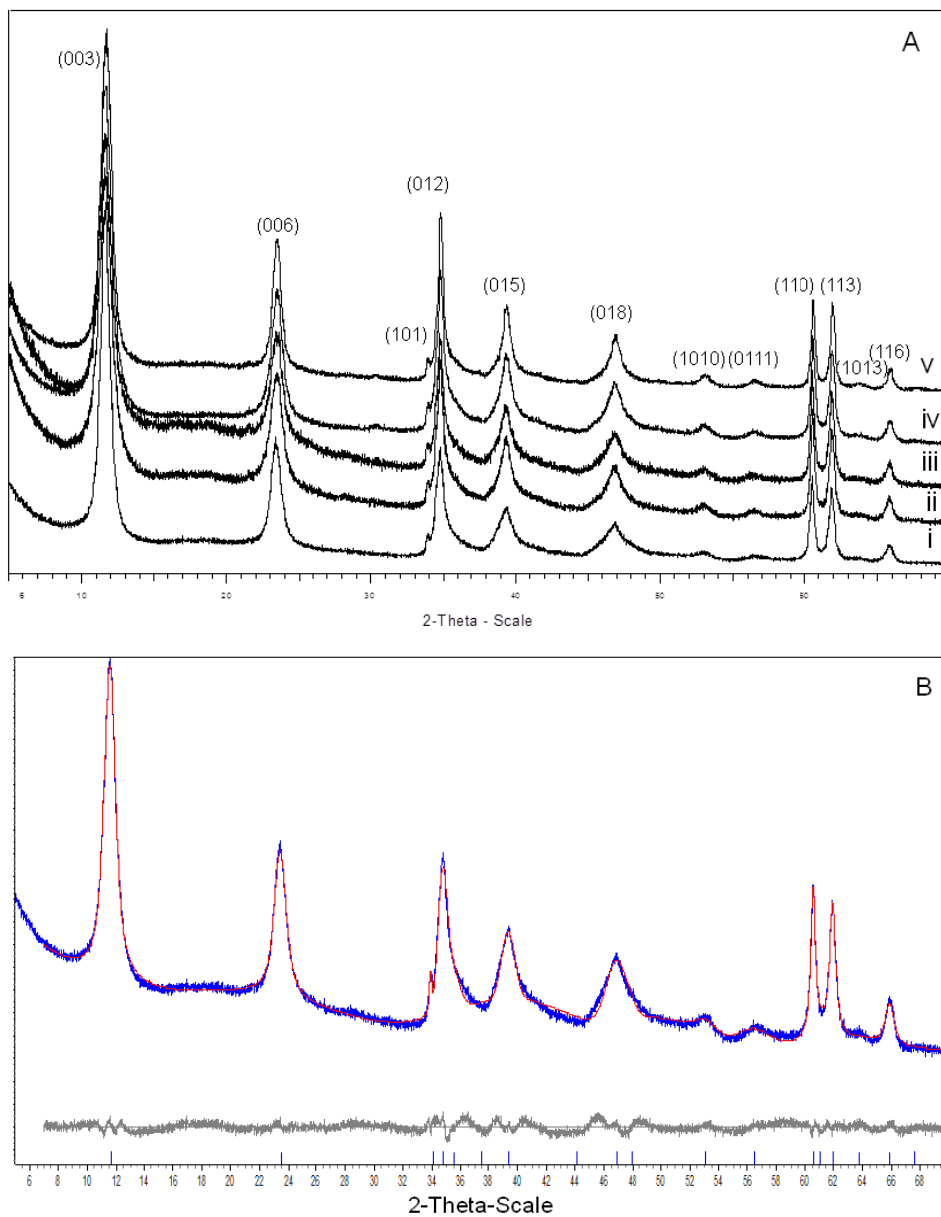


Figure 4.2.10. A) Normalised PXRD diffractograms for HT2 series: i) HT2as; ii) HT2RM24; iii) HT2RUS0.5; iv) HT2RUS2 and v) HT2RUS10. B) Rietveld refinement using the anisotropic peak broadening model for sample HT2as. Experimental diffractogram (blue), calculated (red) and difference (grey).

This decrease in crystallinity with respect to HT1 series was also confirmed by BET measurements, which showed higher specific surface area values for those samples containing magnesium (Table 4.2.5). Moreover, a marked influence on the specific surface area was not observed among the as-synthesised (HT2as) and the hydrothermally treated samples and only sample HT2RUS10 showed a significant decrease in surface area.

Changes in acid-base properties were also observed in these materials and an enhancement of basic-strength as well as basic sites was produced when the magnesium is introduced into the structure. The CO₂ desorption of the calcined (HT2c) sample gave a profile with a main peak at low temperature and a small peak at high temperature, while reconstructed samples showed three main peaks at about 400 K (weak strength), 600 K (medium strength) and 800 K (high strength) (Figure 4.2.11 A). The peak at the highest temperature is predominant in samples submitted to ultrasonication with a contribution of around 70% of the total CO₂ evolved. These peaks are attributed to strong Lewis basic sites which can be associated with unsaturated O²⁻ linked to Al or low coordinatively unsaturated Mg species. Moreover, peaks shifted at higher temperatures from sample rehydrated mechanically to ultrasonicated ones. For instance, the maxima for the high strength basic sites were observed at 765 K, 795 K and 781 K and 776 K for HT2RM24, HT2RUS0.5, HT2RUS2 and HT2RUS10, respectively.

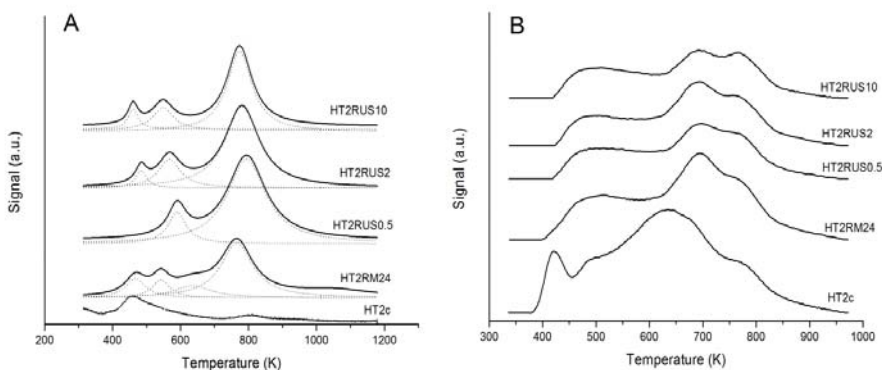


Figure 4.2.11. CO₂ (A) and NH₃ (B) desorption profiles obtained by temperature programmed desorption (TPD) for HT2 series.

The low temperature peak is more intense on calcined sample and can be ascribed to an adsorption at Lewis sites identified to oxygens linked to Mg cations located on basal planes or CO₂ species adsorbed on weakly basic OH⁻ groups.⁴¹

4.2. STRUCTURE EVOLUTION OF LDH ACTIVATED BY INDUCED RECONSTRUCTION

The rehydrated samples showed peaks at medium temperatures which can be assigned to the decomposition of bicarbonate species, formed by adsorption of CO₂ on the Brønsted basic sites.

The number of basic sites increased with the hydrothermal treatment and a maximum was found in sample HT2RUS2. As in HT1 series, the total concentration of acid sites in HT2 series decreased from the mixed oxide to the rehydrated samples. (Figure 4.2.12).

Changes in the total concentration of basic and acid sites were observed with the different treatments applied to the samples. Thus, ultrasonication has an effect on the population of these active centres. The total acidity and basicity of ZnMgAl hydrotalcites was found to increase with respect to those of ZnAl hydrotalcites. Since the aqueous solution of a Mg-based hydrotalcite is more basic than the corresponding aqueous solution of a Zn-based HT, the incorporation of Mg to form a ZnMgAl HT should produce an increase as much in number of basic sites as in basic strength. The increase in acidity (total number of basic sites per mass unit) may be due to a better dispersion of the active centres.

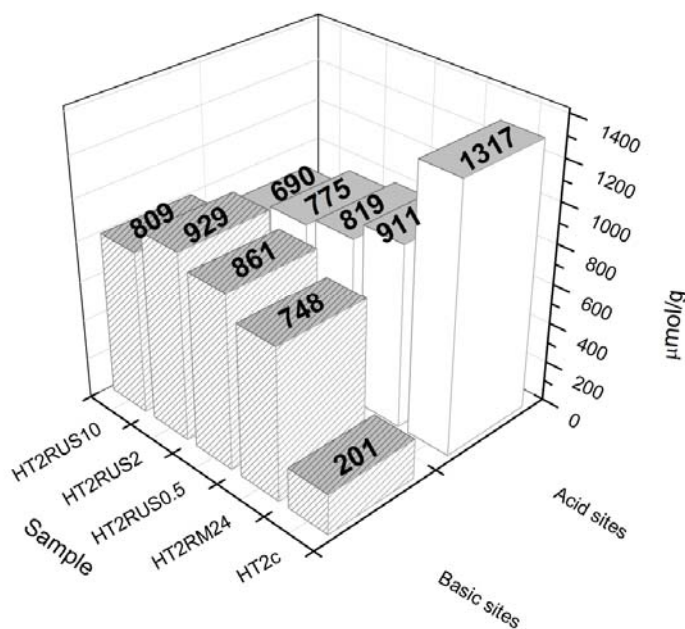


Figure 4.2.12. Total acidity and basicity of HT2 series samples determined by TPD of NH₃ and CO₂.

ii. Carbonylation of glycerol with urea

The carbonylation of glycerol with urea to glycerol carbonate (GC) was selected as a test reaction to analyse the acid-base properties of the reconstructed HT1 and HT2 series. Under identical conditions similar conversion values of glycerol were obtained for all the rehydrated materials, while calcined ones showed less activity. In this sense, the comparison of the activities of the reconstructed LDH materials were expressed in terms of the apparent turnover frequencies (TOF) by normalizing the reaction rates by the total surface area and the ratio between the total ammonia and total CO₂ uptake determined by TPD-NH₃ and TPD-CO₂ respectively. This involves the assumption that the number of active sites is proportional to the acid-base bifunctional pairs of the hydrotalcites materials. From the Table 6 the HT1c and HT2c mixed oxides presented similar TOF values of 2.4·10⁻³ and 2.6·10⁻³ mol/h·m², respectively. After rehydration the TOF values increased progressively for the both series of materials. As observed previously in Figures 4.2.8 and 4.2.12, it is noticeable that the ultrasound assisted hydrothermal treatment affected the population of the acid and basic sites. This effect was mirrored in the TOF values represented in Table 4.2.6. In fact, for both series, the rehydration process induced a nearly total number of acid and basic sites. It seems that the population of the both acid and base sites are determinant for the carbonylation reaction of glycerol with urea. Previous works^{42,43} reported that the reaction between urea and glycerol can be improved using an adequate combination of acid and base sites. The acid sites are able to activate the carbonyl group of the urea, whereas the base sites are engaged for the nucleophilic attack of the adsorbed glycerol. From its respective series the HT1US10 and HT2US10 materials exhibited the highest TOF values of 54.5·10⁻³ and 34.7·10⁻³ mol/h·m², respectively. For the HT2 materials the incorporation of Mg decreased the intrinsic total acid sites. The TOF values obtained for this HT2 samples presented lower values compared to the correspondent ones in the HT1 samples.

Table 4.2.6. Catalytic behaviour of HT1 and HT2 series

Catalyst	Basic sites (μmol/g)	Acid sites (μmol/g)	A/B	Conversion	TOF (mol/h)	TOF (mol/h m ²) (10 ⁻³)
HT1C	136	853	6.27	0.78	0.29	2.6
HT1RM24	598	753	1.26	0.89	1.53	30.0
HT1RUS0.5	575	685	1.19	0.84	1.55	34.4
HT1RU2	631	644	1.02	0.88	1.89	42
HT1RUS10	796	647	0.81	0.86	2.40	54.5
HT2C	201	1317	6.55	0.75	0.25	2.4
HT2RM24	748	911	1.22	0.89	1.63	19.4
HT2RUS0.5	861	819	0.95	0.82	1.89	20.3
HT2RUS2	929	775	0.83	0.82	2.13	23.2
HT2RUS10	809	690	0.85	0.86	2.22	34.7

4.2. STRUCTURE EVOLUTION OF LDH ACTIVATED BY INDUCED RECONSTRUCTION

4.2.4. Conclusions

Two families of hydrotalcites HT1 and HT2 series (ZnAl and ZnMgAl, respectively) were synthesised and characterised by several physico-chemical techniques. It was observed that crystallinity of samples is affected by the hydrothermal treatment. In HT1 series, ultrasound led to an increase in crystallinity with respect to the parent material (HT1as). So, this study showed that sonication enhances and/or alter the dissolution-precipitation/recrystallisation processes of the hydrotalcites leading to an improved crystal quality of the HTs. In HT1 series, ultrasound led to an increase in crystallinity with respect to the parent material (HT1as). Moreover, a segregation of ZnO was found when the samples were rehydrated, especially in those rehydrated by means of ultrasound. This ZnO could come from the crystallisation of amorphous ZnO existing in the parent material or the segregation of Zn from the brucite-like layers could occur. Due to the absence of ZnO in parent material determined by Rietveld refinements, the first possibility seems to be negligible. The enhancement of crystallinity affected all the plane families equally and has been associated to Ostwald ripening phenomena.

The incorporation of Mg into the structure seems to stabilise it and no significant segregation of Zn was observed. Moreover, the amount of Mg incorporated into the brucite-like layers is higher than the Zn cations. These samples showed lower crystallinity degree than the ZnAl-HT (HT1 series) and higher structural disorder.

It was noteworthy the influence of the rehydration treatment on the structural, textural and acid-base properties of hydrotalcites. Based on NH_3/CO_2 -TPD data obtained for two families of hydrotalcites (ZnAl-HT and ZnMgAl-HT), it seems that when the hydrotalcites are submitted to the ultrasound-assisted rehydration the population of the surface acid-base sites changes. The composition of the parent material also had an influence on the proportion of weak, medium and strong-strength basic sites and the hydrothermal treatment can induce changes in the population of the basic sites, therefore they must affect the catalytic behaviour of these materials. In our case, we have observed a different catalytic behaviour in the carbonylation of glycerol with urea when the glycerol conversion is normalised by taking into account the acid-base sites ratio.

Reference

1. D.G. Evans, X. Duan, Ed., Layered Double Hydroxides, Springer-Verlag, Berlin (2006).
2. Corma, S.B. Abd Hamid, S. Iborra, A. Velty, *J. Catal.* 234 (2005) 340.
3. B.F. Sels, D.E. De Vos, P.A. Jacobs, *Catal. Rev.* 43 (2001) 443.
4. A.L. McKenzie, C.T. Fishel, R.J. Davis, *J. Catal.* 138 (1992) 547.
5. J.I. Di Cosimo, V.K. Diez, M. Xu, E. Iglesia, C.R. Apesteguia, *J. Catal.*, 178 (1998) 499.
6. K.K. Rao, M. Gravelle, J.S. Valente, F. Figueras, *J. Catal.*, 173 (1998) 115.
7. J. Roelofs, A. J. van Dillen, K. P. de Jong, *Catal.Today* 60 (2000) 297.
8. S. Kannan, R.V. Jasra, *J. Mater. Chem.*, 10 (2000) 2311.
9. S. K. Sharma, P. K. Kushwaha, V. K. Srivastava, S. D. Bhatt, R. V. Jasra, *Ind. Eng. Chem. Res.*, 46 (2007) 4856.
10. D. Kishore, S. Kannan, *App. Catal. A*, 270 (2004) 227.
11. R.J. Chimentao, S. Abelló, F. Medina, J. Llorca, J.E. Sueiras, Y. Cesteros, P. Salagre, *J. Catal.*, 252 (2007) 249.
12. F. Prinetto, G. Ghiotti, R. Durand, D. Tichit, *J. Phys. Chem. B*, 104 (2000) 11117.
13. S. Abelló, F. Medina, D. Tichit, J. Pérez-Ramírez, Y. Cesteros, P. Salagre, and J.E. Sueiras, *Chem. Commun.* (2005) 1453.
14. P. Cagliotti, A. Paoletti, F.P. Ricci, *Nucl. Inst. and Meth.*, 3, (1958) 223.
15. U. Constantino, F. Marmottini, M. Nocchetti, R. Vivani, *Eur. J. Inorg. Chem.*, 1439-1446 (1998).
16. TOPAS, General Profile and Structure Analysis Software for Powder Diffraction Data, V4.2, 2009, Bruker AXS GmbH, Karlsruhe, Germany.
17. R.J. Hill, C.J. Howard, *J. Appl. Crystallogr.*, 20 (1987) 467.
18. B. Ravel, M. Newville, *J. Synchrotron Radiation*, 12 (2005) 537.
19. M. Newville, *J. Synchrotron Radiation*, 8 (2001) 322.
20. J.J. Rehr, R.C. Albers, *Rev. Modern Physics*, 72 (2000) 621.
21. V. Rives, M. A. Ulibarri, *Coord. Chem. Rev.*, 181, 61 (1999).
22. A. De Roy, C. Forano, J.P. Besse in *Layered Double Hydroxides: Present and Future*; (V. Rives, Ed.); Nova Sci. Pub. Co., Inc., New York, Chapter 1 (2001).
23. G.H. Williamson, W.H. Hall, *Acta Metall.* 1, 22-31 (1953)
24. A. Ennadi, A. Legrouri, A. De Roy, J.P. Besse, *J. Mater. Chem.*, 10 (2000) 2337.

4.2. STRUCTURE EVOLUTION OF LDH ACTIVATED BY INDUCED RECONSTRUCTION

25. A.R. Stokes, A.J.C. Wilson, *Proc. Camb. Phil. Soc.*, **38** (1942) 313.
26. R.D. Shannon, *Acta Crystallogr. Sect. A*, **32** (1976) 751.
27. N.E. Brese, M. O'Keefe, *Acta Crystallogr. Sect. B*, **47** (1991) 192.
28. T. P. Trainor, G.E. Brown Jr., G.A. Parks, *J. Colloid and Interface Sci.*, **231** (2000) 359.
29. W. Hofmeister, H. von Platen, *Cryst. Rev.*, **3** (1992) 3.
30. M. Vucelic, W. Jones, G.D. Moggidge, *Clays Clay Miner.*, **45** (1997) 803.
31. C.J. Serna, J.L. Rendon, J.E. Iglesias, *Clays Clay Miner.*, **30** (1982) 180.
32. M.G. Álvarez, A.M. Segarra, S. Contreras, J.E. Sueiras, F. Medina and F. Figueras, *Chem. Eng. J.*, **161** (2010) 340.
33. M.G. Álvarez, R.J. Chimentão, F. Figueras, F. Medina, *Appl. Clay Sci.*, **58** (2012) 16-24.
34. K.S.W. Sing, D.H. Everett, R.A.W. Haul, L. Moscou, E. Pierotti, J. Rouquerol, T. Seminiewska, *Pure Appl. Chem.*, **57** (1985) 603.
35. W. Ostwald, *Zeitschr Phys. Chem.*, **34** (1900) 495.
36. P.W. Voorhees, *Encyclopedia of Materials: Sci. and Technol.*, 1255.
37. F. Cavani, F. Trifiro, A. Vaccari, *Catal. Today* **11** (1991) 173.
38. F. Winter, X. Xia, B.P.C. Hereijgers, J.H. Bitter, A.J. van Dillen, M. Muhler, K.P. de Jong, *J. Phys. Chem. B* **110** (2006) 9211-9218.
39. A. Viani, A.F. Gualteri, G. Artioli, *Am. Miner.*, **87** (2002) 966.
40. A.V. Radha, P.V. Kamath, C. Shivakumara, *J. Phys. Chme. B*, **111** (2007) 3411.
41. G.Wu, X.Wang, Y. Sun, *Appl. Catal. A: Gen.*, **377** (2010) 107.
42. P. Ball, H. Füllmann, W. Heitz, *Angew. Chem., Int. Ed. Engl.* **19** (1980) 718.
43. M. J. Climent, A. Corma, P. De los frutos, S. Iborra, M. Noy, A. Velty, P. Concepción, *J. Catal.* **269** (2010) 140.

CHAPTER 5

GENERAL CONCLUSIONS

UNIVERSITAT ROVIRA I VIRGILI

HYDROTALCITE-LIKE COMPOUNDS FOR THE VALORISATION OF RENEWABLE FEEDSTOCKS

Mayra García Álvarez

Dipòsit Legal: T. 724-2012

CHAPTER 5

GENERAL CONCLUSIONS

Several hydrotalcite-based materials have been designed, prepared and characterised, as well as studied their catalytic behaviour in the valorisation of glycerol towards glycerol carbonate in a green and efficient method under soft conditions.

- Activated hydrotalcite-like compounds (calcined, rehydrated and anion exchanged hydrotalcites) have shown their capability for obtaining glycerol carbonates by transesterification of glycerol with DEC. The relation among the type of basicity as well as the amount of basic sites and the activity was established.
- The preparation of hydrotalcites supported in carbon nanofibers led to a much greater catalytic activity in the transesterification reaction than bulk activated hydrotalcites. In particular, calcined catalyst (HT-CNFC) showed a catalytic activity almost 300 times higher than that showed by bulk catalyst (HTc). The stability of these catalysts to both rehydration treatment and reaction medium was confirmed.
- The preparation of hydrotalcites supported on particles of alpha and gamma-alumina of controlled size allows to operate in a flow reactor, then to evaluate the extent deactivation of catalysts as a function of time on stream at full conversion of glycerol. Stable catalysts are obtained when $\alpha\text{-Al}_2\text{O}_3$ is the support.

CHAPTER 5. GENERAL CONCLUSIONS

- All these catalysts (bulk and supported catalysts) showed being stable and reusable in the transesterification of glycerol with DEC.
- The LDHs submitted to ultrasound assisted rehydration presented larger crystallite size than those rehydrated mechanically and noteworthy changes in the population of the acid-base sites were observed. The carbonylation of glycerol with urea was used to study the catalytic behaviour of these materials. Changes in catalytic activity were observed when the glycerol conversion is normalised by taking into account the acid-base sites ratio.

UNIVERSITAT ROVIRA I VIRGILI

HYDROTALCITE-LIKE COMPOUNDS FOR THE VALORISATION OF RENEWABLE FEEDSTOCKS

Mayra García Álvarez

Dipòsit Legal: T. 724-2012

UNIVERSITAT ROVIRA I VIRGILI

HYDROTALCITE-LIKE COMPOUNDS FOR THE VALORISATION OF RENEWABLE FEEDSTOCKS

Mayra García Álvarez

Dipòsit Legal: T. 724-2012

APPENDIX 0

DETERMINATION OF PRODUCTS

UNIVERSITAT ROVIRA I VIRGILI

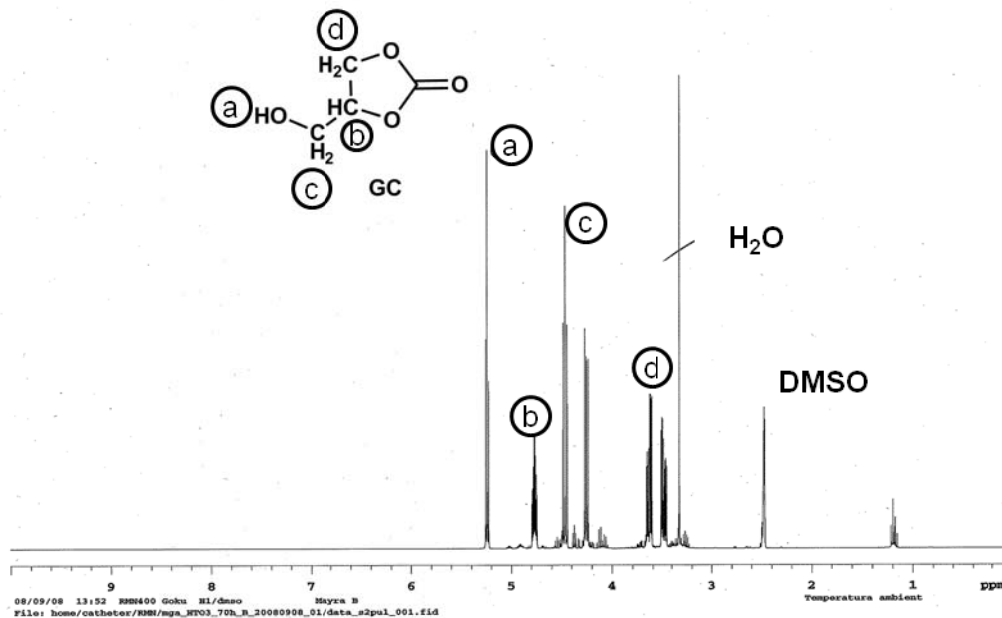
HYDROTALCITE-LIKE COMPOUNDS FOR THE VALORISATION OF RENEWABLE FEEDSTOCKS

Mayra García Álvarez

Dipòsit Legal: T. 724-2012

¹H NMR

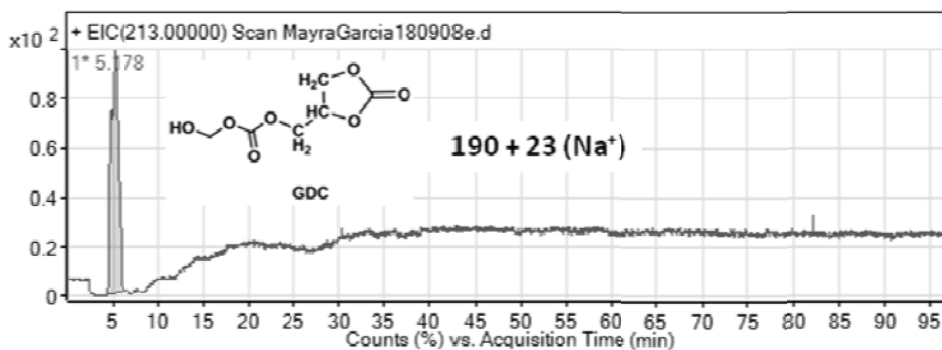
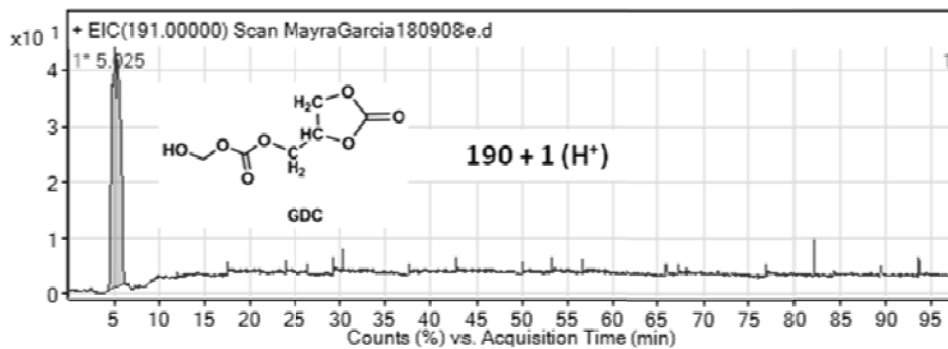
First product of transesterification: Glycerol carbonate



¹H NMR (400 MHz, DMSO-d₆): δ (ppm) = 5.29 (t, 1H, OH, J = 5.6 Hz), 4.81–4.76 (m, 1H, CH), 4.48 (dd, 1H, OCH₂ J₁ = 8.0 Hz, J₂ = 8.4 Hz), 4.28 (dd, 1H, OCH₂CH, J₁ = 8.0 Hz, J₂ = 6.0 Hz), 3.65 (ddd, 1H, CH₂OH, J₁ = 12.4 Hz, J₂ = 5.6 Hz, J₃ = 2.8 Hz), 3.50 (ddd, 1H, CH₂OH, J₁ = 12.4 Hz, J₂ = 5.6 Hz, J₃ = 3.2 Hz).

HPLC-TOF

Second product of transesterification: Glycerol dicarbonate



M.W.: 190 g/mol

APPENDIX I

LIST OF ABBREVIATIONS

UNIVERSITAT ROVIRA I VIRGILI

HYDROTALCITE-LIKE COMPOUNDS FOR THE VALORISATION OF RENEWABLE FEEDSTOCKS

Mayra García Álvarez

Dipòsit Legal: T. 724-2012

LIST OF ABBREVIATIONS

AAS	Atomic Absorption Spectroscopy
BET	Brunauer Emmett Teller approximation
CAS	Chemical Abstract Service
CNF	Carbon nanofibers
DEC	Diethyl carbonate
DMA	Dimethyl acetamide
DMC	Dimethyl carbonate
DMF	Dimethyl formamide
DMSO	Dimethyl sulphoxide
EC	Ethylene carbonate
EG	Ethylene glycol
EU	European Union
EXAFS	Extended X-ray Absorption Fine Structure
FID	Flame Ionization Detector
FTIR	Fourier Transform Infrared Spectroscopy
FWHM	Full Width at Half Maximum
GC	Glycerol carbonate
GC-MS	Gas Chromatography-Mass Detector
GDC	Glycerol dicarbonate
HT	Hydrotalcite
ICDD	International Centre for Diffraction Data
ICP	Induced Couple Plasma
IR	Infrared Spectroscopy
JCPDS	Joint Committee on Powder Diffraction Standards
LDH	Layered Double Hydroxide
MIBK	Methyl isobutyl ketone
MPV	Merwein-Ponndorf-Verley reduction
MS	Mass Spectroscopy
NMR	Nuclear Magnetic Resonance
PXRD	Powder X-ray Diffraction
TCD	Thermal Conductivity Detector
TEA	Triethyl amine
TOF	Turnover Frequency

TPD	Temperature Programmed Desorption
UV	Ultraviolet Spectroscopy
XANES	X-ray Absorption Near Edge Structure

APPENDIX II

INDEX OF TABLES

UNIVERSITAT ROVIRA I VIRGILI

HYDROTALCITE-LIKE COMPOUNDS FOR THE VALORISATION OF RENEWABLE FEEDSTOCKS

Mayra García Álvarez

Dipòsit Legal: T. 724-2012

INDEX OF TABLES

Table 1.1.1. Types of heterogeneous basic catalysts.....	Page 6
Table 2.1.1. Base-catalysed reactions involving hydrotalcite-like compounds.....	Page 30
Table 2.1.2. Transesterification reactions (biodiesel production) involving hydrotalcite-like compounds.....	Page 32
Table 2.2.1. Characterisation of catalysts. Chemical composition, PXRD analysis and BET surface areas.....	Page 39
Table 2.2.2. Results of basic properties for the catalysts.....	Page 40
Table 2.2.3. Synthesis of glycerol carbonate or dicarbonate from glycerol under standard conditions with different catalysts.....	Page 44
Table 2.2.4. Reutilisation of catalyst HTr4.....	Page 45
Table 2.3.1. Composition, textural and crystalline properties of the prepared materials.....	Page 53
Table 2.3.2. Thermogravimetric analysis of rehydrated and anion-exchanged hydrotalcites.....	Page 58
Table 2.3.3. Basic properties found for the mixed oxides and rehydrated catalysts.....	Page 60
Table 2.3.4. Catalytic behaviour for all the catalysts tested in the transesterification of glycerol under standar conditions.....	Page 65
Table 2.3.5. Quantitative results obtained by EDX analysis.....	Page 66
Table 2.3.6. Results of Hammett indicator for calcined, rehydrated and anion-exchanged catalysts.....	Page 68
Table 2.3.7. Comparison of the basic properties of the calcined, rehydrated and fluorine-exchanged catalysts.....	Page 69
Table 2.3.8. Catalytic properties of reused HT4-F catalyst.....	Page 71
Table 3.2.1. Physico-chemical properties of the different materials.....	Page 88
Table 3.2.2. Initial reaction rates for transesterification of glycerol with DEC with the HT catalysts under the same standard conditions.....	Page 90

Table 3.2.3. Catalytic behaviour of the different materials tested in the transesterification of glycerol under standard conditions.....	Page 91
Table 3.3.1. BET specific surface area, textural properties and XRD characterisation of catalysts and supports.....	Page 105
Table 3.3.2. Results of basic properties for the samples.....	Page 108
Table 3.3.3. Properties of the tested solvents.....	Page 110
Table 3.3.4. Catalytic behaviour of catalysts with different Mg/Al molar ratio.....	Page 108
Table 4.2.1. Structural parameters (in Å) obtained by Rietveld refinements.....	Page 135
Table 4.2.2. Mean crystallite size estimation (in Å) for the different hkl families.....	Page 137
Table 4.2.3. Structural parameters (first two shells) of ZnAl-HT (HT1 series) obtained by EXAFS fitting.....	Page 142
Table 4.2.4. Textural properties of ZnAl-HT (HT1 series) obtained by adsorption-desorption of N ₂ at 77 K.....	Page 144
Table 4.2.5. Structural (in Å) and textural parameters of HT2 series obtained by Rietveld refinement, EXAFS fitting and BET measurements	Page 147
Table 4.2.6. Catalytic behaviour of HT1 and HT2 series.....	Page 151

APPENDIX III

INDEX OF FIGURES

UNIVERSITAT ROVIRA I VIRGILI

HYDROTALCITE-LIKE COMPOUNDS FOR THE VALORISATION OF RENEWABLE FEEDSTOCKS

Mayra García Álvarez

Dipòsit Legal: T. 724-2012

INDEX OF FIGURES

Figure 1.2.1. Projection of a brucite-like layer.....	Page 7
Figure 1.2.2. Idealised structure of a layered double hydroxide (LDH).....	Page 8
Figure 1.2.3. Relationship between the triple hexagonal cell with axes OE,OF,OG to the primitive rhombohedral cell with axes OA, OB, OC.....	Page 9
Figure 1.2.4. Association of divalent and trivalent cations in LDHs.....	Page 11
Figure 1.2.5. Possible applications of LDH compounds.....	Page 16
Figure 1.3.1. Distribution of various uses of glycerol.....	Page 17
Figure 2.2.1. Thermogravimetric analysis of the hydrotalcite samples....	Page 40
Figure 2.2.2. CO ₂ losses during temperature-programmed desorption experiments.....	Page 41
Figure 2.2.3. Conversion of glycerol vs. reaction time.....	Page 42
Figure 2.2.4. PXRD patterns for fresh and used catalysts.....	Page 45
Figure 2.3.1. Powder X-ray diffractograms of as-synthesised, calcined and rehydrated hydrotalcite.....	Page 54
Figure 2.3.2. Nitrogen adsorption isotherms for the prepared materials. A) As-synthesised hydrotalcites; B) calcined hydrotalcites and C) rehydrated hydrotalcites.....	Page 56
Table 2.3.3. TPD-CO ₂ profiles of: A) calcined hydrotalcites and B) rehydrated hydrotalcites.....	Page 59
Figure 2.3.4. Catalytic behaviour of calcined and rehydrated catalysts at 403 K and a glycerol : DEC molar ratio 1:17.....	Page 62
Figure 2.3.5. Influence of the Mg/Al molar ratio in the catalytic activity of calcined and rehydrated catalysts.....	Page 62
Figure 2.3.6. Effect of the compensating anion in the glycerol conversion at 403 K and standard reaction conditions.....	Page 67
Figure 2.3.7. TPD-CO ₂ profile of fluorine-exchanged catalysts (HT4-F). Insert: MS analysis.....	Page 69
Figure 2.3.8. X-ray patterns for fresh and used catalyst HTr3.....	Page 70

Figure 3.2.1. X-ray diffraction patterns of a) HT-CNFas; b) HT-CNFrl; c) HT-CNFrg; d) HT-CNFrl after 1 run and e) HT-CNFrg after 1 run.....	Page 86
Figure 3.2.2. TEM images of A) HT-CNFas; B) HT-CNFrg; C) and D) HT-CNFrl.....	Page 86
Figure 3.2.3. Thermogravimetric analyses of supported hydrotalcites HT-CNFas, HT-CNFrl and HT-CNFrg.....	Page 87
Figure 3.2.4. Catalytic behaviour of the different catalysts at 403 K and a glycerol : DEC molar ratio 1:17. Insert: Catalytic behaviour of bulk hydrotalcites under the same standard conditions.....	Page 89
Figure 3.2.5. Catalytic performance of HT-CNFc catalyst in three consecutive runs under standard reaction conditions.....	Page 93
Figure 3.2.6. Transesterification profiles for HT-CNFc and removing of catalyst. Reaction was performed at 403 K and with a glycerol : DEC molar ratio 1:17.....	Page 94
Figure 3.3.1. PXRD diffractograms of: A) Alpha-alumina supported catalysts and B) Gamma-alumina supported catalysts.....	Page 104
Figure 3.3.2. TPD-CO ₂ profiles of: A) catalysts supported onto alpha-alumina and B) catalysts supported onto gamma-alumina.....	Page 106
Figure 3.3.3. Glycerol conversion found for catalyst HTO2-Alpha for the three different solvents tested at 403 K and a fixed feed flow of 0.1 mL/min.....	Page 109
Figure 3.3.4. Results of the variation in HTO2-Alpha catalyst performance for the transesterification of glycerol with diethyl carbonate at 403 K by varying the feed flows. Insert: variation of the selectivity to glycerol carbonate and glycerol dicarbonate with the conversion.....	Page 111
Figure 3.3.5. Catalytic behaviour (conversion and selectivity) of calcined catalysts at 403 K and a feed flow of 0.05 mL/min. A) HTO2-Alpha and B) HTO2-Gamma.....	Page 114
Figure 3.3.6. Catalytic activity for rehydrated catalysts at 403 K and a feed flow of 0.05 mL/min. A) HTr2-Alpha and B) HTr2-Gamma.....	Page 115
Figure 3.3.7. Catalytic activity for catalysts with higher Mg content at 403 K and a feed flow of 0.05 mL/min.: A) calcined catalyst, HTO4-Alpha and B) rehydrated catalyst, HTr4-Alpha.....	Page 117
Figure 3.3.8. Selectivities of the catalysts supported on α -alumina as a function of the conversion. Insert: variation of the conversion with the amount of CO ₂ adsorbed.....	Page 118

Figure 4.2.1. A) Normalised PXRD diffractograms for HT1 series: i) HT1as; ii) HT1RM24; iii) HT1RUS0.5; iv) HT1RUS2 and v) HT1RUS10. B) Rietveld refinement using the anisotropic peak broadening model for sample HT1as.....	Page 134
Figure 4.2.2. Williamson-Hall plots for HT1 series. a) HT1as; b) HT1RM24; c) HT1RUS0.5; d) HT1RUS2 and e) HT1RUS10.....	Page 138
Figure 4.2.3. ^{27}Al NMR of the HT1 series. a) HT1c (calcined HT1as at 723 K); b) HT1RM24; c) HT1RUS0.5; d) HT1RUS2 and e) HT1RUS10...	Page 139
Figure 4.2.4. XANES spectra of ZnAl hydrotalcites (HT1 series) after the hydrothermal treatment at Zn k-edge.....	Page 140
Figure 4.2.5. Zn k-edge Fourier transform of HT1 series. Distances are given without phase shift correction.....	Page 141
Figure 4.2.6. Experimental (blue) and calculated (red) Zn environmental radial distribution and EXAFS Fourier transform modulus for sample HT1.....	Page 142
Figure 4.2.7. N_2 adsorption-desorption isotherms at 77 K of HT1 series	Page 143
Figure 4.2.8. Total acidity and basicity of HT1 series samples determined by TPD of NH_3 and CO_2	Page 145
Figure 4.2.9. CO_2 (A) and NH_3 (B) desorption profiles obtained by temperature programmed desorption (TPD) for HT1 series.....	Page 146
Figure 4.2.10. A) Normalised PXRD diffractograms for HT2 series: i) HT2as; ii) HT2RM24; iii) HT2RUS0.5; iv) HT2RUS2 and v) HT2RUS10. B) Rietveld refinement using the anisotropic peak broadening model for sample HT2as.....	Page 148
Figure 4.2.11. CO_2 (A) and NH_3 (B) desorption profiles obtained by temperature programmed desorption (TPD) for HT2 series.....	Page 149
Figure 4.2.12. Total acidity and basicity of HT2 series samples determined by TPD of NH_3 and CO_2	Page 150

UNIVERSITAT ROVIRA I VIRGILI

HYDROTALCITE-LIKE COMPOUNDS FOR THE VALORISATION OF RENEWABLE FEEDSTOCKS

Mayra García Álvarez

Dipòsit Legal: T. 724-2012

APPENDIX IV

INDEX OF SCHEMES

UNIVERSITAT ROVIRA I VIRGILI

HYDROTALCITE-LIKE COMPOUNDS FOR THE VALORISATION OF RENEWABLE FEEDSTOCKS

Mayra García Álvarez

Dipòsit Legal: T. 724-2012

INDEX OF SCHEMES

Scheme 1.3.1. Compilacion of the main glycerol modifications.....	Page 18
Scheme 1.3.2. Synthesis of glycerol carbonate.....	Page 19
Scheme 1.3.3. Synthesis of glycerol carbonate from glycerol and urea..	Page 20
Scheme 2.2.1. Consecutive hydrotalcite-catalysed transesterification reaction of glycerol with DEC.....	Page 43
Scheme 3.3.1. Consecutive transesterification reaction of glycerol with DEC.....	Page 111
Scheme 3.3.2. Proposal of mechanism of hydrotalcite-catalysed transesterification of glycerol with DEC.....	Page 112

UNIVERSITAT ROVIRA I VIRGILI

HYDROTALCITE-LIKE COMPOUNDS FOR THE VALORISATION OF RENEWABLE FEEDSTOCKS

Mayra García Álvarez

Dipòsit Legal: T. 724-2012

APPENDIX V

CONTRIBUTIONS TO CONFERENCES

UNIVERSITAT ROVIRA I VIRGILI

HYDROTALCITE-LIKE COMPOUNDS FOR THE VALORISATION OF RENEWABLE FEEDSTOCKS

Mayra García Álvarez

Dipòsit Legal: T. 724-2012

CONTRIBUTIONS TO CONFERENCES

Authors: M.G. Álvarez, A.M. Segarra, S. Contreras, F. Figueras, F. Medina, J.E. Sueiras
Title: Influence of Lewis and Brønsted basic sites on activated hydrotalcites for transesterification of glycerol.
Participation: Oral communication
Conference: 6^o International Conference in Acid and basic Catalysis. Genova (Italy).

Authors: M.G. Álvarez, A.M. Segarra, S. Contreras, F. Figueras, F. Medina, J.E. Sueiras
Title: Activated Hydrotalcites as Catalysts for glycerol conversion to Commodity Chemicals.
Participation: Poster communication
Conference: CLEAR Summer School (ACENET and EFCAT). Porto Karras (Greece).

Authors: M.G. Álvarez, A.M. Segarra, S. Contreras, F. Figueras, F. Medina, J.E. Sueiras
Title: Hydrotalcite-like compounds for transesterification of glycerol to more valuable products.
Participation: Poster communication
Conference: EUROPACAT 09. Salamanca (Spain).

Authors: M.G. Álvarez, M. Pliskova, A.M. Segarra, F. Medina, F. Figueras
Title: Continuous transesterification of glycerol with diethyl carbonate using supported hydrotalcites as catalysts.
Participation: Poster communication
Conference: 4th Workshop on Fats and Oils as Renewable Feedstock for the Chemical Industry. Karlsruhe (Germany).

Authors: M.G. Álvarez, R.J. Chimentao, A.M. Segarra, F. Medina, F. Figueras
Title: Revalorización de glycerol: Estudio de catalizadores tipo hidrotalcita empleando reactores en batch y continuo.
Participation: Poster communication
Conference: SECAT 2011. Zaragoza (Spain).

Authors: M.G. Álvarez, A.M. Segarra, F. Medina, F. Figueras
Title: Alumina supported hydrotalcites: Preparation and catalytic study in continuous transesterification of glycerol.
Participation: Poster communication
Conference: EuropaCat 2011. Glasgow (Scotland).

Authors: M.G. Álvarez, R.J. Chimentao, N. Barrabés, S. Reimann, K. Föttinger, F. Medina

Title: Examination of the defect structure evolution by induced reconstruction of layered double hydroxides.

Participation: Poster communication

Conference: EuropaCat 2011. Glasgow (Scotland).

APPENDIX VI

LIST OF PUBLICATIONS

UNIVERSITAT ROVIRA I VIRGILI

HYDROTALCITE-LIKE COMPOUNDS FOR THE VALORISATION OF RENEWABLE FEEDSTOCKS

Mayra García Álvarez

Dipòsit Legal: T. 724-2012

LIST OF PUBLICATIONS

Authors: Mayra G. Álvarez, Anna M. Segarra, Sandra Contreras, Jesús E. Sueiras, Francisco Medina and François Figueras

Title: Enhanced use of renewable resources: Transesterification of glycerol catalysed by hydrotalcite-like compounds

Journal: Chemical Engineering Journal

Volume: 161

Pages: 340-345

Year: 2010

Authors: Mayra G. Álvarez, Martina Pliskova, Anna M. Segarra, Francesc Medina and François Figueras

Title: Synthesis of glycerol carbonates by transesterification of glycerol in a continuous system using supported hydrotalcites as catalysts.

Journal: Applied Catalysis B: Environmental

Volume: 113-114

Pages: 212-220

Year: 2012

Authors: Mayra G. Álvarez, Ricardo J. Chimentao, Francesc Medina and François Figueras

Title: Tunable basic and textural properties of hydrotalcite derived materials for transesterification of glycerol.

Journal: Applied Clay Science

Volume: 58

Pages: 16-24

Year: 2012

Authors: Mayra G. Álvarez, Ricardo J. Chimentao, Noelia Barrabés, Karin Föttinger, Francesc Gisper-Guirado, Evgeny Klemeynov, Didier Tichit and Francesc Medina

Title: Structure evolution of layered double hydroxides activated by induced reconstruction

Journal: Microporous and Mesoporous Materials (*To be submitted*)

Authors: Mayra G. Álvarez, Anne M. Frey, Harry J. Bitter, Anna M. Segarra, Krjin P. de Jong and Francesc Medina

Title: From glycerol to glycerol carbonate: Transesterification over hydrotalcites supported on carbon nanofibers as highly active heterogeneous catalysts. (*To be submitted*)

Authors: Noelia Barrabés, Karin Föttinger, Mayra G. Álvarez, Ricardo J. Chimentao, Evgeny Klemeynov, Atshushi Urakawa, Didier Tichit and Günther Rupprechter

Title: XAFS *in situ* study of the reducibility of Cu-derived hydrotalcite catalysts. (*To be submitted*)

UNIVERSITAT ROVIRA I VIRGILI

HYDROTALCITE-LIKE COMPOUNDS FOR THE VALORISATION OF RENEWABLE FEEDSTOCKS

Mayra García Álvarez

Dipòsit Legal: T. 724-2012